



UNIVERSITÀ DEGLI STUDI DI MILANO

FACOLTA' DI MEDICINA E CHIRURGIA

CORSO DI DOTTORATO DI RICERCA IN

MEDICINA TRASLAZIONALE

CICLO XXXVI

DIPARTIMENTO DI "Clinical Sciences and Community Health"

TESI DI DOTTORATO DI RICERCA

The role of Beta-Klotho protein in NAFLD pathogenesis

Settore scientifico disciplinare

MED/09

Candidato Roberto Piciotti

Matricola N° R13168

Tutor: Prof. Rosa Lombardi

Co-Tutor: Prof. Vincenzo La Mura

Coordinatore del Dottorato: Prof. Chiarella Sforza

Anno Accademico (A.A.)

2022-23

SUMMARY:

.....	1
ABSTRACT	6
INTRODUCTION	9
1. NAFLD: prevalence and pathogenesis.....	9
2. NASH progression to HCC and tumor EMT transition.....	13
3. Nomenclature and classification updating in the context of fatty liver disease.....	14
4. Impact of genetics in NAFLD.....	15
5. KLB: protein structure, activity, transcriptional regulation, protein localization and post-translational shedding.....	20
6. KLB-mediated intracellular signaling in the liver.....	22
7. KLB role in NAFLD pathogenesis: clinical and preclinical evidence.....	26
8. Clinical Management of NAFLD and relevancy of KLB as novel therapeutical target.....	30
RATIONALE OF THE STUDY.....	34
AIMS OF THE STUDY.....	36
METHODS	37
1. Patients' cohort:.....	37
2. In <i>in vitro</i> experiments:.....	39
Generation of KLB Knockout model in HepG2 cells through CRISPR/Cas9 technology.....	39
Cell culture and Treatments.....	40
Protein extraction, quantification, and Western Blot.....	41
Extraction of nuclear and cytosolic portion.....	41
Gene expression analysis.....	41
ORO staining.....	42
Lipid secretion.....	43
Immunofluorescence analysis.....	43
Apoptosis assay for Annexin V and caspase 3/7 by the Incucyte® SX5 platform.....	44
Apoptosis assay by flow cytometric analysis:.....	44
Cell cycle analysis using flow cytometry:.....	45
Inflammation and Stem Cell gene Panels with TaqMan OpenArray:.....	45
Cytokine secretion.....	46
Cell proliferation analysis using the Incucyte® platform.....	46
Cell Proliferation Assays EdU.....	47
Wound Healing Assay.....	48
Spheroid assay.....	48
Statistical analyses.....	49
RESULTS	54
AIM1: Impact of the KLB Knock-out on the hepatocyte homeostasis and on the onset of NAFLD traits.....	54

1. Generation and characterization of a stable KLB full knock-out in vitro model:.....	54
2. Effects KLB KO on FGFR4 activation.....	54
3. Effects of KLB KO on FGFR4/KLB signaling	55
4. KLB depletion impairs lipid metabolism.....	57
5. Effects of lipid overload on KLB-/- cells	59
6. KLB depletion may impair cholesterol metabolism and promote BA production in in vitro model 61	
7. KLB depletion induces severe hepatic damage in <i>in vitro</i> model.....	63
8. KLB depletion promotes cell apoptosis in <i>in vitro</i>	65
9. KLB depletion impairs the autophagic flux	67
10. Effects of KLB depletion on inflammation:.....	71
11. KLB deficiency drives cells toward a malignant phenotype:	74
12. KLB depletion promotes the switching towards a mesenchymal phenotype:	78
AIM2: Characterization of the rs12152703 KLB variant in pediatric and adult patients with NAFLD 82	
2.1 KLB rs12152703 variant may be protective against severe liver disease in NAFLD patients... 82	
2.2 Circulating levels and hepatic expression of KLB in association with the rs12152703 variant genotypes in a subset of pediatric patients.....	83
DISCUSSION	85
CONCLUDING REMARKS.....	91
FUTURE PERSPECTIVES	93
BIBLIOGRAPHY	94

FIGURE INDEX

INTRODUCTION AND METHODS:

Figure A: Mechanism underpinning NAFLD/NASH progression.....	
Figure B: Genetic influence on NAFLD development and progression to severe liver damage.....	
Figure C: In silico predictions of the human KLB protein structures.....	
Figure D: KLB/FGFR4/FGF19 signaling pathways in the liver.....	
Figure E: Impact of the KLB rs17618244 variant on NAFLD traits and on liver homeostasis in adult and pediatric patients with NAFLD.....	

RESULTS:

Figure 1: Characterization of a stable KLB full knock-out <i>in vitro</i> model.....	
Figure 2: Effects of <i>in vitro</i> KLB KO on FGFR4/KLB signaling.....	
Figure 3: Effects of <i>in vitro</i> KLB depletion on lipid metabolism.....	
Figure 4: Effects of lipid overload on KLB ^{-/-} cells.....	
Figure 5: Effects of <i>in vitro</i> KLB depletion on cholesterol metabolism and BA production	
Figure 6: Impact of <i>in vitro</i> KLB depletion on ER and oxidative stress.....	
Figure 7: KLB depletion impact on cell apoptosis in <i>in vitro</i>	
Figure 8: Effects of <i>in vitro</i> KLB depletion on the autophagic flux.....	
Figure 9: Effects of <i>in vitro</i> KLB depletion on inflammation.....	
Figure 10: Effects of <i>in vitro</i> KLB depletion on cell proliferation and growth.....	
Figure 11: Effects of <i>in vitro</i> KLB depletion on the acquisition of pro-tumorigenic features.....	
Figure 12: Effects of <i>in vitro</i> KLB depletion on stemness and pluripotency features	
Figure 13: Effects of <i>in vitro</i> KLB depletion on EMT transition.....	
Figure 14: Impact of the KLB rs12152703 variant on NAFLD traits and on KLB expression in patients	

TABLES INDEX

Table 2: Antibodies reagents code.....	
Table 3: RT-qPCR SYBER Green primers sequences.....	
Table 4: RT-qPCR Taqman probes codes.....	

ABSTRACT

Non-Alcoholic Fatty Liver Disease (NAFLD) is the most prevalent and progressive liver condition characterized by the accumulation of fat in more than 5% of hepatocytes in the absence of excessive alcohol consumption. Considered a spectrum of liver disorders, NAFLD ranges from simple steatosis, where fat buildup is the primary feature, to Non-Alcoholic Steatohepatitis (NASH), a more severe form associated with inflammation and liver cell damage. As a burgeoning public health concern, NAFLD poses risks of progression to advanced liver diseases, including fibrosis, cirrhosis, and hepatocellular carcinoma and its evolution is closely linked to metabolic risk factors such as obesity, insulin resistance, and dyslipidemia. In addition, a genetic burden strongly underpins NAFLD pathogenesis, and several at-risk genetic variations have been found to predispose patients to the onset of liver disease. In this concern, our group previously reported that the rs17618244 G>A variant in the β -Klotho (KLB) gene dampened the KLB hepatic/plasma levels, leading to inflammation, ballooning, and fibrosis in NAFLD patients. KLB protein, functioning as coreceptor for fibroblast growth factor receptors 4 (FGFR4), mediates in the liver the hormonal activity of FGF19 and plays a central role in the regulation of lipid metabolism and in bile acids' biosynthesis. Thus, a stable *KLB* full knock-out model in HepG2 hepatoma cells (*KLB*^{-/-}) has been generated by using Crispr/Cas9 technology, with the aim to reproduce *in vitro* the effects of the *KLB* rs17618244 variant. Then, in a cohort of 1311 NAFLD patients, among which 261 were children, the new intronic *KLB* rs12152703 T>G variant was associated with NAFLD traits and the hepatic/plasma levels of KLB were determined.

Our results outlined that *KLB*^{-/-} cells have altered cell homeostasis and reported the impairment of several hepatocyte typical features. Indeed, *KLB*^{-/-} cells showed the downregulation of important genes involved in lipid metabolism and in cholesterol production and uptake. Furthermore, an increase in the endoplasmic reticulum (ER) and oxidative

stress were observed in *KLB*^{-/-} cells. Cell homeostasis was further affected by the enhancement of cell apoptosis and by the impairment of the autophagic flux, mirroring in *in vitro* the progression to severe liver damage. Accordingly, in our model the release of pro-inflammatory cytokines was increased and a panel of 586 genes associated to inflammation revealed the upregulation of important mediators related to the inflammatory response. Additionally, tumorigenic features were acquired after KLB depletion, resulting in increased cell growth, proliferation and invasiveness. Interestingly, in KLB depleted cells a reduction in the response to anti-cancer therapy was observed, along with the establishment of a pro-tumorigenic environment, supported by the upregulation of several oncogenes and by the increasing of cell self-renewal activity. We further reported that the absence of KLB *in vitro* may mediate the transition to a mesenchymal phenotype through the downregulation of important epithelial markers and the upregulation of mesenchymal mediators. Finally, in patients we evaluated a new variant, the KLB rs12152703, showing its possible protective action against advanced liver disease in term of reduction of transaminases levels, NAFLD activity score (NAS) and predisposition to developing NASH. This action may be mediated by an increase in circulating and hepatic KLB mutated protein, as demonstrated in a pediatric patient with the rs12152703 TT homozygous genotype we evaluated.

In conclusion, our results outlined that *KLB* KO induced in HepG2 cells may drive important changes in liver cells metabolism and homeostasis, as consequence of the altered KLB signaling. In these cells, lipid and cholesterol metabolism were the mainly affected, thus possibly speculating that KLB depletion may lead to the loss of important hepatocyte-specific properties. Moreover, *KLB*^{-/-} cells showed features resembling the switching towards progressive forms of liver damage observed in patients, pinpointing the possible involvement of KLB in NAFLD progression. Moreover, the acquisition of several pro-carcinogenic traits,

such as enhanced proliferation, invasiveness and acquisition of stemness features may indicate that the absence of KLB further contributes to the shift towards a more aggressive cancerous phenotype.

As for the translational approach, we determined for the first time the potential protective role of another variant of KLB, the rs12152703, on liver disease which is correlated to an increase in KLB levels, observed in those patients carrying the TT mutation. These evidence highlights the potentiality of KLB as novel clinical targets to refine the NAFLD prognosis. Moreover, the recombinant isoforms of KLB could be used for the treatment of NASH and might have stronger effects in those patients reporting KLB downregulation.

INTRODUCTION

1. NAFLD: prevalence and pathogenesis

Non-alcoholic fatty liver disease (NAFLD) is a multifactorial and complex liver disorder, emerged as the principal chronic liver disease and one of major public health concerns worldwide. It encompasses a spectrum of liver conditions, ranging from simple hepatic steatosis, characterized by excessive lipid accumulation in hepatocytes, to non-alcoholic steatohepatitis (NASH), cirrhosis and lastly hepatocarcinoma (HCC) [2]. NAFLD is closely associated with metabolic risk factors, such as obesity, insulin resistance, type 2 diabetes mellitus, metabolic syndrome and dyslipidemia [3]. It is also well established that genetic factors predispose individuals to NAFLD and the vast majority of people diagnosed with NAFLD have polymorphisms in genes involved in lipid handling [4]. These predisposing factors interact synergistically to disrupt hepatic lipid homeostasis, leading to the aberrant accumulation of lipids in the liver. Notably, the prevalence of NAFLD has dramatically increased over the past few decades, closely mirroring the escalating rates of obesity and metabolic syndrome worldwide [5]. At present, NAFLD affects approximately one-quarter of the global population, with the highest prevalence in individuals with obesity and diabetes, reaching up to 70-90% in these patient populations [3, 6]. NAFLD prevalence varies substantially among different populations and is closely related to lifestyle and socio-economic factors [7, 8]. In developed countries, the prevalence of NAFLD ranges from 20% to 30%, while in emerging economies, it has reached alarming rates of up to 40% [6, 8]. The escalating epidemic of obesity, sedentary lifestyle, and unhealthy dietary habits has significantly contributed to the increasing burden of NAFLD in both adults and children, posing a significant burden on healthcare systems. As consequence, NAFLD has become a major global health concern, affecting individuals across diverse age groups and ethnic backgrounds and further contributes to a substantial economic burden through its

association with cardiovascular events, diabetes, and other obesity-related comorbidities[9]. The pathogenesis of NAFLD is a complex interplay of various mechanisms involving genetic predisposition, environmental factors, and systemic metabolic imbalances. Basically, insulin resistance along with excessive caloric intake and a sedentary lifestyle led to increased levels of free fatty acids (FFAs) in the blood stream. The accumulation of free fatty acids (FFAs) within hepatocytes results in the creation of lipid droplets, primarily composed of triglycerides [10, 11]. These lipid droplets serve as observable indicators of hepatic steatosis, which is the defining characteristic of NAFLD. In this phase, dysregulated uptake of fatty acids from the bloodstream and impaired export of triglycerides as very-low-density lipoproteins (VLDL) accumulate lipids into hepatocytes which in turn upregulate de novo lipogenesis (DNL), leading to increased fatty acids synthesis also from non-lipid precursors [12]. As consequence, accumulation of toxic lipid intermediates impairs insulin signaling and promotes cell death. The higher lipid availability in the liver initially stimulates the hepatic mitochondrial capacity promoting excessive hepatic oxidative stress and reducing mitochondrial functionality [10]. When the liver is no longer capable to manage the lipid overload, it flows into mitochondrial dysfunction, firstly impairing the mitochondrial electron transport chain (ETC) and the oxidative phosphorylation process (OXPHOS). Impaired mitochondrial function can lead to ATP deficiency, affecting energy-dependent processes in the liver with a major impact on important cellular functions, including repair and regeneration, essential for liver health [13]. Accordingly, dysfunctional mitochondria prompt the production of excessive ROS as a byproduct of inefficient ETC activity, contributing to hepatocellular damage. Indeed, reactive oxygen species exert detrimental effects on cellular components, including lipids, proteins, and nucleic acids. The cumulative impact of oxidative stress and mitochondrial dysfunction lead to severe hepatocyte injury and inflammation [14]. Inflammation is a central feature in the pathogenesis of NAFLD and characterize liver disease progression to NASH [12]. In this step, the activation of innate immune cells, such

as Kupffer cells and neutrophils activate in turn the nuclear factor-kappa B (NF- κ B) pathway which promotes the production of pro-inflammatory cytokines, including tumor necrosis factor-alpha (TNF- α), interleukin-6 (IL-6), and interleukin-1 beta (IL-1 β) [15]. These inflammatory mediators induce hepatocyte injury activating the hepatic stellate cells (HSCs), which initiates the fibrotic process [16, 17]. Notably, activated HSCs are the major cellular source of extracellular matrix (ECM) components in the liver. In response to inflammatory signals, HSCs undergo a process of activation, transforming from a quiescent state to a proliferative and fibrogenic phenotype. Activated HSCs deposit excessive ECM proteins, primarily collagen type I, in the liver parenchyma, leading to the development of fibrosis [18]. At this stage, the transforming growth factor-beta (TGF- β) signaling stands out as a central player, regulating various cellular processes, including proliferation, differentiation, apoptosis, and extracellular matrix synthesis which aggravates liver fibrosis [19]. The presence of persistent inflammation, hepatocyte injury, and fibrosis in NASH sets the stage for hepatocarcinogenesis, creating a microenvironment conducive to malignant transformation. In this process, factors such as oxidative stress, DNA damage, and cellular senescence are main contributors for the establishment of neoplastic changes [15]. Not least, the gut-liver axis has emerged as a key player in NAFLD pathogenesis. Alterations in the gut microbiota composition, intestinal barrier dysfunction, and increased gut permeability have been associated with NAFLD development and progression. This dysbiosis-driven gut-liver crosstalk is thought to contribute to the translocation of gut-derived bacterial products into the liver, triggering hepatic inflammation and injury. Given the rising prevalence of obesity and metabolic syndrome worldwide, NAFLD has become the leading cause of chronic liver disease and a significant risk factor for the development of cirrhosis, hepatocellular carcinoma, and liver-related morbidity and mortality [20].

Therefore, a comprehensive understanding of the pathogenesis of NAFLD is crucial for the development of targeted therapeutic strategies to manage and prevent the progression of this burgeoning global health problem.

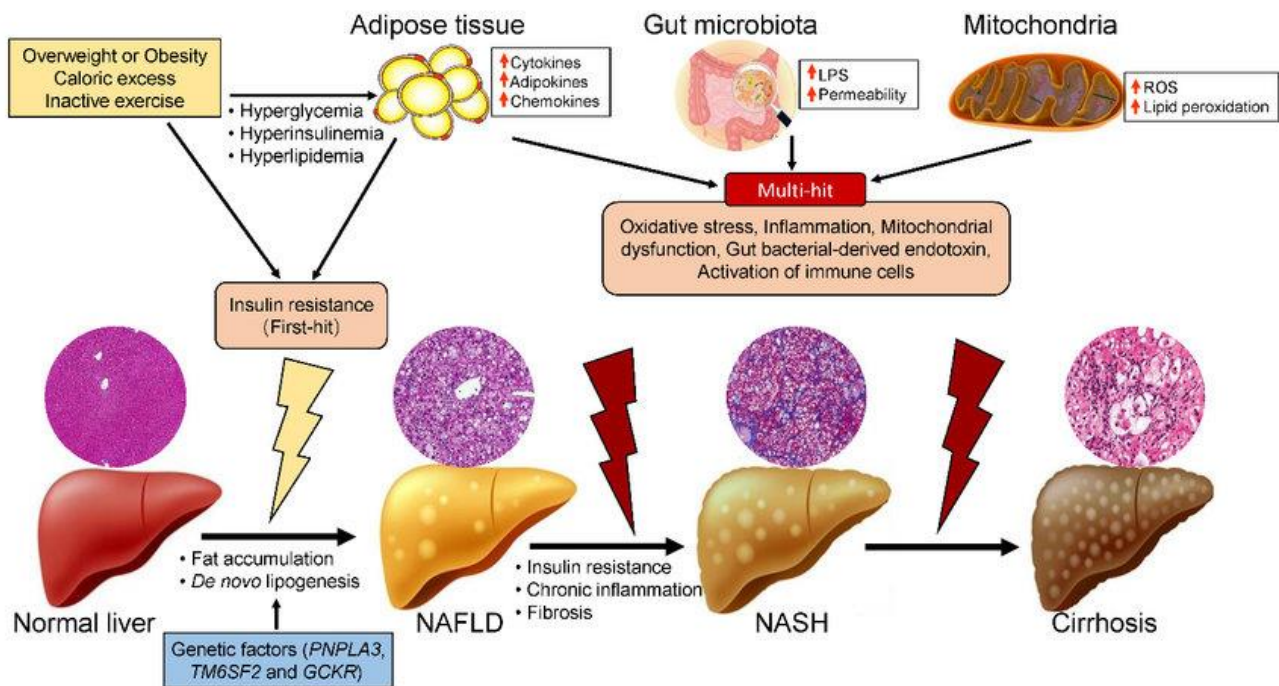


Figure A: Mechanism underpinning NAFLD/NASH progression. Unhealthy diet, physical inactivity, drugs, and hepatitis virus infection give insults to the healthy liver. Insulin resistance and dysfunctional adiposity represent the first hits and along with genetic and environmental factors promote the onset of steatosis, which represents NAFLD first stage. Lipid overload affects expression of genes regulating oxidative stress, lipid peroxidation, mitochondrial damage, and inflammation, setting the stage for NASH development. The onset of fibrosis along with oxidative damage and liver inflammation dictate the progression to cirrhosis finally evolving to HCC in the final stages. From Xu et al., *Int J Mol Sci.* 2019 [21].

2. NASH progression to HCC and tumor EMT transition

The transition from NASH to HCC is a complex process influenced by a combination of genetic, epigenetic, and environmental factors. Chronic inflammation and oxidative stress in the liver contribute to cellular damage and genomic instability, which, in turn, drive the development of preneoplastic lesions. Over time, these lesions can transform into fully developed HCC [5]. The exact molecular mechanisms that underlie the progression from NASH to HCC remain not completely understood. However, various signaling pathways, such as the Wnt/ β -catenin pathway and Notch signaling, have been implicated in promoting liver cancer development [22]. Additionally, dysregulation of several key transcription factors and non-coding RNAs may play crucial roles in the transition from NASH to HCC [23, 24]. During this intricate process, the Epithelial-mesenchymal transition (EMT) has emerged as a critical biological phenomenon involved in cancer progression. Notably, EMT is known for its implication in promoting tumor invasion and metastasis in various cancer types, including HCC [25]. EMT consists in the transformation of epithelial cells which lose their characteristic features and acquire a mesenchymal phenotype characterized by enhanced cell motility and invasiveness [26]. Furthermore, EMT confers cancer stem cell-like properties to tumor cells, contributing to therapy resistance and tumor recurrence, crucial challenges in HCC treatment. The orchestration of EMT is mediated by an intricate interplay of various molecular factors, including transcription factors, non-coding RNAs, epigenetic modifiers, and signaling pathways. In particular, transcription factors such as Snail, Slug, ZEB1, ZEB2, and Twist act as master regulators of EMT, leading to the repression of epithelial markers (e.g., E-cadherin) and activation of mesenchymal markers such as Vimentin [26, 27]. Even so, multiple signaling pathways converge to regulate the EMT process as for the TGF- β signaling which is one of the most potent inducers of EMT in HCC [27], as well as the dysregulated activation of the Wnt/ β -catenin pathway, frequently observed in HCC.

Similarly, the activation of Notch signaling induces EMT-like changes in HCC cells, further fueling cancer progression [28]. To date, numerous studies have demonstrated the clinical significance of EMT in HCC and the increased expression of several EMT-inducing transcription factors is closely associated with aggressive clinicopathological features, advanced tumor stage, and poor prognosis [29-31]. Hence, the identification of molecular markers and genetic signatures associated with EMT holds substantial promise in improving the categorization of patients and shaping the design for individualized therapeutic approaches in HCC.

3. Nomenclature and classification updating in the context of fatty liver disease.

In recent years, the understanding and characterization of fatty liver diseases have undergone significant evolution, leading to a refinement in their nomenclature and classification. One notable shift in terminology that has garnered attention within the medical community is the transition from Non-Alcoholic Fatty Liver Disease (NAFLD) to Metabolic Associated Fatty Liver Disease (MAFLD) and recently to Metabolic dysfunction-Associated Steatotic Liver Disease (MASLD) [32]. This change reflects a deeper comprehension of the multifaceted nature of the condition and its close association with metabolic dysfunction beyond mere fat accumulation in the liver, emphasizing the potential progression to more severe forms of liver damage, such as steatohepatitis and fibrosis. This further acknowledges the clinical spectrum of the disease, ranging from simple steatosis to non-alcoholic steatohepatitis (NASH), cirrhosis, and hepatocellular carcinoma [33].

Historically, NAFLD served as the prevailing term to describe hepatic steatosis in individuals without significant alcohol consumption. However, as research advanced, it became evident that NAFLD encompasses a spectrum of liver disorders with diverse pathophysiological mechanisms and clinical presentations [34]. Furthermore, the term "non-alcoholic" has been

criticized for its imprecise and potentially stigmatizing connotations, as it merely defines the condition by what it is not rather than by its underlying metabolic drivers [32]. In response to these limitations, the concept of MASLD was introduced to better encapsulate the metabolic underpinnings of the disease. Indeed, the designation "Metabolic Associated" underscores the strong association between fatty liver disease and metabolic dysregulation, including obesity, insulin resistance, dyslipidemia, and hypertension. By integrating metabolic factors into the nomenclature, MASLD aims to provide a more accurate and comprehensive description of the condition while facilitating early identification, risk stratification, and targeted interventions [35].

For consistency with the original name of this study which is part of larger project funded by the Italian Ministry of Health and for relevance with the poster presented at national and international congresses, during this dissertation will be adopted the old terminology, NAFLD, to refer to the pathological condition.

4. Impact of genetics in NAFLD

Alongside to metabolic factors, genetic and epigenetic variations are implicated in NAFLD pathogenesis, influencing disease susceptibility and phenotypic heterogeneity of liver disease. In support, Genome-wide association studies (GWAS) identified numerous candidate genes involved in lipid metabolism, inflammation, and fibrosis. Subsequently, the identification of genetic variants associated with NAFLD has provided crucial insights into the molecular mechanisms underpinning disease development and has opened up new avenues for personalized therapeutic interventions [31, 36].

Among the genetic variants identified as predictors of NAFLD progression the most extensively studied is the rs738409 C>G polymorphism in the patatin-like phospholipase domain-containing 3 (PNPLA3) gene [37]. The G allele of this variant has been consistently associated with increased hepatic lipid accumulation and inflammation, thereby predisposing individuals to NAFLD development. Therefore, the PNPLA3 variant has been clinically correlated to the progression from simple steatosis to more severe forms of the disease, including NASH and fibrosis, being considered the most robust genetic predictor of NAFLD severity [36, 38]. Another significant genetic modifier is the TM6SF2 (Transmembrane 6 superfamily member 2) gene, which affects lipid metabolism in hepatocytes. Several genetic variants in the TM6SF2 gene have been identified and associated with hepatic fat accumulation, elevated transaminases levels, NASH development, and fibrosis progression in NAFLD patients. These variants impact on lipid handling within hepatocytes, leading to alterations in very-low-density lipoprotein (VLDL) secretion and triglyceride levels, ultimately influencing NAFLD phenotypes [37]. Similarly, membrane-bound O-acyltransferase domain-containing 7 (MBOAT7) variants have been associated with changes in hepatic lipid composition and NAFLD development, underscoring the intricate interplay between lipid metabolism and disease pathogenesis. MBOAT7, is an important enzyme involved in the synthesis of triglycerides and phospholipids, thus mutations in its sequence drive to lipid accumulation in hepatocytes and development of fatty liver with subsequent liver damage [39, 40]. Moreover, genetic variations in the MBOAT7 gene have been directly linked to increased NAFLD risk and to increased susceptibility to lipotoxicity and inflammation in the liver, ultimately promoting NAFLD progression [40]. Others genetic variants found in key genes involved in glucose homeostasis play significant role in NAFLD pathogenesis as well [41]. For instance, the rs1260326 C>T variant in the glucokinase regulatory protein (GCKR) gene leads to impaired glucose homeostasis and dysregulated lipogenesis, fostering hepatic fat accumulation.

Altered glucose influx into hepatocytes due to GCKR variations leads to increased *de novo* lipogenesis (DNL) and finally contributes to NAFLD development [38]. Moreover, the coexistence of genetic variants in genes governing hepatic lipid handling, such as apolipoprotein B (APOB) and microsomal triglyceride transfer protein (MTTP), may promote VLDL retention, further aggravating hepatic lipid accumulation and disease severity [42]. Consistently, it has been found that the genetic signature in genes involved in the generation of lipid droplets (LDs) predispose to NAFLD onset. In this regard, genetic variants in genes like perilipin-2 (PLIN2) and perilipin-5 (PLIN5) impact LD formation, stability, and lipid storage, influencing cellular stress responses [43, 44]. In addition, mitochondrial dysfunctions have been closely linked to the progression from simple steatosis to NASH and variants in genes regulating mitochondrial oxidative flux, such as superoxide dismutase 2 (SOD2) and the uncoupling proteins (UCPs), contribute to oxidative stress and mitochondrial damage, amplifying hepatic injury [45, 46]. Interestingly, increasing evidence claims that the genetic variant, rs72613567 in the HSD17B13 gene confers protection against histological steatohepatitis, fibrosis, and cirrhosis [47].

The interaction between more genetic variants may affect more widely disease severity and progression [48]. For instance, the co-presence of PNPLA3 and GCKR variants exacerbate NAFLD, NASH, and HCC odds [49], while the HSD17B13 variant can mitigate the impact of the PNPLA3 variant on liver damage, but not hepatic fat accumulation [50]. However, even if increasing evidence are demonstrating that NAFLD development and progression is strongly affected by numerous single nucleotide polymorphisms (SNPs) in genes involved in lipid metabolism, insulin resistance, inflammation, oxidative stress, each individual SNP has a relatively small effect size on the NAFLD risk [38]. For these reasons, there is impelling need to assess genetic risk in a cumulative manner evaluating multiple genetic variants along with others NAFLD risk factors. In this regard, the Polygenic Risk Score (PRS) is a

statistical method that utilizes genome-wide association study (GWAS) data and other genetic information to assess an individual's genetic predisposition to develop NAFLD generating a predictive risk score for each patient [51]. The construction of a PRS involves the selection of relevant genetic variants associated with NAFLD from large-scale genetic databases and cohort studies. Each SNP is assigned a weight based on its effect size, which is determined by its association with the disease in previous studies. Using these weights, PRS is calculated for each individual, based on the genotype information for the selected SNPs. The resulting PRS represents an individual's genetic predisposition to NAFLD, with higher scores indicating a greater risk [52].

In recent times, particular emphasis was given to genetic variants in the β -Klotho (KLB) gene and their association with NAFLD severity. As proved, these genetic variants can alter KLB's function, impacting its ability to mediate Fibroblast Growth Factors (FGFs) signaling effectively [53, 54]. Specifically, a variant known as rs17618244 (p.R728Q KLB) has been a focal point of investigation given that, individuals carrying the minor allele A, exhibit an increased predisposition to NAFLD. This association resulted in more severe liver damage, including increased inflammation, ballooning, and NASH, in pediatric and adult populations. Moreover, this genetic variation has been linked to advanced fibrosis, especially in the presence of obesity, highlighting the interaction between genetic and environmental factors in NAFLD pathogenesis [55, 56]. In summary, even if the interplay between genetic factors and environmental cues, such as diet and lifestyle, further complicates the disease's complexity, understanding how they contribute to NAFLD pathogenesis and progression is crucial for identifying high-risk individuals and for developing targeted therapies aimed to improve patient outcomes. Genetic profiling, indeed, could facilitate risk stratification, early diagnosis, and the identification patients eligible for targeted interventions.

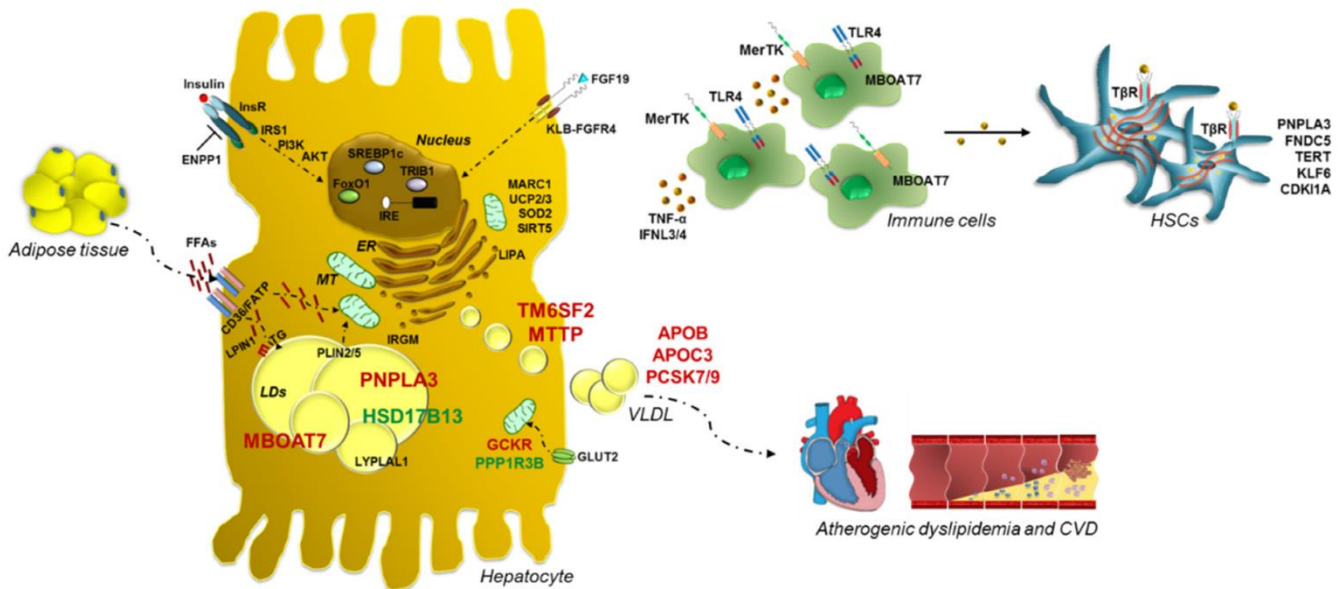


Figure B: Genetic influence on NAFLD development and progression to severe liver damage. Visual representation of key inherited variations impacting the advancement of NAFLD. Specifically, within hepatocytes, PNPLA3, situated on the surface of lipid droplets, facilitates the breakdown of triglycerides (TG). The p.148M variant results in increased hepatic TG accumulation due to the build-up of mutant proteins, hindering TG metabolism. TM6SF2 participates in very-low-density lipoprotein (VLDL) formation within the endoplasmic reticulum (ER) and its release, while MBOAT7 transfers arachidonoyl-CoA to Lyso-PI, ensuring membrane fluidity. Variations in these genes decrease VLDL secretion and membrane flexibility, respectively. Conversely, genetic variants in *HSD17B13* may protect against NAFLD. Inherited variations, including those in *ApoB*, *PLIN* genes, and *MTTP*, could also impact glucose and insulin signaling, free fatty acid uptake, fat accumulation, and VLDL clearance, contributing to fatty liver. Recently, common single nucleotide polymorphisms (SNPs) in genes influencing mitochondrial function, such as *SOD2*, the *UCPs*, and *SIRT5*, have been suggested as significant contributors to the transition from fat accumulation to NASH and fibrosis. Additionally, variants in genes regulating the inflammatory response and the activation of hepatic stellate cells may accelerate the progression from fatty liver to more severe conditions. From *Meroni et. al; Biomedicines, 2021 [57]*.

5. KLB: protein structure, activity, transcriptional regulation, protein localization and post-translational shedding

KLB gene is located in chromosome 14,4p and consists of 5 exons encoding for a type I transmembrane protein that weighs approximately 130-kDa and counts 1014 amino acids [58]. The amino acid sequence of KLB was found to be 41.2% homologue to that of α -Klotho (KI) resulting in similar domain and structure organization [59]. Nevertheless, KLB was primarily detected in the liver and in the adipose tissue where acts as a membrane coreceptor [60], whereas KI is mainly present in the kidney [61] where operates as multifunctional protein. KI is implicated in anti-aging processes, in the regulation of FGF23 activity and in ion homeostasis [62] while KLB is assembled in a heterodimer complex with fibroblast growth factor receptor 1c (FGFR1c) or with FGFR4 to serve as obligate coreceptor for the internalization of endocrine FGF21 and FGF19, respectively [63]. The structure of β -Klotho protein contains a signal sequence at the N-terminus, a single transmembrane domain and a short cytoplasmic domain. An extracellular portion is also reported and consists of two internal repeats (KL1 and KL2) with high homology to family 1 glycosidases but with poor enzymatic activity [64]. Soluble forms of KLB have been detected in humans and other mammals and exert their biological effects on distant organs or tissues. These forms derive from the shedding of the extracellular domain or the alternative splicing of the protein [65]. The shedding of KLB soluble portion is possibly mediated by the metalloproteinases ADAM10 and ADAM17, firstly studied on KI and supposed to acts similarly on KLB, as well. These proteins could generate the cleavage of sKLB next to the transmembrane domain (α -cut) or between the KL1 and KL2 subunits (β -cut) resulting in soluble full-length Klotho or KL1 and KL2 fragments [66]. A recent study used X-ray crystallography to determine the structure of β -Klotho soluble portion [67], highlighting the strong association with the human cytosolic β -glucosidase, enzyme involved the hydrolysis of disaccharides and oligosaccharides. Two tandem glycoside hydrolase-like domains,

named D1 and D2, characterize sKLB domain and are connected with an unstructured and flexible linker, similar to the one found in the active sites of glycoside hydrolase family-1 (GH1) enzymes. Despite this homology, two key glutamates conserved in GH1 enzymes for their crucial role in the catalytic activity are substituted in sKLB structure and are correlated to the loss of the enzymatic function. These peculiarities identify Klotho proteins as new and distinct protein family (KL family) in the context of the glycosidase family 1 superfamily [67]. Interestingly, a short amino acids helix leads to the occlusion of the corresponding pocket to the GH1-substrate-binding region on KLB and constitute part of the FGF21-binding site. FGF21 was found to bind KLB in a cooperative manner in two distinct binding sites located in the regions D1 and D2 of the peptide, respectively. The mode of interaction between KLB and FGF21 resembles the mechanism used for the oligosaccharide substrates recognition in GH enzymes. Indeed, a common sugar-mimicking Ser-Pro-Ser motif found in glycoside hydrolases is shared with FGF21 and is also contained at the C-terminus of FGF19. This may explain the evolution of the glycoside hydrolase active site to become a specific receptor for endocrine FGFs. Another study performed hydrogen deuterium exchange (HDX) coupled to mass spectrometry (MS) followed by site-directed mutagenesis to propose a cooperative action of two distinguished ligand-binding sites in KL1 and in KL2, and two corresponding co-receptor binding sites on the C-terminal domain of FGF19 and FGF21 [68]. As reported, the optimized FGF-KLB complex formation requires the concomitant occupancy of both the receptor binding sites and a single amino acid substitution in either region was sufficient to abolish β -Klotho binding impairing FGF21 functional activities. In this regard, *in vitro/in vivo* experiments testing the removal of the distal binding region by truncation or proteolytic cleavage resulted in the complete inactivation of FGF21 signal [69]. Despite the lack of studies directly finalized on the binding of FGF19 to KLB, the strong similarities between FGF21 and FGF19 and the specificity of these two hormones towards β -Klotho suggest the presence of common co-receptor binding elements. You Shi et Al.

further supported this hypothesis demonstrating that the two segments on the C-terminal domain of FGF19 interact with the same two regions of KLB engaged by FGF21 in highly conserved spot, partially explaining the interchangeable effects of FGF19 and FGF21 on glucose and lipid homeostasis [68].

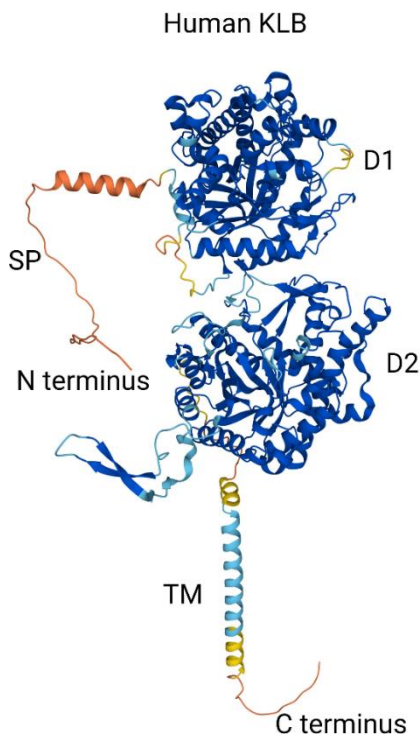


Figure C: In silico predictions of the human KLB protein structures. Total peptide was represented and D1 and D2 catalytic regions were highlighted. N and C terminal domains were represented. Colors reflect model confidence (dark blue: very high (pLDDT >90); light blue: confident (90 < pLDDT > 70); yellow: low (70 > pLDDT > 50); orange: very low (pLDDT < 50). D1: domain 1 (residues 53-507); D2: domain 2 (residues 521-968); SP: signal peptide; TM: transmembrane region. From Aaldijk et. al, *Front. Endocrinol.*, 2023 [1]

6. KLB-mediated intracellular signaling in the liver

The signaling cascade initiated in the liver by the binding of FGF19 with FGFR4/KLB receptor complex exerts profound effects on the regulation of different metabolic processes and on the bile acids (BAs) production. Specifically, FGF19, which is released from the small intestine, binding to FGFR4/KLB leads to the autophosphorylation of FGFR4 tyrosine kinases, acting as docking sites for various adaptor proteins, with FGFR substrate 2 (FRS2) taking center a stage. FRS2 facilitates the activation of Ras, a small GTPase protein.

Activated Ras initiates a cascade of phosphorylation events, ultimately culminating in the activation of Mitogen-Activated Protein Kinases (MAPKs), particularly the extracellular signal-regulated kinases 1 and 2 (ERK1/2) [70, 71]. Once activated, ERKs translocate to the nucleus, where exerts influence on the expression of several downstream effectors, thereby impacting on cellular functions ranging from cellular proliferation to differentiation. Activated FRS2 acts as an intermediary, also promoting the activation of p38 MAPK through its phosphorylation. Thus, p-p38 MAPK, translocates to the nucleus influencing the expression of several transcription factors and regulating a variety of cellular responses, including inflammation, stress response and cell differentiation [72]. Simultaneously, the FGF19/KLB/FGFR4 complex triggers the PI3K/AKT pathway. Specifically, after FGFR4 activation, FRS2 recruits the p85 regulatory subunit of phosphoinositide 3-kinase (PI3K). Activated PI3K generates phosphatidylinositol (3,4,5)-trisphosphate (PIP3), a secondary messenger that orchestrates the phosphorylation and activation of protein kinase B (AKT) [70]. AKT, in turn, sets off a cascade of phosphorylation events, affecting downstream targets that influence critical cellular processes, including glucose metabolism regulation, lipid synthesis modulation and cell survival, collectively contributing to metabolic homeostasis [73]. It has also been observed that, KLB can modulate the secretion and availability of Wnt ligands, influencing their binding to cell surface receptors thus initiating downstream signaling events, such as the Wnt/ β -catenin pathway. For these reasons the interplay between KLB and the Wnt/ β -catenin pathway is critical for maintaining liver homeostasis, control differentiation and to prevent carcinogenesis [71]. Moreover, FGF19 binding to KLB/FGFR4 in the liver modulates BAs synthesis by feedback inhibition. Specifically, BAs which are produced in the liver from cholesterol and stored in the gallbladder until needed are regulated by two signaling pathway [74]. Therefore, BAs exert negative feedback on their production through the binding to the nuclear receptor farnesoid X receptor (FXR), which stimulates the expression of SH2 Domain-Containing Protein

Tyrosine Phosphatase (SHP). SHP, in turn, binds to the nuclear factor Hepatic Nuclear Factor α (HNF- α), blocking its role as a transcriptional activator of the Cholesterol 7 Hydroxylase (CYP7A1) gene, which is essential in the biosynthetic pathway of BAs [75, 76]. In addition, the regulation of CYP7A1 have multiple mechanisms and also depends on FGF19, which binding to the KLB/FGFR4 complex activates in the liver the MAP kinase cascade able to inhibit the expression of *CYP7A1* [77]. Additionally, FGF19 acts on the gallbladder, inducing its relaxation and thus leading to BA accumulation. Importantly, in the liver, FGF19 modulates the expression of the enzymes Acetyl-CoA Carboxylase (ACC) and SREBP1, thereby affecting the carbohydrate and lipid metabolism. Specifically, FGF19 reduces insulin's ability to stimulate fatty acid synthesis and in the meantime stimulates glycogen synthesis by inhibiting gluconeogenesis through the downregulation of the transcription factor Peroxisome Proliferator-Activated Receptor-Gamma Coactivator 1 (PGC1- α) [74].

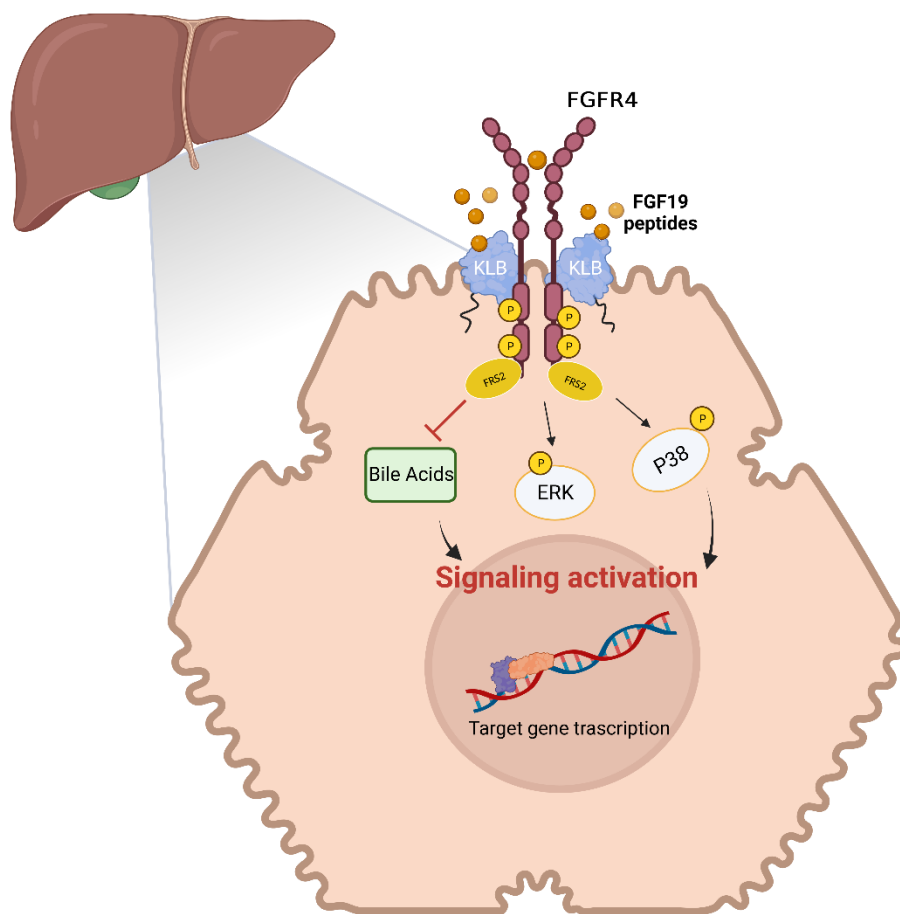


Figure D: KLB/FGFR4/FGF19 signaling pathways in the liver. FGF19, FGFR4, and KLB compose a complex, activated by FGF19 binding. Upon this event, a cascade of pathways is stimulated including RAS/RAF/MAPK and the inhibition of BAs production. FGF19-FGFR4-KLB signal is involved in proliferation, angiogenesis, anti-apoptosis, EMT, invasion.

7. KLB role in NAFLD pathogenesis: clinical and preclinical evidence

Increasing lines of evidence are highlighting the involvement of FGF19/KLB/FGFR4 signaling perturbations in various metabolic disorders [78]. In type 2 diabetes mellitus (T2DM), impaired FGF19 activity was associated with insulin resistance and disturbances in glucose metabolism [79]. In a pioneering study, Alisi and colleagues investigated the association between serum FGF19 levels, KLB, and the severity of liver damage in a cohort of 84 obese pediatric patients with biopsy proved NAFLD, alongside 23 control subjects [80]. Their findings revealed an inverse correlation between serum FGF19 levels and hepatic KLB expression with the presence of non-alcoholic steatohepatitis (NASH), suggesting for the first time the potential role of the FGF19-KLB axis on NAFLD pathogenesis. Subsequently, it was determined that disruption of the KLB/FGFR4 complex resulted in decreased FGF19 levels [81]. In these conditions, the accumulation of lipids in the liver and propagation of the inflammatory responses was promoted, probably due to the inability of FGF19 to explicate its biological functions [82]. To date, four polymorphisms in the KLB gene have been evaluated for their impact on the FGF19/FGF21 signal transduction and consequently, for the influence on the NAFLD spectrum. In 2011, Wong *et al.* reported a novel genetic variant, rs17618244 G>A, within the KLB gene (resulting in the p.R728Q KLB variant). This genetic variation was found to potentially affect the colonic transit in irritable bowel syndrome with diarrhea (IBS-D) impairing protein stability and regulating bile acid production [53]. Building upon these insights, Dongiovanni and Crudele *et al.* in 2020 translated these findings to the clinical context of NAFLD, revealing that pediatric individuals carrying the minor A allele of rs17618244 variant exhibited an increased frequency of NAFLD. Interestingly, the rs17618244 variant was further associated with heightened lobular inflammation, ballooning, and NASH in a cohort of 249 overweight pediatric NAFLD patients compared to 128 healthy age-matched controls, with more pronounced effect in those carrying the minor allele. In the

same study, the downregulation of hepatic and circulating KLB expression was observed in carriers of the minor allele and associated with the rs17618244 gene variation and with disease worsening [55]. Subsequently, in 2021, Panera and Meroni *et al.* confirmed what observed in the pediatric population in a study involving 1111 adult patients with biopsy-proven NAFLD. Here, it was demonstrated that the rs17618244 KLB genetic variation might serve as a novel modifier influencing the susceptibility to advanced NAFLD, primarily by affecting the hepatic signaling of FGF19/KLB. Moreover, differently from children, who exhibited less severe hepatic injury, adult patients carrying the rs17618244 variant showed higher degree of fibrosis, especially in the presence of obesity, posing that the effect size of this variant might be amplified by increased adiposity. Transcriptome analysis on the hepatic tissue of 125 obese individuals confirmed the downregulation of *KLB* expression also in adult subjects carrying the A allele. Accordingly, circulating levels of both KLB and FGF19 were found decreased also in this cohort of patients and associated with the genomic variation [56]. KLB downregulation was further correlated with the expression of genes involved in the fibrogenic processes such as TGF- β , COL1A1, and COL3A, suggesting that KLB expression may prevent to liver fibrosis. Accordingly, the absence of KLB in mice appears to disrupt the normal metabolism of lipids and carbohydrates, which are pivotal factors in NAFLD development [1]. Indeed, *Klb*^{-/-} mice had impaired lipid homeostasis, characterized by reduced plasma triglyceride levels and a tendency toward lower plasma cholesterol. Notably, these effects were reversed when KLB was specifically restored in hepatocytes. Additionally, KLB-deficient mice exhibit altered carbohydrate metabolism, as indicated by decreased hepatic glycogen levels and increased hepatic glucokinase expression. These changes are particularly relevant to glycolysis, implicating a role of KLB in glucose turnover. Noteworthy, *Klb*-deficient mice exhibit altered BA homeostasis characterized by increased *Cyp7a1* expression, which resulted in a more elevated synthesis and excretion of bile acids. Significantly, *Klb*^{-/-} mice showed also an altered BA composition,

unveiling a possible wider role of Klb on BA homeostasis. Consequently, Klb-deficient mice develop a pathological phenotype resembling NAFLD, characterized heightened expression of pro-inflammatory cytokines and macrophage markers, and elevated plasma levels of alanine aminotransferase (ALT) and aspartate aminotransferase (AST). Relevantly, the impact of Klb absence in mice extends to fibrosis, resulting in increased expression of genes related to fibrogenesis, indicating that KLB may play a role in the development of liver fibrosis also in *in vivo* models [83]. In conformity with the previous studies, in *in vitro* the transient downregulation of KLB gene led to increased intracellular lipid accumulation and caused the upregulation of *p62*, *ACOX1*, *ACSL1*, *IL-1 β* and *TNF- α* mRNA levels in HepG2 and in Huh7 cells [55]. Moreover, LX-2 cells transfected with KLB mutated form reported the downregulation of KLB protein and a concomitant increase of protein degradation. *KLB* silencing in LX2 cells was further associated with enhanced proliferation rate and enhanced expression of pro-fibrogenic genes such as α SMA and COL1A1, suggesting that KLB expression prevents the shift towards a myofibroblast-like phenotype [56].

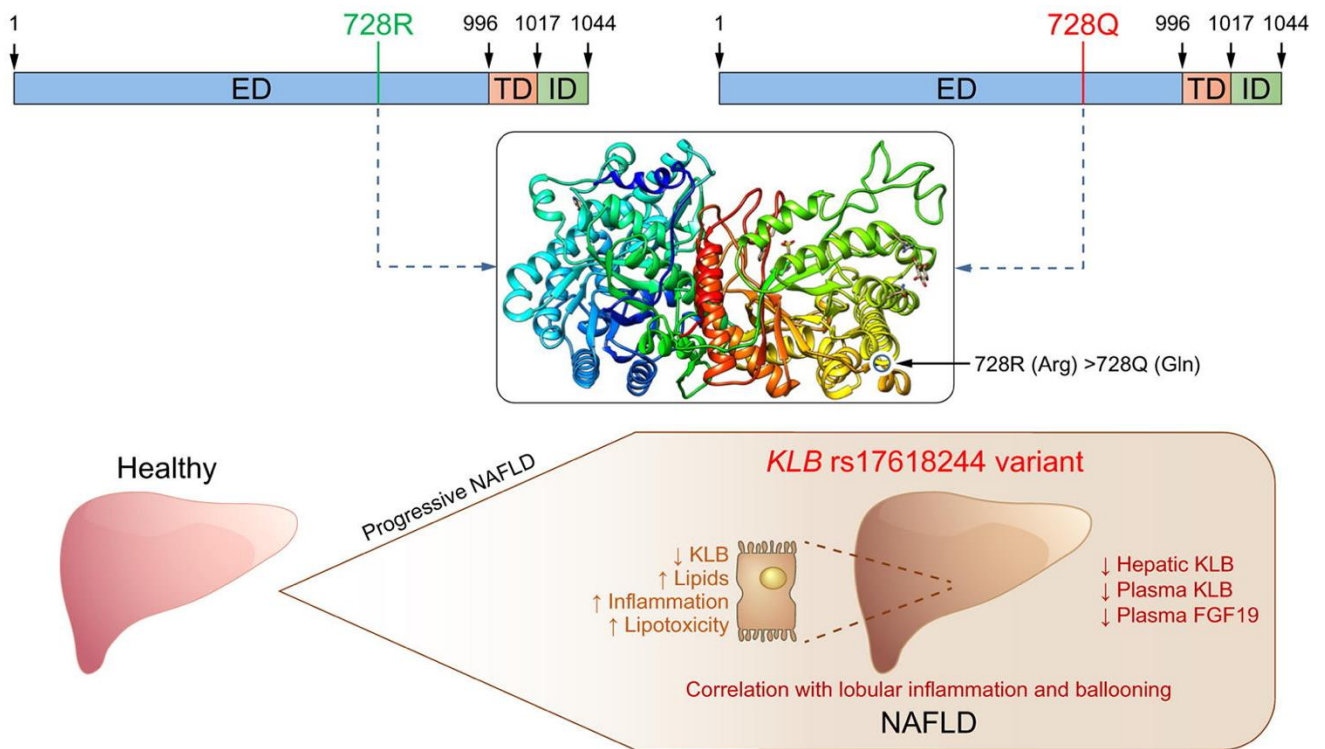


Figure E: Impact of the KLB rs17618244 variant on NAFLD traits and on liver homeostasis in adult and pediatric patients with NAFLD. From *Dongiovanni and Crudele et. al, J Hepatol., 2020 [55]*

8. Clinical Management of NAFLD and relevancy of KLB as novel therapeutical target

At present, the primary approaches to manage with NAFLD/NASH involve non-pharmacological methods aimed at reducing fatty liver through weight loss, exercise, and controlled diets. However, there is no approved pharmacological treatment for NAFLD, yet [84]. Some experimental therapies involve insulin-sensitizing agents like pioglitazone and anti-oxidative compounds such as vitamin E, which have shown some improvements in steatosis, inflammation, and fibrosis. However, their effects are not well-established, and safety concerns have limited the clinical use of pioglitazone, leaving a large medical gap. While numerous drug candidates are currently undergoing clinical trials for NASH, several of these candidates have encountered setbacks during Phase 3 trials. These challenges include the failure in meeting the endpoints that would have a significant impact on NASH resolution or the reduction of fibrosis [81]. On the other hand, patients treated with Obeticholic acid (OCA) reported a modest reduction in fibrosis but hasn't received FDA accelerated approval due to concerns about its overall efficacy compared to potential risks [85]. To date, it is widely accepted that removing the insults like steatosis and inflammation has a positive effect on fibrosis and in worst cases, the bariatric surgery has been shown to be the unique strategy to resolve fibrosis over time [86].

In this scenario, developing targeted and non-invasive therapeutic strategies to counteract the progression of steatosis and the onset of other NAFLD traits before severe liver damage occurs has become a crucial point. Pharmacological targeting of the FGFR-KLB system has shown significant improvements in animal models with obesity, type 2 diabetes (T2D) and NAFLD leading to strong beneficial effects on NASH parameters [87]. This has led to the development of various FGF19- and FGF21-mimetics and of FGFR1c/KLB-targeting antibodies, recognizing KLB as a potential druggable target [1, 81]. Specifically for liver

disease, FGF19 has been proposed as a diagnostic biomarker in NASH, inversely associated to steatosis. Therefore, the hepatic response to FGF19 seemed to be impaired in patients with NAFLD and the lack or the decreased activity of FGF19 may contribute to worsening of NASH, due to accumulation of toxic bile acids catabolites and dysregulation of the intracellular signaling [78, 88]. To this end, the pharmacological administration of FGF19 has shown promising results in improving metabolic disorders such as T2D and NAFLD [89]. However, this approach doesn't seem to be a resolution due to the difficulties in separating the mitogenic signaling, which can lead to cancer, from the metabolic action of FGF19.

Efforts to develop effective pharmacological treatments for NAFLD have sparked increasing interest in targeting the FGF19 pathway, particularly via the KLB/FGFR4 axis. Considering that dysregulation of this axis has been implicated in the pathogenesis of liver disease, clinical trials aimed to modulate FGFR4 activity, either by activating or inhibiting the receptor, to ameliorate liver steatosis, inflammation, and fibrosis have been approved. In line with this, the therapeutic potential of a non-mitogenic engineered analog of FGF19, NGM282 (Aldafermin), designed to activate the FGFR4-KLB receptor, has been investigated in preclinical and clinical studies of liver fibrosis and NASH. This compound has shown metabolic improvements in animal models of NASH, along with enhancements in insulin sensitivity and bile acid-induced toxicity, alongside reductions in hepatic inflammation and fibrosis [90]. A recent placebo-controlled phase 2b clinical study administering NGM282 to 160 patients with compensated NASH-cirrhosis demonstrated promising initial results and after twelve weeks of NGM282 treatment diminished liver fat content (-67-74% in 3 mg groups), improving liver damage markers and histological features of NASH (-1.9 NAS score in 3 mg group) in NASH patients [91]. A second phase 2 clinical trial was then conducted to investigate the efficacy and safety of more prolonged treatment (i.e., 24 weeks) with NGM282 in biopsy-proven NASH patients. Here was demonstrated that NGM282 treatment

decreased plasma C4 levels, liver damage markers ALT and AST, and liver fibrosis biomarker Pro-C3. Histological outcome measures were also improved in NGM282-treated patients with improvements in fibrosis and NAFLD activity score (NAS)(62%), and NASH resolution [92]. However, one safety concern with NGM282 treatment is the increase in plasma low-density lipoprotein (LDL) cholesterol and acute diarrheal events [93].

In another promising clinical trial a recombinant form of FGF21, AKR-001 (Efruxifermin, Akero Therapeutics), has been used to increase the binding affinity with KLB [94]. In this phase 1 clinical trial (NCT01856881) patients with T2D, the four weeks treatment with AKR-001 resulted in reduced atherogenic lipid profile and improved insulin sensitivity with reduced plasma glucose, insulin, and HOMA-IR. Afterwards, in NCT03976401 phase 2a clinical trial NASH patients underwent 16-week of AKR-001 treatment reporting a reduction of the hepatic fat fraction (10.3% - 14.1%), NASH resolution without worsening of fibrosis, and reduction in enhanced liver fibrosis (ELF) scores. Currently, AKR-001 is in phase 2b clinical trials for treating NASH in non-cirrhotic and compensated cirrhotic patients (NCT04767529 and NCT05039450). Furthermore, a recent phase 1b/2a clinical trial based on pegozafermin treatment, a glycoPEGylated FGF21 analog, demonstrated favorable effects on histological and metabolic parameters in individuals with NASH after 20 weeks of treatment. The outcomes included the amelioration of ballooning or lobular inflammation and of serum markers of fibrosis and hepatic damage [95].

Despite the protective effects demonstrated by recombinant FGF19 and FGF21, their clinical utility is limited by factors such as rapid plasma clearance and proteolytic inactivation for FGF21 and potential tumorigenic activity for FGF19. Therefore, deeper investigations into KLB-based drugs are warranted through preclinical and clinical studies and is gaining increasing interest [81, 96].

Against this backdrop, the modulation of KLB expression via the FGF-receptor/KLB axis may impact liver disease progression in a favorable way. A phase 1b study assessing the safety, tolerability, pharmacokinetics, immunogenicity, and pharmacodynamics of BFKB8488A, a bispecific antibody targeting FGFR1c and KLB, was set in patients with T2DM or NAFLD, (NCT04171765 GC41033) [97]. These patients reported improvements in serum lipid levels, hepatic steatosis, and markers associated with liver injury and fibrosis. Notably, a phase 2 clinical trial is underway to evaluate the efficacy and safety of BFKB8488A in individuals with NASH.

Similarly, MK-3655 (NGM313), a humanized monoclonal antibody against the FGFR-1c/KLB complex, demonstrated significant effects on hepatic steatosis, circulating levels of hepatic enzymes, triglycerides, and LDL in obese non-diabetic patients in a phase 1 trial (NCT03298464). A subsequent phase 2b study is currently ongoing in pre-cirrhotic NASH patients (NCT04583423)..

Thus far, clinical trials have generated disappointing results, making it unlikely that FGF19/FGF21 mimetics will serve as a stand-alone treatment for T2D and NAFLD. Nonetheless, even short-term treatment with FGF19 mimetics or FGFR1c/KLB-targeting antibodies results in remarkable reductions of liver fat content and markers of liver damage and fibrosis. For these reasons, KLB-targeting drugs are particularly interesting as a therapeutic strategy for patients with NAFLD.

RATIONALE OF THE STUDY

Nonalcoholic fatty liver disease (NAFLD) is currently the most frequent liver disorder worldwide, with a dramatic increasing trend in the next decade. A recent meta-analysis highlights that the overall global prevalence is approximately 36%-38% with variation by geographical region [98]. Frequency distribution differences may be related to genetic, epigenetic, environmental, or socio-cultural factors, which, in turn may influence inherited susceptibility, fat compartmentalization, and co-occurrence of co-morbidities, including type two diabetes and metabolic syndrome. However, several lines of evidence demonstrated that genetic background is not only an entity that may influence the prevalence of NAFLD, but also a key risk factor associated to disease onset and progression[99].

During the past decade, several genetic loci and SNPs involved in NAFLD susceptibility have been identified by case-control and genome-wide association studies. Panera et al and Dongiovanni et al. previously demonstrated that the rs17618244 KLB variant, G>A (MAF:A=0.181982/10924), increased the risk of developing ballooning and lobular inflammation and was associated with more severe liver damage in pediatric patients with NAFLD [55, 56]. In these studies, the Authors demonstrated that the rs17618244 KLB variant increased the risk of developing ballooning lobular inflammation and was associated with more severe liver damage in a cohort of pediatric patients with NAFLD [55]. Interestingly, a significant reduction in KLB plasma levels was further observed in this cohort of patients compared to healthy individuals, independently of their genetic background, suggesting that KLB may act in also in a soluble form. Moreover, stratifying patients according to the presence of the minor at-risk A allele, the Authors demonstrated that the rs17618244 variant caused a stronger reduction of circulating FGF19/KLB levels in patients carrying the GA/AA genotype compared to non-carriers, reflecting the parallel decrease of KLB hepatic expression in NAFLD subjects carrying the variant. According to this notion,

HepG2 and Huh7 hepatoma cell lines exposed to a lipid overload, a condition resembling NAFLD, displayed a severe reduction of intracellular and secreted KLB protein confirming what observed in patients. In addition, *KLB* transiently silenced hepatocytes upregulated markers of oxidative stress and inflammation such as *p62*, *ACOX1*, *ACSL1*, *IL-1 β* and *TNF- α* , suggesting a protective role of KLB protein against lipotoxicity and inflammation in hepatocytes. Afterwards, in the sequel published study, the impact of the KLB rs17618244 variant on histological liver damage was investigated in larger cohort of adult patients with biopsied-proven NAFLD (n=1111) [56]. Here, KLB rs17618244 variant was further correlated with development of hepatic fibrosis. After stratifying patients according to the presence of obesity (body mass index (BMI)>35), it was reported that the minor A allele was more associated with fibrosis, with lobular inflammation and cirrhosis in this patient's subset. Finally, new insights on KLB protein structure and its intracellular activity have been provided through the study of the prediction model. Indeed, it was proved that the Arg728Gln substitution, associated to the rs17618244 variant, could impact on the stability of KLB protein, possibly explaining the reduced KLB expression observed in carriers of the variant. Similarly, to the KLB rs17618244 variant, other two variants in KLB gene, namely the rs7674434 and the rs12152703, have been previously associated with an increase in alanine aminotransferase (ALT) levels, index of hepatic inflammation and liver injury, in a Chinese cohort of NAFLD patients [54]. However, the impact of these variants on the histological spectrum of NAFLD has not been investigated yet.

AIMS OF THE STUDY

Therefore, the aim of this study is to reproduce in *in vitro* the effects of the loss of function of KLB rs17618244 variant observed in NAFLD patients, by exploiting HepG2 cells silenced for *KLB* through the CRISPR/Cas9 technology. In order to clarify the impacts of KLB on the NAFLD spectrum, we will determine in our model the effects of KLB depletion on hepatocyte homeostasis. With this goal, we will investigate typical NAFLD traits and several markers of NAFLD progression, such as perturbations in the lipid and glucose metabolism, the activation of ER and oxidative stress, impairment in the apoptosis and the autophagy processes and the activation of necro-inflammation (**AIM1**). Moreover, we evaluated the frequency distribution of the KLB rs12152703 variant, G>T (MAF: T=0.256701/8639), firstly been characterized in a Chinese cohort [54], in both pediatric and adult patients with NAFLD. Thus, we will assess the correlation with typical histological and molecular NAFLD traits in the overall patient's cohort and we will determine the impact of this variant on soluble and hepatic form of KLB in a subset of pediatric patients (**AIM2**).

METHODS

Patients' cohort:

The retrospective cohort of 1050 adult patients with NAFLD consists of Italian subjects enrolled consecutively at the Metabolic Liver Diseases outpatient clinic at the IRCCS Cà Granda Foundation between January 1999 and December 2021. Inclusion criteria for this study are the presence of liver biopsy performed for suspected NASH or severe obesity. We excluded from the study other causes of liver disease including alcohol abuse, autoimmune or viral hepatitis, hereditary hemochromatosis, or genetic alpha-1 antitrypsin deficiency. The retrospective cohort of Italian pediatric patients (n=261) with confirmed NAFLD by biopsy was evaluated at the Bambino Gesù Pediatric Hospital (OPBG) between September 2015 and May 2021, after excluding other causes of liver disease including alcohol abuse, autoimmune or viral hepatitis, hereditary hemochromatosis, or genetic alpha-1 antitrypsin deficiency. The 128 pediatric control children without liver disease were obtained from the population participating in special liver disease screening programs conducted by OPBG every year.

Anthropometric and Biochemical Data:

Since these are retrospective cohorts, the anthropometric and biochemical data of the patients were retrieved from a pseudonymized database with respective codes associated with samples preserved for genetic analysis, transferred into an excel file for each cohort and analyzed individually or in aggregate.

Histological Assessment of Liver Damage and NAFLD scores:

Since these are retrospective cohorts, histological data of the patients were retrieved from a pseudonymized database with respective codes associated with samples preserved for genetic analysis and transferred into a file for each cohort and analyzed individually or in

aggregate. Liver biopsies were classified according to the scoring system recommended by the Clinical Research Network [100].

Genotyping:

Controls and cohorts of patients (pediatric and adult) with NAFLD were genotyped for the rs12152703 variant of the KLB gene using Taqman 5'-nuclease probes and the QuantStudio 3 platform (Thermo Fisher, Waltham, MA, USA). The obtained results were used to calculate the allelic frequency of this mutation, which was compared with the allelic frequency found in the control cohort, consisting of healthy individuals of European origin participating in the 1000 Genomes Project and with the children control cohort, respectively.

Measurement of circulating levels and the hepatic tissue expression of the KLB protein:

Circulating KLB levels were measured in a subgroup of 137 pediatric patients belonging to the genetically characterized cohort who had a sufficient biological sample for analysis. A commercial ELISA kit (LS-F11894 - LifeSpan BioSciences, Seattle, WA, USA) was used for the measurement of circulating KLB levels. Protein expression of KLB was assessed in liver tissue from a subgroup of 80 pediatric children from the pediatric cohort, with and without NASH, stratified for KLB rs12152703 genotype, using the quantitative analysis of immunofluorescent assays. Immunofluorescence was performed on 2 µm thick sections obtained from formalin-fixed, paraffin-embedded tissue. Sections were incubated overnight at 4 °C with primary anti-KLB antibody (dilution 1:300, Abcam, Cambridge, MA, USA) and detected with fluorophore-conjugated secondary antibody (Alexa Fluor 488 dilution 1:500, Applied Biosystems). Nuclei were counterstained with 4',6-diamidino-2-phenylindole (DAPI) for 5 minutes, and sections were mounted with PBS/glycerol (1:1) using a coverslip. Image acquisition was performed using a confocal microscope Olympus Fluoview FV1000

equipped with FV10-ASW software version 4.1, using a 40x objective. Quantitative image analysis was conducted as previously described [80].

In *in vitro* experiments:

Generation of KLB Knockout model in HepG2 cells through CRISPR/Cas9 technology

Cas9 inducible HepG2 cell line: lentiviral infection and selection with puromycin:

The KLB full-knockout (KO) model was generated by the Laboratory of Hepatic and Metabolic Diseases at the Fondazione IRCCS Ca' Granda Ospedale Policlinico of Milan by using CRISPR/Cas9 technology. To achieve a complete knockout, sgRNAs were designed to target the exon 2 of the KLB gene, aiming to disrupt the gene's function or prevent its synthesis through Cas9-induced double-strand breaks (DSBs) and subsequent non-homologous end joining (NHEJ) repair with insertions/deletions at the gene's origin. The sgRNA used in this study reported a 70% targeting efficiency to the prediction tool, with no predicted off-targets. To obtain the model, a stable cell line containing Cas9 under the control of doxycycline-inducible promoter and puromycin resistance as selection marker was generated as previously described [101].

Exon2 KLB

GCTCACTCGAAAGTTTGGCATAACTACAACACACATTTCCGCCACATCAGAAGGGTTGGTT
ATC

GATCACGTTGGGATCTCATTGGATCGAGCCAAACCGGTTCGGAAAACA[CGATTGGATATATT
CA

gRNA: **AAACCGGTTCGGAAAACACGA** **TGG**

5' CCGG - AAACCGGTTCGGAAAACACGA 3' guida exon 2 FW TOP

5' AAAC - TCGTGTTCCTCCGACCGGTTT 3' guida exon 2 RV BOTTOM

Cell culture and Treatments

The HepG2 Cas9 and the HepG2 KLB $-/-$ cell were cultured in DMEM High Glucose supplemented with 10% FBS, 100 U/mL penicillin, 100 μ g/mL streptomycin, and 1% L-glutamine (complete growth medium) and incubated at 37 °C under 5% CO₂ atmosphere. All cell lines were used for no more than 20 passages after thawing, as the increase in the number of passages may affect cell phenotype and alter experimental results. Quiescence medium: DMEM, 0.5% BSA, 100 U/mL penicillin, 100 μ g/mL streptomycin was added overnight before isolating cell pellet for protein and RNA extraction or performing biochemical kits. Starvation medium: DMEM, 1% FBS, 100 U/mL penicillin, 100 μ g/mL streptomycin was added overnight before cell proliferation and cell cycle experiments. A mixture of palmitic and oleic acids (PAOA) at the final concentration of 0.25 mM (ratio 1:2, Sigma-Aldrich) was added to the quiescent medium and incubated for 24 hours to perform lipid load challenge experiments. Sorafenib (Santa Cruz Biotechnology, Dallas, TX) was added to the complete growth medium to the final concentration 5 μ mol/L plus dimethyl sulfoxide DMSO (0.6%) and incubated for 24,48,72,120 hours, respectively to perform MTS assay. Treatments were freshly prepared and administered daily. The FGF19 hormone (R&D Systems, CAT 969-FG-025/CF) was added at the final concentrations of 100 μ g/ml to starvation medium and incubated for 15', 30' and 2h, then cell pellet was isolated. Treatments with Chloroquine and with Rapamycin were performed on cell seeded in 6 well plate at 70% of cell confluence. Chloroquine was added to the complete growth medium at the final concentration of 20 μ M and incubated for 2h, then cell pellets were isolated. Rapamycin cell stock 100mM was resuspended in DMSO and was added to the complete growth medium at the final concentration of 100nM and incubated for 30', 2h, 3h and 24h, then cell pellets were isolated.

Protein extraction, quantification, and Western Blot

Protein expression analysis and subsequent quantification were performed on cellular pellets obtained from the HepG2 Cas9 and HepG2 KLB $-/-$ cell lines. Extraction was carried out using RIPA buffer (10 mM Hepes, 1 mM EDTA, 60 mM KCL, 2% Nonidet P40) containing phosphatase and protease inhibitors. The extracted proteins were quantified using the Pierce BCA Protein Assay kit (660 nm, ThermoFisher) and loaded equimolarly (20 μ g/well) onto SDS-page gels. Proteins were electrophoretically separated on 4-15% polyacrylamide SDS-page gels (depending on molecular weight) and then transferred to a nitrocellulose membrane (BioRad, Hercules, CA). The membranes were subsequently incubated with 3% BSA (Sigma Aldrich, St Louis, MO) or 5% Nonfat Dry Milk (Cell Signaling Technology) for 45' to block nonspecific sites. Subsequently, membranes were incubated overnight with specific primary antibodies, as listed in **Table 2**. Membranes were rinsed 3 times with TBS 1X for 5' minutes each and then incubated for 1 hour with secondary antibodies against the species of the primary antibodies present (dilution 1:5000), **Table 2**. Protein bands were detected using ECL (Bio-Rad Laboratories Inc.), and images were captured using the iBright imaging system (Thermo Fisher Scientific-Invitrogen) or with ChemiDoc XRS+ System (BioRad). Band densities were measured using Image J v3.91 software and normalized to β -actin/GAPDH/VINCULIN signal.

Extraction of nuclear and cytosolic portion

Nuclear/cytosolic portion have been extracted from HepG2 Cas9 and HepG2 KLB $-/-$ cell lines by using Nuclear/Cytosol Extraction Kit (ab289882, K266). Extraction have been carried out accordingly to the manufacturer disposition.

Gene expression analysis

RNA was extracted from cultures cell lines using Trizol reagent (Life Technologies-ThermoFisher Scientific, Carlsbad, USA). One/two μ g of total RNA were retrotranscribed

with SuperScript VILO cDNA Synthesis (Invitrogen). Quantitative real-time PCR (qRT-PCR) was performed by an ABI 7500 fast thermocycler, using the TaqMan Universal PCR Master Mix (Life Technologies, Carlsbad, USA) or SYBR Green chemistry (Fast SYBR Green Master Mix; Life Technologies, Carlsbad, USA). Human Taqman probes and SYBR Green primers used in this study are listed in **Table 3** and **Table 4**. All reactions were reproduced at least in triplicate. Data were normalized to glyceraldehyde 3-phosphate dehydrogenase (GAPDH) housekeeping gene and results were expressed as fold increase (Arbitrary units (AU) of $2^{-\Delta\Delta CT}$ mean value \pm standard deviation (SD).

ORO staining

Cells were plated on a 6-well plate (5×10^5 cells/well) in triplicate and left overnight in complete growth medium. Then cells were kept for 24 hours in starvation medium, containing 0.5% bovine serum albumin (BSA), 1% L-glutamine, and 1% penicillin/streptomycin. The day after, we performed ORO staining, a soluble red powder with high affinity for neutral TAGs and lipids stored in the LDs. Quiescent medium was removed, and the 6-well plates were gently rinsed with 2 mL sterile phosphate-buffered saline 1X. Next, cells were fixed with paraformaldehyde 4% for 10 minutes at room temperature and washed with sterile water. Subsequently, 60% isopropanol was added for 5 minutes. Concurrently, we prepared ORO working solution by mixing 3 parts of ORO stock solution (300 mg of Red Oil powder in 100 mL di-isopropanol 100%) and 2 parts of sterile water and filtered the resulting solution for 2 times. ORO working solution (1 mL/well) was added to each sample and incubated for about 40 minutes. Finally, plates were rinsed with tap water, paying attention not to disrupt the monolayer. LD content was visualized in pink-red color and photos were acquired to the phase-contrast microscope (20X magnification). The ORO-positive area was quantified by ImageJ software in 10 random micrographs by

calculating the ORO-positive area as a percentage of pixels above the threshold value with respect to the total pixels per area.

Lipid Tox red Assay

The HepG2 KLB *-/-* and wild-type Cas9 cells were seeded at a density of 20.000 cell/well in a 4 well chamber suitable for microscopy. Then, cells were maintained in complete growth medium until 70% of cell confluence was reached. After washing with PBS 1X cells were incubated with 100 μ L of 4% PFA/PBS 1X fixative solution for 10' at RT. Fixative solution was removed and cells were washed 3 times with buffer solution. Afterwards, 1000X LipidTOX™ Neutral Lipid Stain was diluted 1:1000 in PBS and added 100 μ L/well directly on cells in solution with nuclear marker (hoechst) 1:3000, for 30' RT. Images acquisition was performed at the fluorescence microscope without washing out the solution, at 500 nm. Isoprpanol was used 100% as white for reading.

Lipid secretion

Supernatants were collected and concentrated using the Vivaspin 20/10 KDa polyethersulfone twin membrane (Sartorius Stedim Biotech, France), with the purpose to quantify apolipoprotein B (ApoB) release through enzyme linked immunosorbent assay (ELISA), which detects both ApoB main isoforms, the intestinal ApoB-48 and the hepatic ApoB-100. The assay has been performed according to the manufacturer's instructions (ThermoFisher Scientific). The lower limit of ApoB detection was 0.21 ng/mL.

Immunofluorescence analysis

The HepG2 KLB *-/-* and wild-type Cas9 cellular models were seeded at a density of 20.000 cell/well then treatments were performed on cells grown in complete growth medium until 70% of cell confluence was reached. Then, cells were fixed in a mixture of methanol/acetone (3:1) and incubated for 10' at -20°; after this cells were permeabilized with Triton™ X-100 (Sigma-Aldrich, St. Louis, MO) 1X for 10' at RT. Non-specific sites were blocked with BSA

5% for 45' at RT. Cells were then incubated with the primary antibody directed against the protein of interest and detected using secondary antibodies conjugated with the Alexa Fluor® 488 (green) fluorophore (dilution 1:500; Invitrogen) or Alexa Fluor® 555 (red) (dilution 1:500; Invitrogen). The cell nuclei were stained with DAPI (Invitrogen™), (blue), (dilution 1:10,000). Images were analyzed using the Olympus FluoView FV1000 microscope.

Apoptosis assay for Annexin V and caspase 3/7 by the Incucyte® SX5 platform

Cells were seeded in quintuplicate for each condition (5000 cells/well) in a ViewPlate-96 Black plate in 50 µL of DMEM medium with 10% FBS and incubated at 37°C overnight. The following day, 50 µL of DMEM 2X 'working reagent' was added to each well, supplemented with either Annexin V Green reagent or Caspase-3/7 Green reagent (Sartorius, Essen Bioscience) at the final concentration of 1 mM plus 1 mM CaCl₂ for Annexin V and at the final concentration 1 mM for Caspase 3/7. Subsequently, the cells were placed in the Incucyte® platform applying the modality "Adherent Cell Line Protocol" and analyzed with the Incucyte®Live-Cell Imaging analysis system. The instrument acquired 4 images for each well every 2/3 hours for 48 consecutive hours in brightfield at 10x magnification and in fluorescence at the specific wavelength for the Annexin V and Caspase 3/7 fluorescent probes, indicated by the manufacturer. Cellular apoptosis was assessed for each probe based on the Fluorescence Integrated Intensity (GCU/µm²) value and normalized to the cell mask acquired in brightfield at t₀. The images were the analyzed, and the data were generated using the automated software algorithm of the IncuCyte™ software.

Apoptosis assay by flow cytometric analysis:

Apoptosis was assessed using the Fluorescein-5-isothiocyanate (FITC) Annexin V Apoptosis Detection Kit I (Becton Dickinson). Cell lines were plated in triplicate for each condition (100.000 cells/well) in a 12-well plate and incubated with complete growth medium

at 37°C overnight. The following day, cells were washed twice with cold PBS and resuspended in 1X Annexin Binding Buffer. Subsequently, cells were stained with 5 µL/well of Annexin V FITC and 5 µM Propidium Iodide (PI) for 15 minutes prior to analysis. Analysis was performed using a FACSCanto II flow cytometer, employing DiVa Software version 6.3 (Becton Dickinson) and data provided as number of cells on the total amount of the events positive for the staining.

Cell cycle analysis using flow cytometry:

Cell cycle phases distribution was analyzed by flow cytometry using propidium iodide (PI) staining (Sigma-Aldrich, St. Louis, Missouri, USA). Cells were collected by trypsinization, washed with PBS 1X, then fixed in a cold solution of methanol/acetone (4:1). Cells were first incubated with RNase A at 37 °C then stained with a solution containing 100 µg/ml PI, at 37 °C for 20'. Stained nuclei were analyzed for DNA-PI fluorescence using a Becton Dickinson FACSCanto II flow cytometer (Becton-Dickinson, Milan, Italy). The proportions of cells in G0/G1, S phase, and G2/M phases of the cell cycle were analyzed by DiVa Software, version 6.3 (Becton-Dickinson) and plotted as percentages on the total number of live cells.

Inflammation and Stem Cell gene Panels with TaqMan OpenArray:

The analysis of gene panels associated with immune response and stem cell/pluripotency features were conducted using the OpenArray™ Human Inflammation Panel and the OpenArray™ Human Stem Cell Panel, respectively, on a QuantStudio system. RNA was isolated from cell lines using the Norgen Total RNA Isolation Kit (Norgen Biotek Corp) and quantified with NanoDrop Technologies instrument (Wilmington). Subsequently, 2 µg of total RNA was reverse-transcribed using the SuperScript™ VILO™ cDNA kit (Thermo Fisher Scientific-Invitrogen). The resulting cDNA was employed to perform gene panels containing 586 inflammation-related genes and 609 stem cell-related genes, respectively. Each panel also included the analysis of 21 housekeeping genes for endogenous control. Real-time

PCR was carried out using the QuantStudio™ 12K Flex analysis system (Thermo Fisher Scientific-Applied Biosystems). Each sample was assessed in quadruplicate. Cartridge loading and machine operations have been performed following the manufacturer's instructions. The relative quantification (RQ) of gene expression values was calculated using an open-source Thermo Fisher Scientific cloud platform. The RQ of each gene in different samples was normalized to the respective GAPDH and fold change was calculated compared to the gene expression levels of their respective controls.

Cytokine secretion

Supernatants media were concentrated using the Vivaspın 20/10 KDa polyethersulfone twin membrane (Sartorius Stedim Biotech, France) and then exploited to quantify cytokine secretion through ELISA assays specific for TNF- α , IL6, and IL1 β (R&D Systems, Minneapolis, USA). The lower limits of detection were 15.6, 3.9, and 9.4 pg/mL, respectively. Data were normalized to the total protein content.

Cell proliferation analysis using the Incucyte® platform

Cell proliferation was evaluated by using the Incucyte® SX5 platform (Sartorius-Biopharma) applying the Incucyte® Label-Free Cell Proliferation Assay protocol and analyzed using the Incucyte® Live-Cell Imaging analysis system. This approach allows evaluate cell proliferation through live imaging by calculating the real-time cell confluence. HepG2 KLB -/- and wild-type Cas9 cells were plated in quintuplicate at a density of 5000 cells per well in 96-well plates (ViewPlate-96 Black, Optically Clear Bottom) in 100 μ L of DMEM supplemented with 1% FBS and incubated at 37 °C overnight to synchronize the cell cycle. Subsequently, cells were placed in the Incucyte® Live-Cell platform and analyzed using the modality "Adherent Cell Line Protocol". Images were captured in bright-field by the instrument at 10x magnification at various time points over 48 hours. Cell confluence analysis was performed using the IncuCyte™ analysis software.

Cell Proliferation Assays EdU

The measurement of cell proliferation and cell cycle S-Phase have been assessed with Click-iT EdU Cell Proliferation Assays® (Thermofisher). In this assay, EdU (5-ethynyl-2'-deoxyuridine) is incorporated during DNA synthesis and detected using a click reaction a copper(I)-catalyzed reaction between an azide and an alkyne. 500.000 cells/well have been seeded in a 6 well plate with three replicates for each condition and incubated in DMEM 1% FBS, at 37° overnight. The next day, Click-it Edu reagent was added to the complete growth medium at the concentration 10 uM and incubated for 2h. Cells were rinsed with Wash Buffer and trypsinised, then the cell pellet was resuspended in 100 ul of Click-it fixative buffer and incubated for 15'. Cells were pelleted in 1 ml of Wash Buffer and resuspended in 100 ul of Click-iT permeabilization reagent 1X and incubated for 15'. Subsequently, cells were stained with 500ul of Click-iT Plus reaction cocktail added to the volume and incubated for 30' out of light. The analysis was performed using a FACSCanto II flow cytometer (Alexa Fluor 594 picolys azide; Ex 532/561 nm, Em 620 nm), utilizing DiVa Software, version 6.3 (Becton Dickinson).

Cell growth rate and cytotoxicity assay using MTS

Cells were seeded in a 96-well plate in quadruplicate and incubated in DMEM 1% FBS overnight, to synchronize cell cycle. Cell growth rate was measured at the baseline using the CellTiter96-Aqueous One Solution Cell Proliferation Assay (MTS:3-(4,5-dimethylthiazol-2-yl)-5-(3-carboxymethoxyphenyl)-2-(4-sulfophenyl)-2H-tetrazolium) kit (Promega Corporation, Fitchburg, WI) according to the manufacturer's instructions. Fresh growth media was provided for 24-48-72 h and 1 week. MTS reagent (20 µL/well) was added to the cells at each timepoint followed by incubation for 4 hours in a 5% CO₂ humidified incubator at 37°C, and the absorbance was measured to the spectrophotometer at 490 nm. At least 3 independent experiments were performed. Administration of sorafenib (Santa Cruz

Biotechnology, Dallas, TX) at very low concentrations (1 and 2.5 $\mu\text{mol/L}$) was effective to modulate cell survival, whereas the higher concentrations (10 and 50 $\mu\text{mol/L}$) showed a high mortality rate. Therefore, after a day at 37°, 5% CO₂, cells were treated with sorafenib at a final concentration of 5 $\mu\text{mol/L}$ plus DMSO (0.6%), which is further consistent with the current literature [102, 103]. Subsequently MTS assay was performed at the baseline without treatment and at for the following timepoints: 24-48-72 h and 1 week, after treatment. Cell medium was changed every day, not affecting the drug concentration.

Wound Healing Assay

Cells were seeded in 6-well plate ($8 \times 10^5/\text{well}$) and incubated with complete growth media until approximately 90% confluency was reached. A fine scratch was introduced using a sterile pipette tip in the middle of cells monolayer. The wounds were photographed at bright field microscope (objective, 100X) at 24 and 48 hours. Each experiment was performed in triplicate. Scratch width was measured at each timepoint by ImageJ software in 5 random photos for each condition. Means of scratch widths with SD of the selected photos were plotted and analyzed.

Spheroid assay

HepG2 KLB $-/-$ and wild-type Cas9 cells were seeded 10^5 cells/well for each condition in 100 μl of complete growth medium on 96 Ultra-Low Attachment (Corning Life Sciences, Amsterdam, Netherlands). The plate was incubated in Incucyte® SX5 platform and Tumour spheroids (TS) growth was monitored over 96h after from the seeding. After 96 hours TS of around 250 μm in diameter were achieved and the assay was stopped. TS generation was assessed by using the modality Incucyte® 3D Multi-Tumor Spheroid Assays and analyzed by the Incucyte® Image Analysis system. Photos were acquired every 6 hours (DF® Brightfield acquisition, 10X magnification). TS size and growth was measured using the InCuCyte™ analysis software.

Statistical analyses

For descriptive statistics, continuous variables were reported as means and SD or as the median and interquartile range for highly skewed biological variables. The results are shown as means \pm SD or median and interquartile range, of at least three independent experiments, each containing triplicates or quadruplicates. Data are expressed as fold change (Arbitrary Unit (AU) vs controls. Real-time quantitative PCR raw data were analyzed by using the 2(-Delta CT) Livak method [104]. Variables with skewed distribution were logarithmically transformed before analyses. Statistical analyses were performed using JMP Pro 16.0 (SAS, Cary, NC) and Prism software (version 9.5.0, GraphPad Software). Differences between groups were calculated by using t-tests analysis and one-way analysis of variance (ANOVA) which was followed by post hoc t-tests adjusted for the number of comparisons when multiple groups were involved (Bonferroni correction). Genetic analyses conducted on patients were based on additive and recessive models of generalized linear regression. Specifically, continuous traits were analyzed with generalized linear models, while binary traits (presence of NASH or severe fibrosis) were analyzed using logistic regression or ordinal regression for the analysis of ordinal traits (e.g., histological components of NAFLD). *p-values* lower than 0.05 (at two-tailed) were considered statistically significant (*** $P < 0.0001$, ** $P < 0.001$, * $P < 0.01$).

Reagents:

Dulbecco's modified Eagle's medium (DMEM), phosphate-buffered saline (PBS), fetal bovine serum (FBS), L-glutamine, penicillin/streptomycin, Trypsin/EDTA, Hank's balanced salt solution, and fast SYBR green master mix were obtained from ThermoFisher Scientific (Waltham, USA). Cell culture flasks, plates, and polyester membrane inserts (12 mm diameter, 0.4 μm pore diameter) were obtained from Corning (Cambridge, MA, USA). Sorafenib was acquired from Santa Cruz Biotechnology (Dallas, TX). Human Taqman

probes were provided by from ThermoFisher Scientific (Waltham, USA) and SYBR Green primers were custom made and provided by Sigma-Aldrich (St Louis, MO). BSA was purchased from Sigma-Aldrich (St Louis, MO). PCR Master Mix 2x was purchased from BiotechRabbit (Hennigsdorf, Germany). Clarity Western ECL substrate was obtained from Bio-Rad Laboratories. CellTiter 96 AQueous One Solution Cell Proliferation Assay (MTS) was purchased from Promega Corporation. The TAG quantification kit was purchased from BioVision, Inc (Milpitas, CA). Triglyceride Quantification Kit was purchased from BioVision (Milpitas, United States). The ATP Assay Kit, MAK190 (colorimetric or fluorometric tests), the ATP synthase activity kit and the NAD/NADH Quantitation Kit MAK037 (colorimetric tests) were all purchased by Sigma-Aldrich (St Louis, MO). The Cholesterol Colorimetric Assay Kit– high density lipoprotein (HDL) and Low-density lipoprotein/ very low-density lipoprotein (LDL/VLDL), Reactive oxygen species/Reactive nitrogen species (ROS/RNS) Colorimetric Assay Kit, Hydrogen Peroxide Assay Kit, Lipid Peroxidation (malondialdehyde) Assay Kit (colorimetric/fluorimetric), DNA Damage Colorimetric Assay Kit (apurinic/apyrimidinic (AP) sites), and MitoBiogenesis In-Cell Enzyme-Linked Immunosorbent Assay Kit were purchased from Abcam. VectaMount AQ Mounting Medium was obtained from Maravai Life Sciences, Inc. The Anti-Cas9 antibody was purchased from Novus Biologicals (Littleton, U.S.A.). The antibiotics Blastocidin, Ampicillin, and Puromycin, as well as the competent bacterial cells DH5- α , the Super Optimal Broth with Catabolite repression (S.O.C. medium), and Lipofectamine 3000 for transfection, were obtained from ThermoFisher Scientific (Waltham, United States). The PCR Master Mix 2X was acquired from BiotechRabbit (Hennigsdorf, Germany). The plasmid pGL3-U6-sgRNA-PGK-puromycin (51133) was purchased from Addgene (Teddington, UK), while the lentiviral vector Edit-R Inducible lentiviral Cas9 Nuclease was acquired from GE Healthcare Dharmacon Inc. Chloroquine (MedChemExpress- cat: HY-17589/CS-3811). Rapamycin (Cell Signaling- cat 9904S). Triton™ X-100 (Sigma-Aldrich, St. Louis, MO).

Table 2: Antibodies reagents code

Antibody and used dilution	Manufacturer and reagents code
PGC1- α (1:1000 WB)	Novus Biologicals NBP1-04676
p-(Ser473)-Akt (1:1000 WB)	Cell Signaling 9271S
Cytokeratin 18	antibodies.com A86656
Histone H3 (1: 2000 WB)	Abcam ab1791
P38 (1:1000 WB)	Cell signaling 8690
p-P38 (Thr180/Tyr182) (1:1000 WB)	Cell signaling 4511
KLB (1:500 WB)	Abcam
ERK (1:1000 WB)	Cell signaling 4695
p-ERK (Thr202/Tyr204) (1:1000 WB)	Cell signaling 4370 (WB) Santa Cruz sc-81492 (IF)
NRF-2 (1:1000 WB)	Cell signaling 12721
BAX (1:1000 WB)	Cell signaling 5023
Cas3 (1:1000 WB)	Cell signaling 9662
Cas3-cleaved (1:1000 WB)	Cell signaling 9664
p-Beclin (1:1000 WB)	Cell signaling BK14717S
LC3 β (1:1000 WB)	Cell signaling 43110T
P62 (1:1000 WB)	Cell signaling 43110T
LAMP2 (1:1000 WB) (1:500 IF)	Santa Cruz AU-SC-200
NF- κ B p65 (1:1000 WB)	Abcam ab16502
p-NF- κ B p 65 (Ser536) (1:500 IF)	Cell signaling 303s
PCNA (1:1000 WB)	Cell signaling
JNK (1:1000 WB)	Biotech AF1387
p-JNK (1:1000 WB)	Biotech AF1205
E-CADHERIN (1:1000 WB)	Cell signaling 3195
Vimentin (1:1000 WB)	Cell signaling 5741S
p-FAK (1:500 IF)	Santa Cruz sc-81493
FGFR4 (1:1000 WB)	Abcam ab262718
p-FGFR4 (Y642) (1:1000 WB)	Abcam ab192589

β -actin (1:5000 WB)	Abcam ab6276
Vinculin (1:2000 WB)	Abcam ab207440
GAPDH (1:2000 WB)	Cell signaling 5174s
ACSL4	Santa Cruz sc-365230

Table 3: RT-qPCR SYBER Green primers sequences

Gene	Forward 5'→3'	Reverse 5'→3'
<i>ABCG5</i>	GATTGTCGTCCTCCTGGTGGAA	TCTCCGAAGCTCAGGATGGCAA
<i>ABCG8</i>	TGTCCTCGCTACAGCAATCCTG	AGAAACAGGGCTGCGAGTGACT
<i>ACSS2</i>	GGTGACCAAGTTCTACACAGCAC	G TTCACCCACTGTGCCTAACAC
<i>ATF4</i>	AAACCTCATGGGTTCTCCAG	GGCATGGTTTCCAGGTCCT
<i>ATF6</i>	AATTCTCAGCTGATGGCTGT	TGGAGGATCCTGGTGTCCAT
<i>BCL2</i>	ATCGCCCTGTGGATGACTGAGT	GCCAGGAGAAATCAAACAGAGGC
<i>cFOS</i>	GCCTCTTTACTACCACTCACC	AGATGGCAGTGACCGTGGGAAT
<i>CYP7B1</i>	CACCAGAGAACAATTGGACAGCC	GCTACCAAGTCTCCCTTTTCGCA
<i>CYP39A1</i>	GAGGATGACCTGGAGAATCTCC	GCAGCCAAAATGGAGACAACATC
<i>cJUN</i>	CCTTGAAAGCTCAGAACTCGGAG	TGCTGCGTTAGCATGAGTTGGC
<i>CPT1</i>	GATCCTGGACAATACCTCGGAG	CTCCACAGCATCAAGAGACTGC
<i>DAGT1</i>	GCTTCAGCAACTACCGTGGCAT	CCTTCAGGAACAGAGAAACCACC
<i>DAGT2</i>	GCTACAGGTCATCTCAGTGCTC	GTGAAGTAGAGCACAGCGATGAG
<i>DHCR7</i>	TCCACAGCCATGTGACCAATGC	CGAAGTGGTCATGGCAGATGTC
<i>HIF1α</i>	TATGAGCCAGAAGAACTTTTAGGC	CACCTCTTTTGGCAAGCATCCTG
<i>HIF1β</i>	CTGTCATCCTGAAGACCAGCAG	CTGGTTCTCATCCAGAGCCATTC
<i>HMGCR</i>	GACGTGAACCTATGCTGGTCAG	GGTATCTGTTTCAGCCACTAAGG
<i>LDLR</i>	GAATCTACTGGTCTGACCTGTCC	GGTCCAGTAGATGTTGCTGTGG
<i>LXRα</i>	TGGACACCTACATGCGTCGCAA	CAAGGATGTGGCATGAGCCTGT
<i>MnSOD2</i>	CTGGACAAACCTCAGCCCTAAC	AACCTGAGCCTTGGACACCAAC
<i>MTPP</i>	GCTTCCGTTAAAGGTCACACA	CAGCTGTTATCGTGACTTGGA
<i>PPARGCA</i>	CCAAAGGATGCGCTCTCGTTCA	CGGTGTCTGTAGTGGCTTGACT
<i>PPARα</i>	ATGGCATCCAGAACAAGGAG	TCCCGTCTTTGTTTCATCACA
<i>SREBP2</i>	CTCCATTGACTCTGAGCCAGGA	GAATCCGTGAGCGGTCTACCAT

<i>β-actin</i>	GCTACAGCTTCACCACCACA	AAGGAAGGCTGGAAAAGAG
----------------	----------------------	---------------------

Table 4: RT-qPCR Taqman probes codes

Gene	Taqman RT-qPCR probe (Life Sciences)
<i>ACSL1</i>	Hs01059101_m1
<i>CD36</i>	Hs00354519_m1
<i>CDH1 (E-caderin)</i>	Hs01023894_m1
<i>CDH2 (N-caderin)</i>	Hs00983056_m1
<i>FASn</i>	Hs01005622_m1
<i>GAPDH</i>	Hs02786624_g1
<i>KLB</i>	Hs01573147_m1 (Exon1-2) Hs00545621_m1 (Exon3-4)
<i>Cytokeratin 18 (KRT18)</i>	Hs_02827483_g1
<i>PPARγ</i>	Hs01115513_m1
<i>ABC1</i>	Hs01059101_m1
<i>SR-B1(SCARB1)</i>	Hs00969821_m1
<i>KLB rs12152703</i>	C__31801563_10 (SNP Genotyping Assays)

RESULTS

AIM1: Impact of the KLB Knock-out on the hepatocyte homeostasis and on the onset of NAFLD traits

1. Generation and characterization of a stable KLB full knock-out in vitro model:

The full knock-out of *KLB* (*KLB KO*) gene was performed by using CRISPR/Cas9 technology in HepG2 cells as reported in method section. In KLB knock-out cells (*KLB*^{-/-}), KLB expression was dramatically dampened both at gene ($p < 0.0001$ vs Cas9) and at protein ($p < 0.0001$ vs Cas9) level, compared to controls (Cas9) (**Figure 1A**).

2. Effects KLB KO on FGFR4 activation

Generally, KLB exploits its functions in the liver by forming a complex with FGFR4, and the subsequent activation of signaling pathways by the FGFR4/KLB complex requires FGF19 binding [74]. Therefore, in our model, we investigated the effects of KLB KO on phosphorylated form of FGFR4 (p-FGFR4), which reflects the FGFR4/KLB complex activation, in the absence or presence of FGF19. Unexpectedly, Cas9 control cells exhibited a basal level of p-FGFR4 also in the absence of FGF19 that was instead decreased ($p < 0.001$ vs Cas9) in *KLB*^{-/-} cells (**Figure 1B**). However, as shown in (**Figure 1B**), Cas9 control cells displayed the activation of the FGFR4 receptor through its auto-phosphorylation, with an increasing trend over the time after the stimulus with FGF19 (Cas9 15', $p < 0.01$ vs Cas9 t0). Conversely, we observed that the absence of KLB in HepG2 cells may cause a decreased auto-phosphorylation/activation of FGFR4, both in the presence and in absence of FGF19 (t15', $p < 0.001$ vs Cas9 t15'; t2h, $p < 0.0001$ vs Cas9 t2h) (**Figure 1B**).

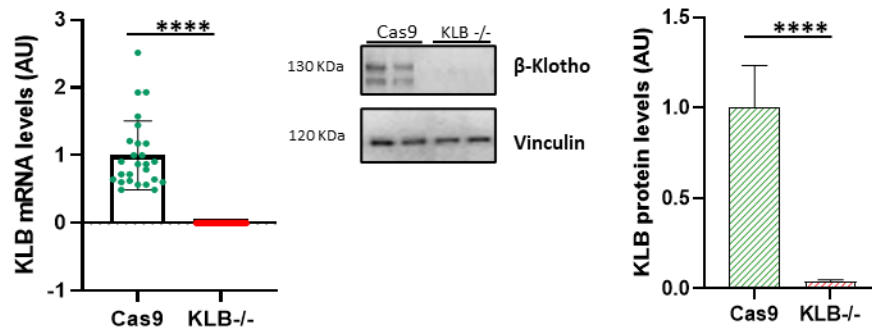
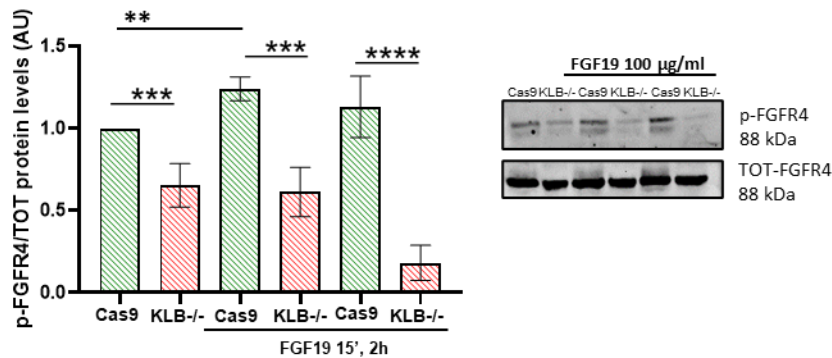
A**B**

Figure 1: (A) KLB mRNA and protein expression were evaluated by reverse transcription quantitative PCR normalized to the *h-GAPDH* housekeeping and Western blot (WB) normalized to the Vinculin housekeeping, respectively. KLB expression was dampened in KLB^{-/-} cells both at gene and at protein level (**** $p < 0.0001$ vs Cas9). FGF19 stimulus was performed on starved cells (0.5% FBS), directly added to culture medium at 100 $\mu\text{g/ml}$ for 15' and 2h. (B) Immunoblot analysis reveal that the activation of p-FGFR4 was downregulated in KLB^{-/-} cells compared to controls also after FGF19 stimulus. p-FGFR4 signal was normalized on TOT-FGFR4 signal (** $p < 0.001$; **** $p < 0.0001$).

3. Effects of KLB KO on FGFR4/KLB signaling

Hence, we next investigated several of the main downstream effectors modulated by the activation of FGFR4/KLB complex signaling. Our results (**Figure 2A**) demonstrated that phosphorylated forms of ERK (p-ERK) and P38 proteins (p-P38), were strongly downregulated in KLB^{-/-} cells (p-ERK/total ERK, $p < 0.0001$ vs Cas9), (p-P38/total P38, $p < 0.0001$ vs Cas9). p-ERK downregulation was also observed by immunofluorescence, evidencing the almost complete absence of the p-ERK positivity in the nuclei of KLB^{-/-} cells. As expected, FGF19 stimulus determined the up-regulation of p-ERK protein levels in control cells (Cas9 t2h, $p < 0.0001$ vs Cas9 t0), confirming the physiological response to the stimulus (**Figure 2B**). Conversely, ERK signaling inhibition (t0, $p < 0.001$ vs Cas9; t15',

p<0.0001 vs Cas9 t15') due to KLB KO was confirmed even after the treatment with FGF19 (Figure 2B)

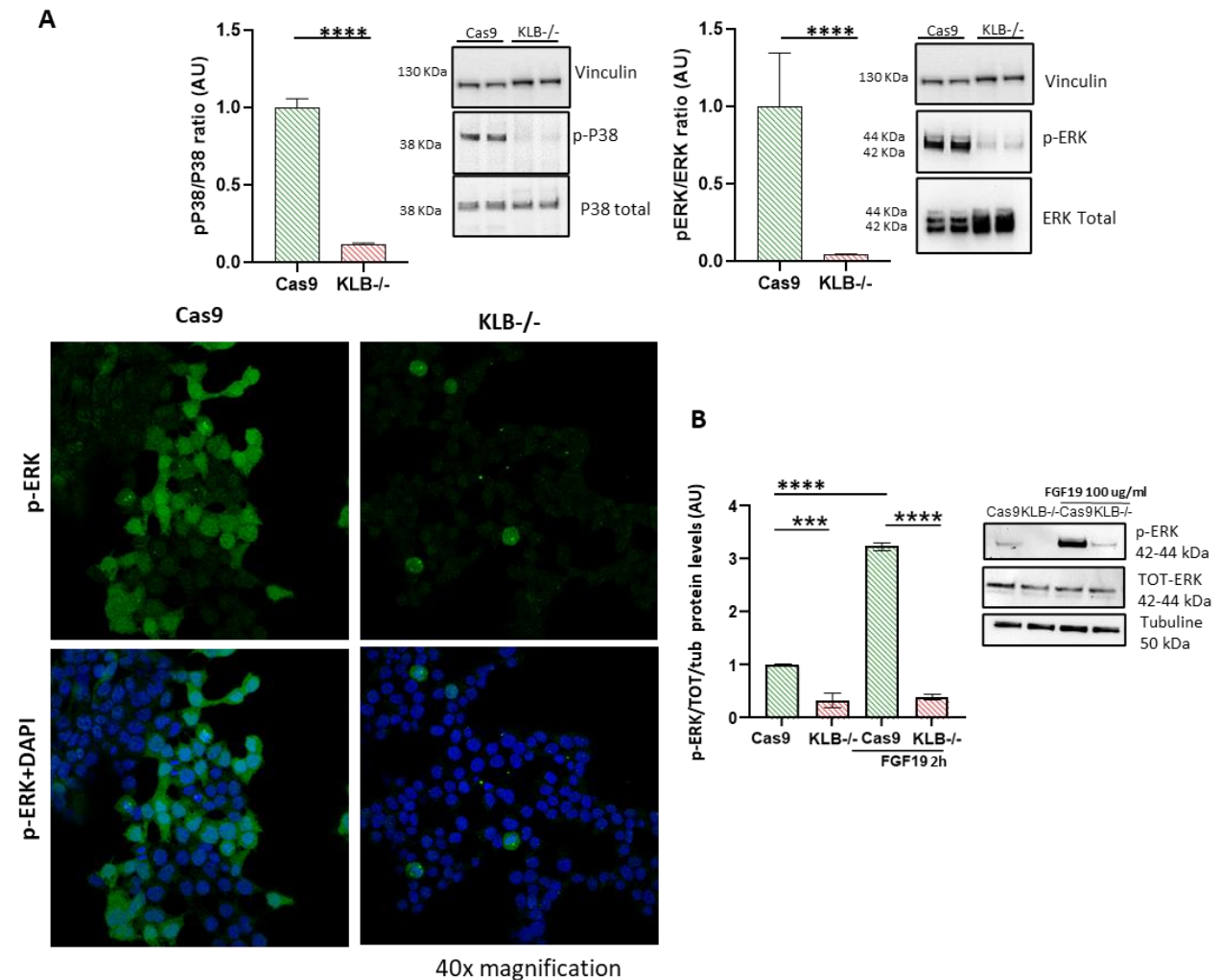


Figure 2. (A) The protein levels of p-P38/total P38 and p-pERK/total ERK were assessed by WB and found significantly decreased in KLB-/- cells (****p<0.0001 vs Cas9). Ratios were measured through ImageJ software and normalized to the vinculin housekeeping. Immunofluorescent assays were performed on fixed cells incubated with specific p-ERK rabbit antibody (1:500, green), and then with specific anti-species secondary antibodies. Nuclei were stained with DAPI (1:10000, blue). Images were acquired at confocal microscopy at 40x magnification. KLB-/- cells showed strongly decreased p-ERK fluorescent signal confined in the nuclei. **(B)** FGF19 stimulus was performed on starved cells (0.5% FBS), directly added to culture medium at 100 ug/ml for 2h. p-ERK protein levels were decreased in KLB-/- cells also after FGF19 stimulus while were increased in controls (Cas9 2h ****p<0.0001vs Cas9). p-ERK signal was double normalized on TOT-ERK and on alpha-tubuline. For bar graphs, data are expressed as means and SE. At least three independent experiments were conducted. Statistical correlations were assessed by unpaired t-test to compare the mean of two independent groups or by one-way/two-way ANOVA test for multiple parameters, adjusted for confounding factors. p values<0.05 (two-tailed) will be considered statistically significant.

4. KLB depletion impairs lipid metabolism

Since lipid metabolism perturbations have onset during NAFLD and widely contributes to the disease progression, we evaluated in our model the expression of several key regulators of the lipid homeostasis. An aberrant lipid metabolism was observed in KLB deficient cells through the downregulation of *Fatty acid synthase (FAS)* and *Peroxisome proliferator-receptor gamma (PPAR γ)*, (*FAS*, $p < 0.0001$ vs Cas9; *PPAR γ* , $p < 0.001$ vs Cas9), both genes involved in lipogenesis and fatty acids (FA) absorption, (**Figure 3A**). Moreover, as shown in **Figure 3A**, *KLB*^{-/-} cells compared to controls showed decreased mRNA levels of several genes including: i) *CD36*, encoding for the scavenger receptor appointed to the intracellular up-take of fatty acids; ii) *Acyl-CoA Synthetase Long Chain Family Member 1 (ACSL1)*, and *4 (ACSL4)*, two proteins involved in the esterification and degradation of fatty acids (*CD36*, $p < 0.0001$ vs Cas9; *ACSL1*, $p < 0.001$ vs Cas9; *ACSL4*, $p < 0.01$ vs Cas9); iii) *Microsomal Triglyceride Transfer Protein (MTTP)* and *ApoB*, involved in lipoprotein assembling (*MTTP*, $p < 0.001$ vs Cas9; *ApoB* $p < 0.01$ vs Cas9).

Furthermore, *KLB*^{-/-} cells have been characterized for the expression of genes regulating triglycerides biosynthesis. In *KLB*^{-/-} cells we found a the downregulation of important mediators of fatty acids β -oxidation and in triglyceride biosynthesis (**Figure 3B**), including *Carnitine Palmitoyltransferase 1 (CPT1)*, ($p < 0.05$ vs Cas9), *Peroxisome Proliferator Activated Receptor Alpha (PPAR α)* ($p < 0.05$ vs Cas9), *PPARG Coactivator 1 Alpha (PGC1 α)*, ($p < 0.0001$ vs Cas9), and *Diacylglycerol O-Acyltransferase 1 (DGAT1)* and *2 (DGAT2)* (*DGAT1*, *DGAT2*, $p < 0.0001$ vs Cas9).

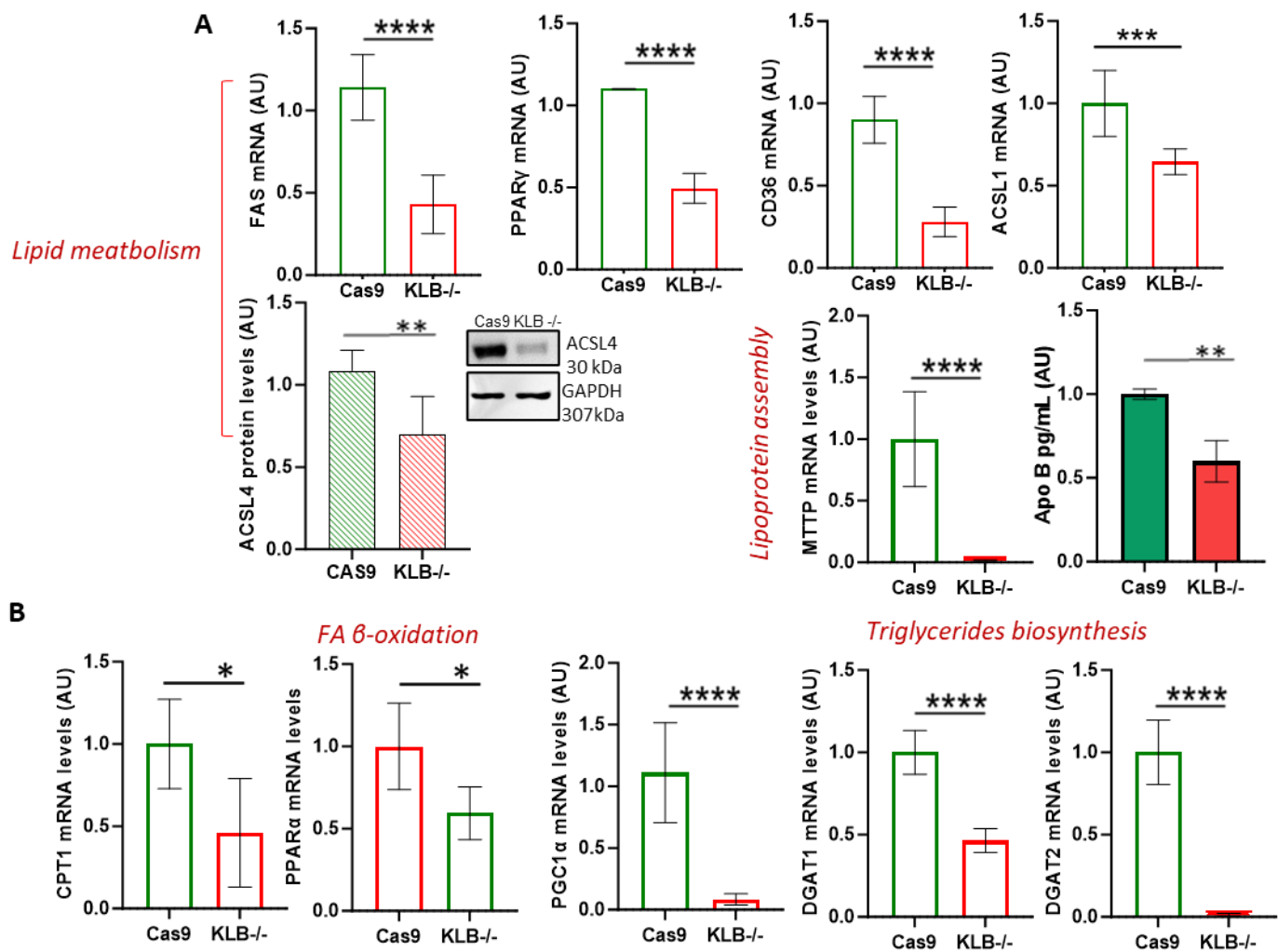


Figure 3. (A) *FAS*, *PPAR γ* , *CD36* and *ACSL1* mRNA levels were downregulated in KLB^{-/-} cells (***p<0.001; ****p<0.0001). Gene expression analyses were performed with TaqMan Real-time qPCR and expression curves were normalized on h-*GAPDH*. Data are expressed as fold increase (Arbitrary Unit (AU) vs controls. Immunoblot analysis performed on cell lysates revealed decreased levels of ACSL4 protein in KLB^{-/-} cells (**p<0.01). Ratios were measured using ImageJ and normalized on hGAPDH protein. Data are expressed as fold change (Arbitrary Unit (AU) vs controls. **(B)** *CPT1*, *PPAR α* , *PGC1 α* , *DGAT1* and *DGAT2* mRNA levels were downregulated in KLB^{-/-} cells (*p<0.05; ****p<0.0001). Gene expression analyses were performed with TaqMan Real-time qPCR and expression curves were normalized on h-*GAPDH*. Data are expressed as fold increase (Arbitrary Unit (AU) vs controls. At least three independent experiments were conducted. Statistical correlations were assessed by unpaired t-test to compare the mean of two independent groups or by one-way/two-way ANOVA test for multiple parameters, adjusted for confounding factors. p values<0.05 (two-tailed) will be considered statistically significant. Data are expressed as fold increase (Arbitrary Unit; AU) vs control. For bar graphs, data are expressed as means and SE.

5. Effects of lipid overload on *KLB*^{-/-} cells

The overall downregulation of FA production and uptake observed in *KLB*^{-/-} cells was further investigated performing Oil Red O (ORO) staining, which specifically labels the intracellular lipid content. The staining was performed at the baseline and after giving a lipid load of palmitic and oleic acids (PAOA) for 24 hours, added directly to the cells culture media (0.025 mM, 1:2). This was aimed to reproduce *in vitro* steatosis, which is a feature of NAFLD. Images of staining were next acquired to the optical contrast phase microscope and quantified (**Figure 4A**, left). We observed that *KLB*^{-/-} cells accumulated fewer lipid droplets than controls after exposure to PAOA ($p < 0.001$ vs Cas9 PAOA). The reduction of the lipid content in *LB*^{-/-} cells was also confirmed by the red staining of neutral lipids in fluorescence (**Figure 4B**, right). In addition, according to what was seen at the gene level, a lower amount of triglycerides content was detected in *B*^{-/-} cells both at the baseline and after PAOA exposure ($p < 0.05$ vs Cas9; $p < 0.0001$ vs Cas9 PAOA) (**Figure 4C**). Furthermore, after the PAOA stimulus, we measured the expression of genes implicated in the lipid metabolism which were previously characterized at the baseline confirming the dampened expression of *DGAT1* ($p < 0.0001$ vs Cas9; $p < 0.0001$ vs Cas9 PAOA), *PGC1 α* ($p < 0.01$ vs Cas9; $p < 0.0001$ vs Cas9 PAOA) and *MTTP* ($p < 0.0001$ vs Cas9; $p < 0.0001$ vs Cas9 PAOA) after PAOA exposure as well as the baseline, (**Figure 4D**).

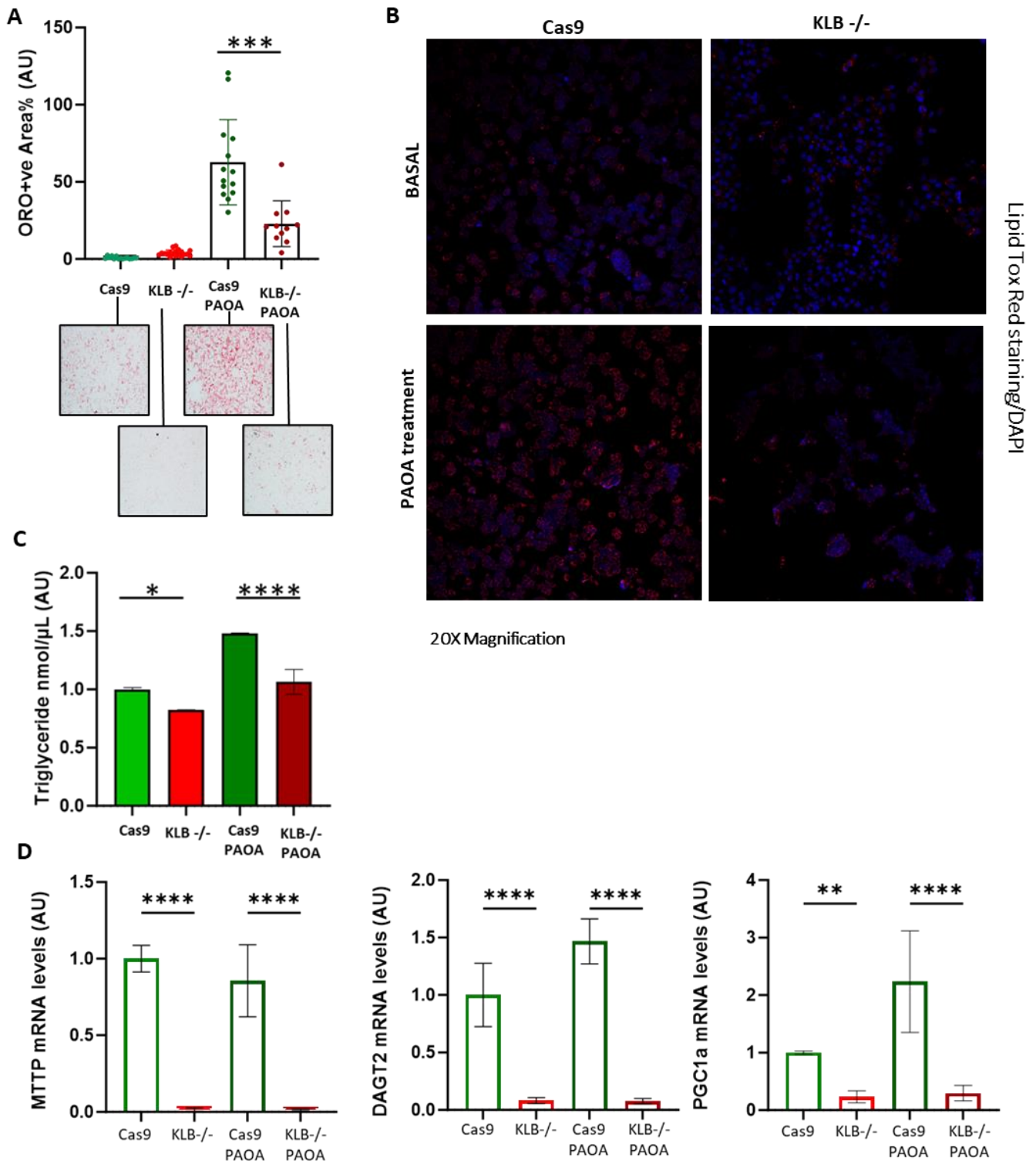


Figure 4 (A) Treatments with PAOA were added directly to culture media at (1:2), 0.025mM for 24h. On the left, intracellular fat accumulation was evaluated by ORO staining both at the baseline and after 24 hours of treatment with PAOA and photos were acquired in bright field at 20x magnification and the red signal was quantified using ImageJ. KLB^{-/-} cells reported significantly lowered fat deposits after PAOA (***p<0.001). (B) On the right, neutral lipid were stained using LipidTOX™ kit (ThermoFisher) and images were acquired at confocal microscopy at 40x magnification. Nuclei were stained with DAPI (1:10000, blue). KLB^{-/-} cells visually showed decreased red signal compared to controls. (C) Intracellular triglycerides content was assessed through fluorometric assay and found significantly reduced in KLB^{-/-} cells also after PAOA lipid load (****p<0.0001 vs Cas9; *p<0.05 vs Cas9). (D) *MTTP*, *DAGT2* and *PGC1a* down-regulation at gene level was maintained also after PAOA lipid load (**p<0.01 vs Cas9; ****p<0.0001 vs Cas9). Data are expressed as fold change (Arbitrary Unit (AU) vs controls. At least three independent experiments were conducted. Statistical correlations were assessed by unpaired t-test to compare the mean of two independent groups or by one-way/two-way ANOVA test for multiple parameters, adjusted for confounding factors. p values<0.05 (two-tailed) will be considered statistically significant. Data are expressed as fold increase (Arbitrary Unit; AU) vs control. For bar graphs, data are expressed as means and SE.

6. KLB depletion may impair cholesterol metabolism and promote BA production in in vitro model

In our model, we also observed an impairment of the cholesterol metabolism. In particular, as shown in **Figure 5A-B**, *KLB*^{-/-} cells exhibited a significant downregulation of genes involved in *de novo* cholesterol synthesis, including *Hydroxymethylglutaryl-CoA Reductase (HMGCoA)* ($p < 0.0001$ vs Cas9), *Sterol Regulatory Element-Binding Transcription Factor-2 (SREBP2)* ($p < 0.01$ vs Cas9) and *Acyl-CoA Synthetase Short Chain Family Member-2 (ACSS2)* ($p < 0.0001$ vs Cas9); and of genes involved in cholesterol alternative synthesis such as *7-Dehydrocholesterol Reductase (DHCR7)* ($p < 0.0001$ vs Cas9). Afterward, we demonstrated a *KLB* KO-dependent impairment of cholesterol export, hepatic transport and up-take through the downregulation of several genes including, *Low Density Lipoprotein Receptor (LDLR)* ($p < 0.001$ vs Cas9), *liver X receptor α (LXR α)* ($p < 0.001$ vs Cas9) and the cholesterol scavenger receptor *SR-B1* ($p < 0.0001$ vs Cas9) (**Figure 5C**). *KLB*^{-/-} cells displayed also decreased expression of genes encoding for the cholesterol membrane transporters such as *ABCA1*, *ABCG5*, and *ABCG8* (ATP-binding cassette transporters) (*ABCA1*, $p < 0.001$ vs Cas9; *ABCG5*, $p < 0.0001$ vs Cas9; *ABCG8*, $p < 0.0001$ vs Cas9), which regulates the cholesterol efflux into the intestinal lumen (**Figure 5D**). Overall, all these results suggest a key effect of *KLB* in cholesterol regulation, as confirmed by a significant decrease of the intracellular cholesterol content in *KLB*^{-/-} cells ($p < 0.0001$ vs Cas9) (**Figure 5E**).

BA production, that uses cholesterol as primary scaffold is directly inhibited by FGF19 in physiological conditions, through *KLB*/*FGFR4* complex activity. As expected, we observed that *KLB*^{-/-} cells had increased mRNA expression of genes implied in BA production, such as *CYP7B1* and *CYP39A1* ($p < 0.001$ vs Cas9) (**Figure 5F**). Moreover, the total BA concentration was increased in *KLB*^{-/-} cells ($p < 0.0001$ vs Cas9) (**Figure 5G**).

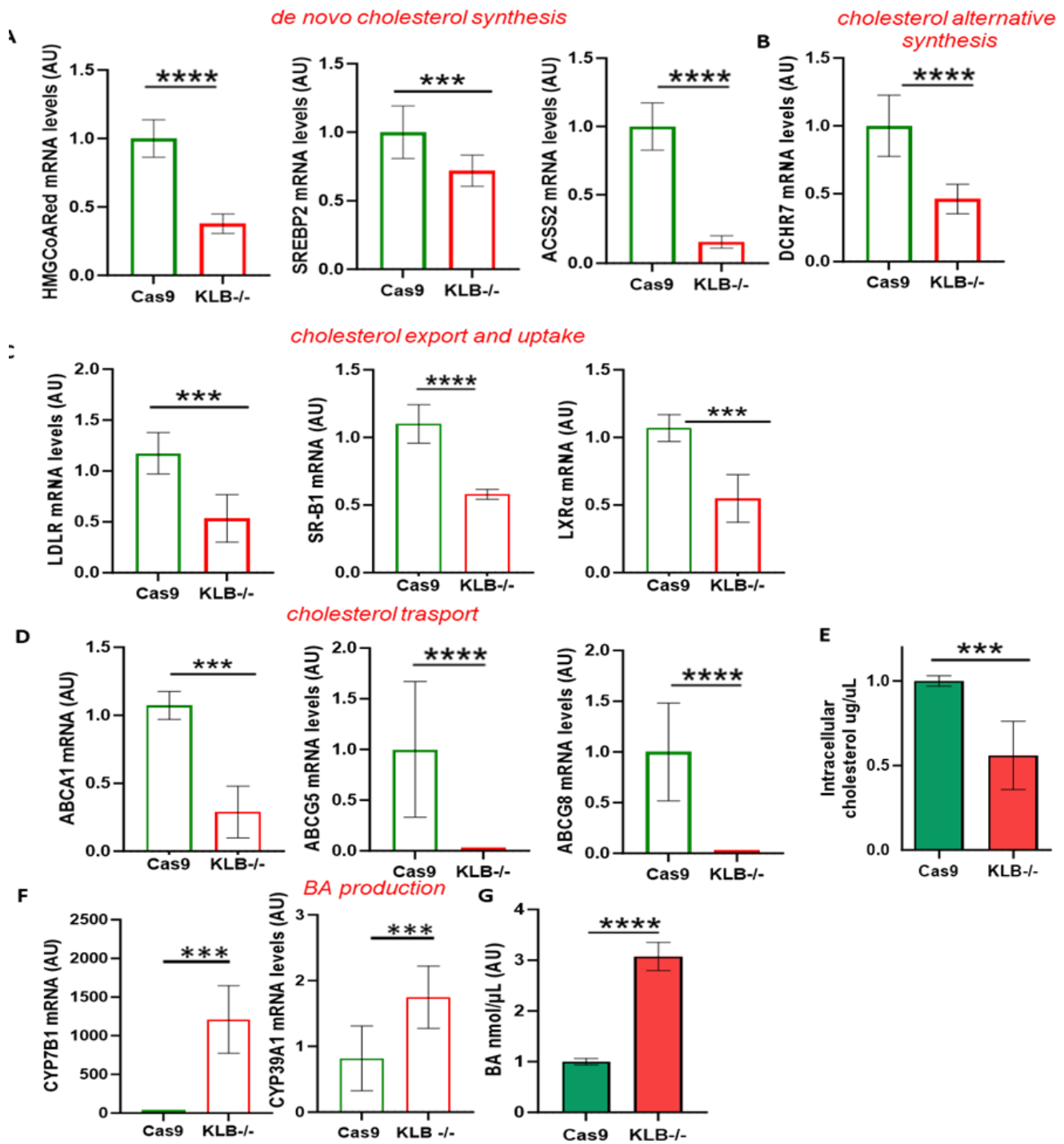


Figure 5. (A) *HMGCARed*, *SREBP2*, *ACSS2*, (B) *DCHR7*, (C) *LDLR*, *LXRα*, *SR-B1*, (D) *ABCG1*, *ABCG5* and *ABCG8* mRNA expression was evaluated by reverse transcription quantitative PCR and normalized to the *h-GAPDH* housekeeping and were found significantly decreased in *KLB-/-* cells compared to control (**** $p < 0.0001$ vs Cas9; *** $p < 0.001$ vs Cas9). (E) Intracellular cholesterol content was assessed through uorometric assay and found significantly reduced in *KLB-/-* cells (*** $p < 0.001$ vs Cas9). (F) *CYP7B1* and *CYP39A1* mRNA expression was evaluated by reverse transcription quantitative PCR, normalized to the *h-GAPDH* housekeeping and was found significantly increased in *KLB-/-* cells compared to control (*** $p < 0.001$ vs Cas9). (G) Intracellular Bile Acids content was assessed through a colorimetric assay and found significantly increased in *KLB-/-* cells (**** $p < 0.0001$ vs Cas9). Data are expressed as fold change (Arbitrary Unit (AU) vs controls. At least three independent experiments were conducted. Statistical correlations were assessed by unpaired t-test to compare the mean of two independent groups or by one-way/two-way ANOVA test for multiple parameters, adjusted for confounding factors. p values < 0.05 (two-tailed) will be considered statistically significant. Data are expressed as fold increase (Arbitrary Unit; AU) vs control. For bar graphs, data are expressed as means and SE.

7. KLB depletion induces severe hepatic damage in *in vitro* model

Since endoplasmic reticulum (ER) and oxidative stress are two of the main pathological processes featuring the advanced stages of liver disease, we evaluated in our model several markers associated with cellular stress to clarify KLB involvement during NAFLD progression. *KLB*^{-/-} cells were predisposed to develop sustained ER stress upregulating the *Activating Transcription Factor 4 (ATF4)* ($p < 0.0001$ vs Cas9) and ATF6 ($p < 0.01$ vs Cas9), two important ER stress mediators (**Figure 6A**). Accordingly, the activation of c-Jun N-terminal kinases (JNK pathway) was further observed in our model ($p < 0.0001$ vs Cas9), (**Figure 6A**). As a consequence of the enhanced ER stress we found an increased oxidative stress in *KLB*^{-/-} cells, resulting into rising of the hydrogen peroxide levels (H_2O_2) ($p < 0.01$ vs Cas9), enhanced release of oxygen reactive species (ROS) ($p < 0.001$ vs Cas9) and nitrogen reactive species (RNS) ($p < 0.001$ vs Cas9) and increased levels of malondialdehyde (MDA) ($p < 0.01$ vs Cas9), (**Figure 6B**). Furthermore, the boost of the oxidative stress led also to the increased ROS-mediated damage on the DNA apurinic sites (DNA-AP-sites) ($p < 0.0001$ vs Cas9), (**Figure 6B**). A possible compensatory effect to counteract the increase of the oxidized species was further observed in our model through the upregulation of *Manganese-Containing Superoxide Dismutase-2 (MnSOD2)* ($p < 0,001$ vs Cas9), the gene encoding for the main antioxidant enzyme that protects cells from oxidative damage and through the upregulation of NRF2 protein, involved in the detoxification and elimination of oxidative stress products ($p < 0.05$ vs Cas9), (**Figure 6C**).

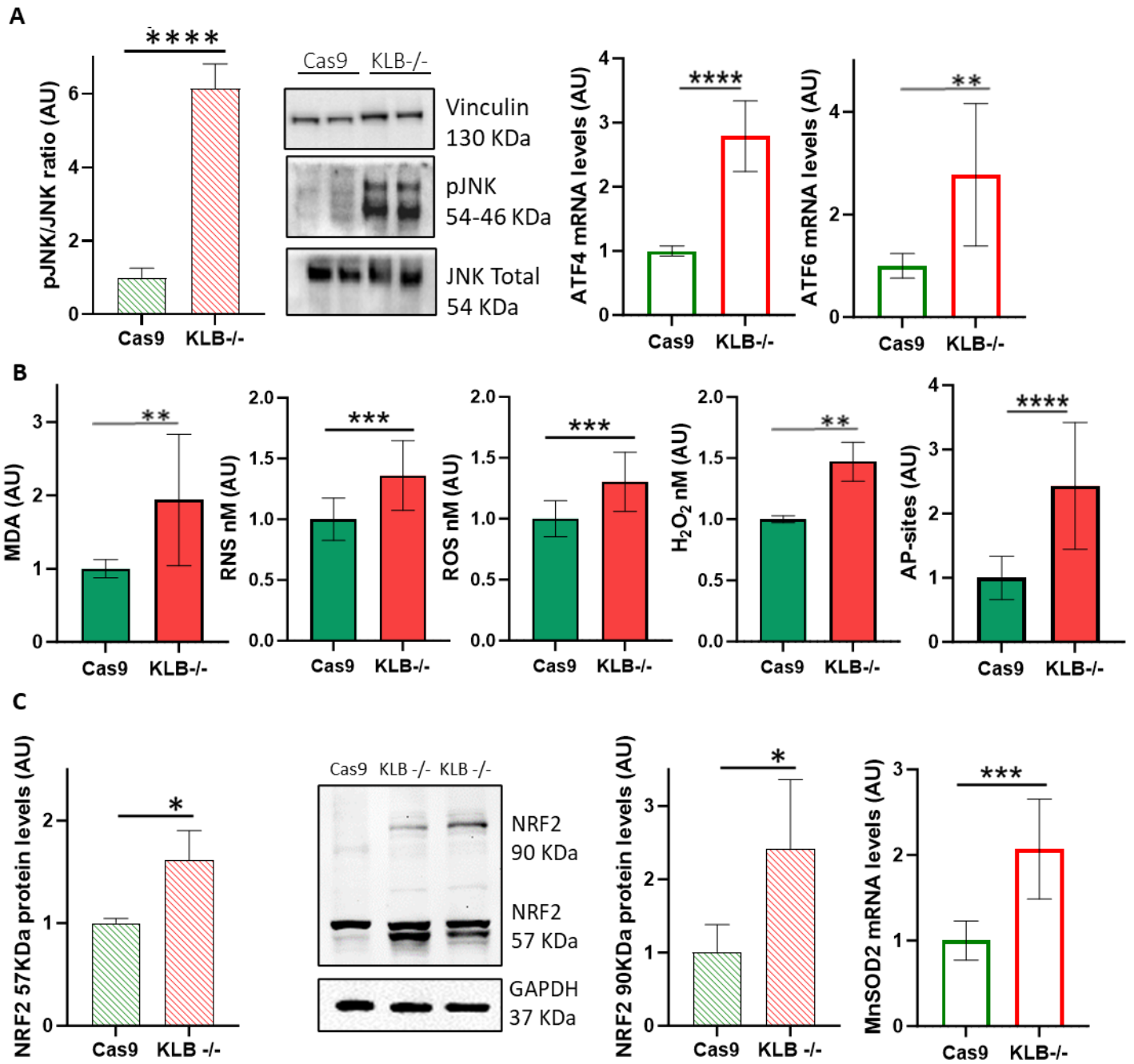


Figure 6: (A) The protein levels of p-JNK/total JNK were assessed by WB, ratios were measured through ImageJ software and normalized to the vinculin housekeeping. pJNK protein levels were increased in KLB^{-/-} cells (**p<0.001vs Cas9). *ATF4* and *ATF6* mRNA expression was evaluated by reverse transcription quantitative PCR and normalized to the h-GAPDH housekeeping and were found significantly increased in KLB^{-/-} cells compared to control (**p<0.01vs Cas9; ****p<0.0001vs Cas9). (B) Intracellular hydrogen peroxide (H₂O₂), malonyldialdehyde (MDA), Reactive nitrogen species (RNS), Reactive oxygen species (ROS) and ROS-mediated damage on AP-sites were assessed through fluorimetric assays and were significantly increased in KLB^{-/-} cells (****p<0.0001vs Cas9; ***p<0.001vs Cas9; **p<0.01vs Cas9). (C) The protein levels of NRF2 were assessed by WB, ratios were measured through ImageJ software and normalized to the vinculin housekeeping. NRF2 protein levels were increased in KLB^{-/-} cells in both his molecular weight bands (**p<0.05 vs Cas9). *MnSOD2* mRNA expression was evaluated by reverse transcription quantitative PCR and normalized to the h-GAPDH housekeeping and was found significantly increased in KLB^{-/-} cells compared to control (**p<0.01vs Cas9; ****p<0.0001vs Cas9). Data are expressed as fold change (Arbitrary Unit (AU) vs controls. For bar graphs, data are expressed as means and SE. At least three independent experiments were conducted. Statistical correlations were assessed by unpaired t-test to compare the mean of two independent groups or by one-way/two-way ANOVA test for multiple parameters, adjusted for confounding factors. p values<0.05 (two-tailed) will be considered statistically significant

8. KLB depletion promotes cell apoptosis in *in vitro*

Next, we investigated the effect of *KLB* KO on the apoptosis process using two different approaches, including FACS analysis and live cell imaging by Incucyte® SX5 platform. FACS analysis was conducted by labeling cells with Annexin V and PI for the evaluation of early and late apoptosis, respectively. As shown in **Figure 7A**, we found a significant increase of both early and late apoptosis in *KLB*^{-/-} cells compared to Cas9 cells (Annexin V, $p < 0.01$ vs Cas9; PI, $p < 0.05$ vs Cas9). The enhancement of the apoptosis was further confirmed by the evaluation of Annexin V (early apoptosis) and caspase 3/7 (late apoptosis) positivity over 24h, by using Incucyte® SX5 platform (**Figure 7B**). In particular, both the markers were found increased in *KLB*^{-/-} cells (Annexin V: 2h, $p < 0.001$ vs Cas9 2h; 4h, $p < 0.05$ vs Cas9 4h; 7h, $p < 0.05$ vs Cas9 7h), (Caspase 3/7: 2h, $p < 0.001$ vs Cas9 2h; 4h, $p < 0.01$ vs Cas9 4h; 8h, $p < 0.05$ vs Cas9 8h), (**Figure 8C**). In addition, we also reported an increase of the protein levels, not only of the known apoptotic marker caspase-3 (Cas 3) and of its active cleaved form (Cas3, $p < 0.01$ vs Cas9; Cas 3-cl, $p < 0.05$ vs Cas9) but also of BAX an important proapoptotic effector ($p < 0.01$ vs Cas9), (**Figure 7C**).

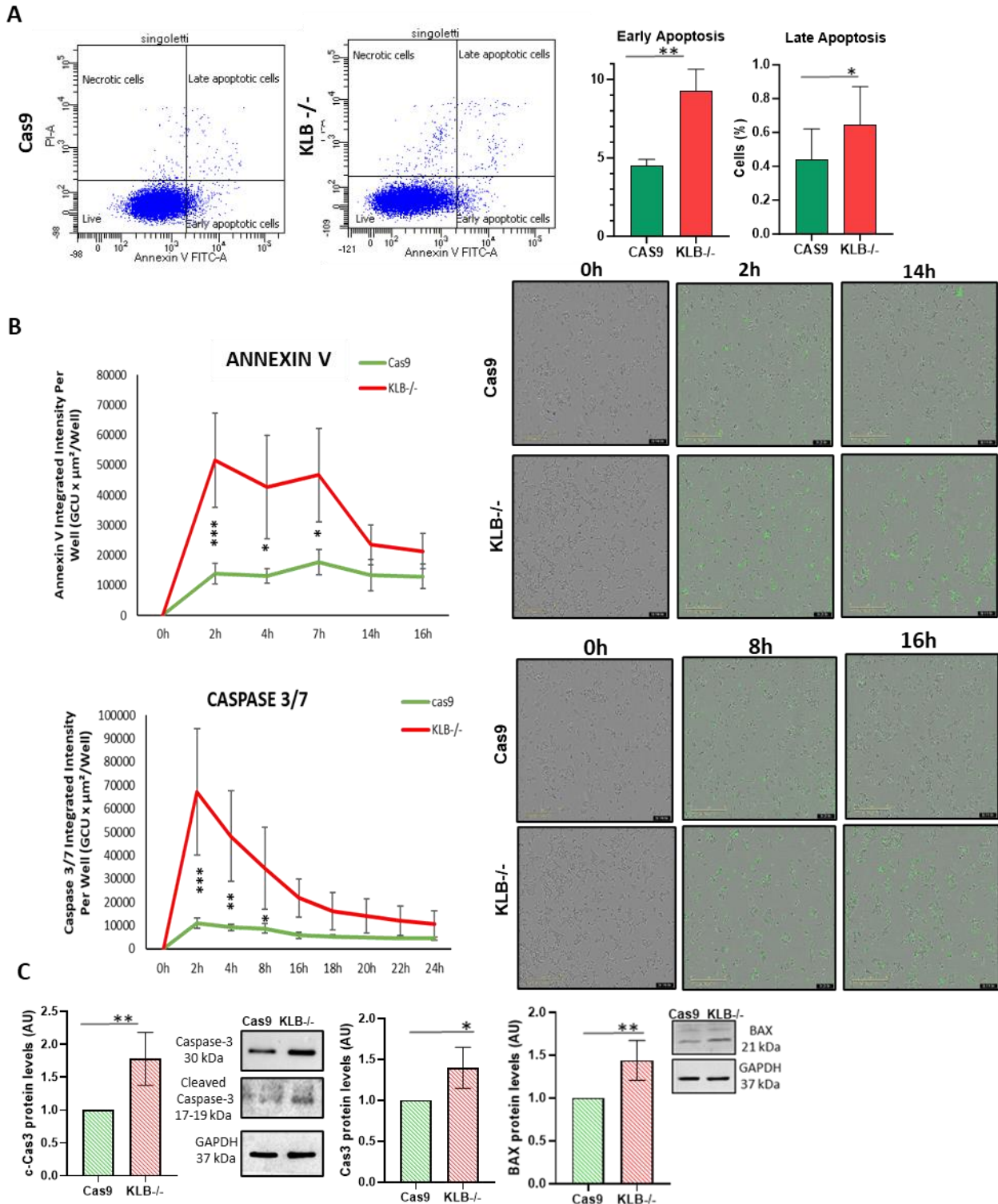


Figure 7. (A) Analysis of the cell apoptosis were performed by using FACS after labelling cells with Annexin V and PI. *KLB* KO model showed increased number of cells in early and late apoptosis compared to controls (** $p < 0.01$, * $p < 0.05$). Apoptotic cells were expressed ad percentage on total cell number. *KLB*^{-/-} showed increased number of cells in early and late apoptosis compared to controls (** $p < 0.01$, * $p < 0.05$). (B) Early and late apoptosis were investigated by testing Annexin V and Caspase 3/7 fluorescent dye (Sartorius) through Incucyte® SX5 platform. Annexin V and Caspase 3/7 signal was expressed as integrated intensity normalized on cell mask and T0 signal. Analyses were performed through the Incucyte software. *KLB*^{-/-} cells had increased positivity for Annexin V and Caspase 3/7 at different timepoints. (C) Immunoblot analysis performed on cell lysate revealed increased Cas3 and Cas3 cleaved form protein levels in *KLB*^{-/-} cells (** $p < 0.01$; * $p < 0.05$) and increased BAX protein levels in *KLB*^{-/-} cells (** $p < 0.01$). Ratios were measured using ImageJ and normalized on hGAPDH protein. Data are expressed as fold change (Arbitrary Unit (AU) vs control). At least three independent experiments were conducted. For bar graphs, data are expressed as mean and SE. Statistical correlations were assessed by unpaired t-test to compare the mean of two independent groups or by one-way/two-way ANOVA test for multiple parameters, adjusted for confounding factors. p values < 0.05 (two-tailed) will be considered statistically significant.

9. KLB depletion impairs the autophagic flux

Considering the exacerbation of the ER and oxidative stress found in *KLB*^{-/-} model along with the enhanced apoptotic rate we hypothesized that these cells may accumulate cellular breakdown products which need to be degraded. Thus, also other mechanisms of cellular degradation and recycling involved in NAFLD pathogenesis, such as autophagy, may be modulated in our model. To study the autophagic process we evaluated in *KLB*^{-/-} and in Cas9 cells the expression of: i) LC3 β (Microtubule-associated protein 1 light chain 3 beta), the main marker involved in the formation of the autophagosome; and ii) p62 protein called sequestosome 1 (p62/SQSTM1), which directly interacts with LC3 β , iii) p-Beclin-1, a key upstream autophagic regulation. To better understand the direction of the autophagic flux we have also used drugs inducing or inhibiting autophagy. In particular, we used, the pro-autophagic rapamycin activating the mTOR pathway, and cloroquine (CLQ) that blocks the autophagolysosome formation, thus inducing the intracellular accumulation of p62 and of LC3 β . As expected, we observed a gradual increase of p-Beclin-1 levels in Cas9 controls after the pro-autophagic stimulus with rapamycin for 3h and 24h, indicating a physiological response to the drug, (Cas 3h, $p < 0.01$ vs Cas9; Cas 24h, $p < 0.01$ vs Cas9), (**Figure 8A**). Moreover, *KLB*^{-/-} cells exhibited increased levels of p-Beclin-1 at the baseline ($p < 0.01$ vs Cas9) that were maintained higher compared with the non-treated controls at all the timepoints (3h, $p < 0.0001$ vs Cas9; 24h, $p < 0.0001$ vs Cas9). These results suggested an attempt in *KLB*^{-/-} cells to induce autophagy through upstream modulation. Interestingly, a significant reduction of p62 protein levels was observed in *KLB*^{-/-} cells and maintained also after the stimulus with rapamycin at different time points (baseline, $p < 0.001$ vs Cas9; 30', $p < 0.001$ vs Cas9 30'; 2h, $p < 0.0001$ vs Cas9 2h; 24h $p < 0.0001$ vs Cas9 24), (**Figure 8B**). WB and immunofluorescent analysis for LC3 β marker indicated a slightly increase of the cytosolic LC3 β form (LC3-I) in *KLB*^{-/-} cells, (baseline, $p < 0.0001$ vs Cas9; 30', $p < 0.001$ vs Cas9 30'; 2h, $p < 0.0001$ vs Cas9 2h). However, the consequent increase of LC3-II, the active

lipidated form that is associated with the increase of the autophagosomes number, was significantly downregulated in *KLB*^{-/-} cells both at the baseline and after the stimulus with rapamycin (baseline, $p < 0.0001$ vs Cas9; 30', $p < 0.0001$ vs Cas9 30'; 2h, $p < 0.0001$ vs Cas9 2h; 24h $p < 0.0001$ vs Cas9 24h). Contrarily, Cas9 cells showed a basal level of LC3II protein that was increased progressively after the treatment with rapamycin (Cas9 30', $p < 0.001$ vs Cas9; Cas9 3h, $p < 0.0001$ vs Cas9; Cas9 24h, $p < 0.0001$ vs Cas9); while, p62 levels were progressively hindered after treatment with rapamycin, indicating a physiological response of these cells to autophagic inductors, (Cas9 30', $p < 0.01$ vs Cas9; Cas9 3h, $p < 0.01$ vs Cas9; Cas9 24h, $p < 0.0001$ vs Cas9), (**Figure 8B**).

As expected, the blocking of autophagic flux with CLQ cause a significant increase of p62 protein in Cas9 cells, (Cas9 2h $p < 0.0001$ vs Cas9). A similar trend was observed in *KLB*^{-/-} that reported an accumulation of p62 in response to CLQ, even though at lower level than those observed in Cas9 cells, (baseline, $p < 0.001$ vs Cas9; 2h, $p < 0.001$ vs Cas9 2h), (**Figure 8C**), demonstrating no impairment of p62 turnover in our model. This data was further supported by immunofluorescence analysis acquired at confocal microscopy that showed a decreased p62 signal in *KLB*^{-/-} cells compared with Cas9, where there is a typical p62 round positive structures within the cytoplasm, (**Figure 8D**).

Interestingly, after treatments with CLQ, LC3-II form was accumulated in both *KLB*^{-/-} cells and controls, (Cas9 2h, $p < 0.001$ vs Cas9; *KLB*^{-/-} 2h, $p < 0.001$ vs *KLB*^{-/-}), but to a minor extent in our model, (*KLB*^{-/-} , $p < 0.0001$ vs Cas9; *KLB*^{-/-} 2h, $p < 0.01$ vs Cas9 2h), (**Figure 8C**). Moreover, immunofluorescent analyses performed at the baseline and after CLQ treatment revealed different distribution of LC3 β signal in *KLB*^{-/-} cells compared with Cas9 cells. In particular, *KLB*^{-/-} cells exhibited a more diffused and intense cytoplasmic pattern, indicating LC3-I positivity, while Cas9 cells showed a dotted pattern, typical for LC3-II positivity, (**Figure 8D**). This evidence suggests an impairment of the autophagic flux in *KLB*^{-/-}

/- cells that may fail in generating functional autophagosomes. Accordingly, the expression of the LAMP-2 protein, an essential component of the lysosomal membrane was reduced in *KLB* ^{-/-} cells ($p < 0.01$ vs Cas9), both at WB and immunofluorescence, indicating also a reduction of autophagolysosome number in our model, (**Figure 8E**).

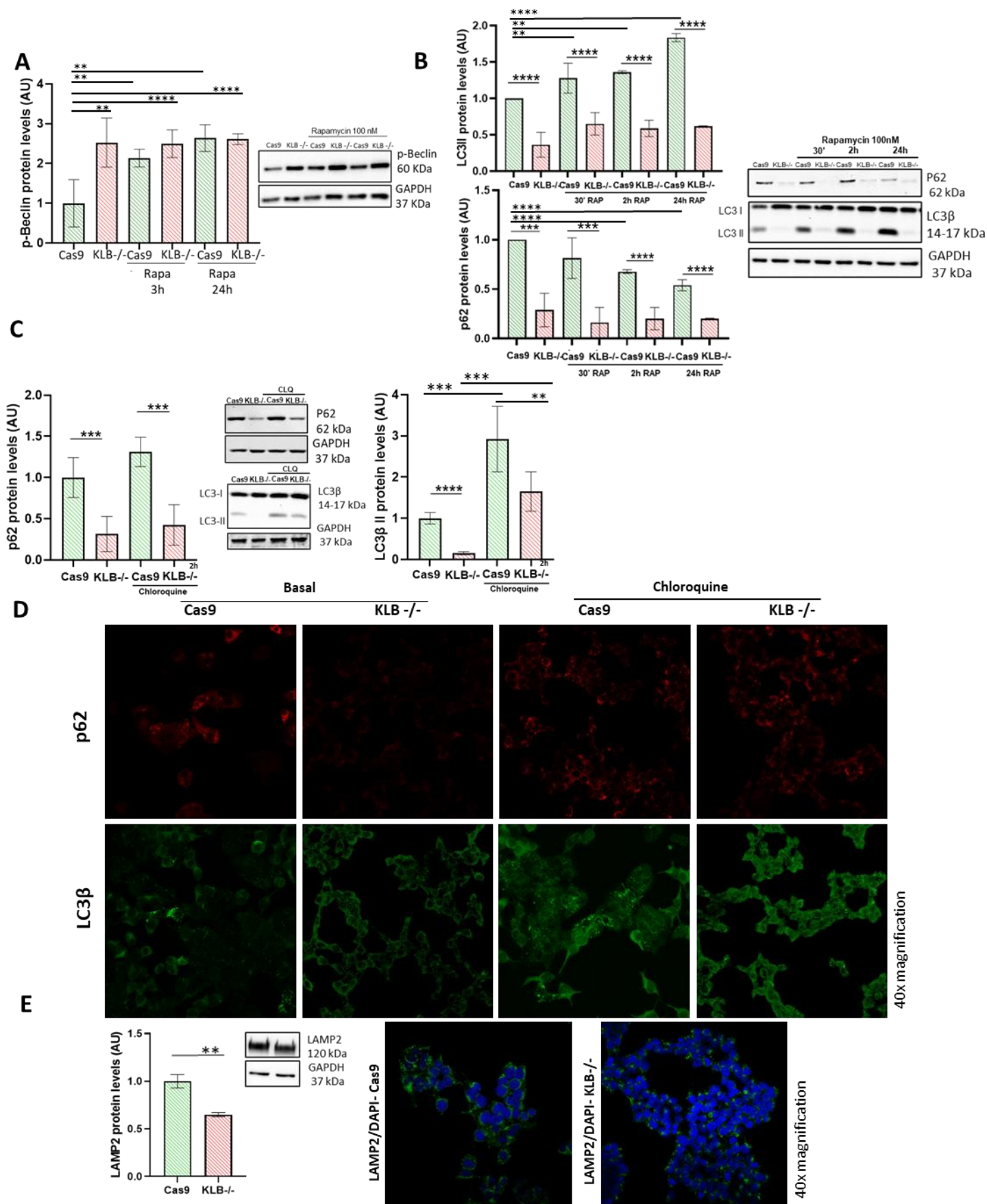


Figure 8. Stimulus with rapamycin 100nM was performed at 4 timepoints, 30', 2h, 3h and 24h. **(A)** Immunoblot analysis were performed on cell lysates and revealed increased pBeclin1 protein levels in KLB^{-/-} (***p*<0.01 vs Cas9) at the baseline and after treatment with rapamycin at 3h and 24h (*****p*<0.0001 vs Cas9). **(B)** p62 and LC3BII protein levels were measured by immunoblot analysis and found decreased in KLB^{-/-} cells, at the baseline and after treatment with rapamycin in all the timepoints (****p*<0.001 vs Cas9; *****p*<0.0001 vs Cas9). **(C)** Treatments with CLQ 10μM were performed on cells for 2h, then immunoblots were performed on extracted proteins. p62 protein was found downregulated in KLB^{-/-} cells at the baseline and after treatment with CLQ (****p*<0.001 vs Cas9; *****p*<0.0001 vs Cas9); LC3BII protein levels were decreased in KLB^{-/-} cells at the baseline and after treatment with CLQ (***p*<0.01 vs Cas9; *****p*<0.0001 vs Cas9); ratios were measured using ImageJ and normalized to hGAPDH protein. **(D)** Images were acquired at confocal microscopy, 40x magnification. KLB^{-/-} cells without CLQ showed less p62 signal and a different distribution of LC3B, compared to Cas9. KLB^{-/-} cells treated with CLQ had increased p62 signal respect to basal condition but fewer compared to Cas9 and a different distribution of LC3B signal is appreciated in KLB^{-/-} cells compared to Cas9. **(E)** WB analysis performed for LAMP2 protein revealed decreased LAMP2 protein levels in KLB^{-/-} cells (***p*<0.01), this evidence was also observed by immunofluorescence, LAMP2 rabbit antibody. Nuclei were stained with DAPI (1:10000, blue). Data are expressed as fold change (Arbitrary Unit (AU) vs controls). For bar graphs, data are expressed as means and SE. At least three independent experiments were conducted. **(F)** Statistical correlations were assessed by unpaired t-test to compare the mean of two independent groups or by one-way/two-way ANOVA test for multiple parameters, adjusted for confounding factors. *p* values<0.05 (two-tailed) will be considered statistically significant.

10. Effects of KLB depletion on inflammation:

Inflammation plays a central role in NAFLD progression, influencing both the transition from simple steatosis to NASH, and predisposing to liver fibrosis development. Thus, we investigated in our *KLB* KO model the activity of the transcriptional factor Nuclear factor kappa B (NF- κ B) that directly stimulates the production of pro-inflammatory cytokines. Notably, *KLB*^{-/-} cells compared to Cas9 cells had higher levels of NF- κ B (p<0.0001 vs Cas9) into the nucleus, and decreased levels of NF- κ B into the cytosol (p<0.0001 vs Cas9) with consequent increase of the NF- κ B nuclear/cytosolic ratio (p<0.0001 vs Cas9), (**Figure 9A**). We confirmed these results by immunofluorescence, which revealed increased nuclear positivity for the active-phosphorylated NF- κ B at the subunit p65 (Ser536) in *KLB*^{-/-} cells compared to controls where the protein exhibited exclusively a cytosolic localization, (**Figure 9B**). As consequence, TNF α (p<0.0001 vs Cas9), IL-1 β (p<0.0001 vs Cas9) and IL-6 (p<0.001 vs Cas9) cytokine and interleukins concentrations were found increased in *KLB*^{-/-} cell supernatants (**Figure 9C**), confirming the triggering of the inflammatory cascade.

To better characterize the role of KLB on the activation of the liver inflammation we performed a gene expression analysis by the Real-time PCR-Taqman OpenArray™ Platform. This method allowed us to evaluate in a multi-gene panel the simultaneous expression of 586 genes associated with pathological inflammatory conditions (OpenArray™ Human Inflammation Panel). From the analysis of this panel, we observed the significant modulation of 120 genes of which 75 genes were upregulated and 45 genes were downregulated in *KLB*^{-/-} cells when compared to Cas9 cells, (**Figure 9D**). Among the upregulated genes we found *IL-15*, (fold: 19.41, p<0.05) that directly promotes the expression of chemokines and several receptors for chemokines. Indeed, we observed the upregulation of genes encoding for chemokines receptors, such as *C-C Motif Chemokine Ligand 25 (CCL25)* and *C-C Motif Chemokine Receptor 9 (CCR9)*, (fold: 2.988, p<0.05; fold:

2.88, $p < 0.05$) which levels are usually increased in patients with NASH and contribute to fibrosis onset. In support of this finding, we also reported the upregulation of the *Chemokine (C-X-C motif) ligand 11 (CXCL11)* and the *C-X-C Motif Chemokine Receptor 6 (CXCR6)*, (fold: 3.02, $p < 0.05$; fold: 2.09, $p < 0.05$), which attract T cells to the liver, and promote liver inflammation and fibrosis. *Lipopolysaccharide-binding protein (LBP)*, which interacts with LPS in the membrane of stellate cells, Kupffer cells and liver macrophages directly inducing TNF-alpha gene expression, was further found upregulated in *KLB -/-* cells, (fold: 3.25, $p < 0.01$). Interestingly, *Toll Interacting Protein (TOLLIP)* that encodes for a negative regulator of TLR and NF- κ B signaling was also reduced in *KLB -/-* (fold: 0.53, $p < 0.01$). Of note, *TOLLIP* acts also as autophagy inducer.

11. KLB deficiency drives cells toward a malignant phenotype:

Considering the outbreak of many typical traits of severe liver damage observed in our model, we investigate whether KLB deletion may prompt the tumorigenic phenotype. With this aim, we first evaluated the impact of the KO on cell proliferation. Thus, we reported that KLB deficient cells displayed enhanced cell growth rate from 48 hours to 1 week at MTS assay ($p < 0.05$ at 48 hours and 72 hours vs Cas9; $p < 0.01$ at 1 week vs Cas9), and less cytotoxicity to anti-cancer therapy at MTS assay over 120h, when exposed to Sorafenib ($p < 0.001$ at 24 hours vs Cas9; $p < 0.05$ at 48 hours and 1 week vs Cas9), (**Figure 10A**). Afterwards, cell proliferation rate was analyzed by using the Incucyte® SX5 platform and FACS. The analysis of cell confluence over 48h, showed that *KLB*^{-/-} cells were more proliferative if compared to control cells ($p < 0.001$ vs Cas9), (**Figure 10B**). Furthermore, cell cycle analysis, through FACS with Propidium Iodide dye, revealed in *KLB*^{-/-} cells a higher number of cells in G2/M phase, than in controls ($p < 0.01$ vs Cas9), (**Figure 10C**), while Click-iT® EdU proliferation assay confirmed also the increase of S-phase in our model ($p < 0.01$ vs Cas9), (**Figure 10D**). The enhancement of cell proliferation was further supported by the increased expression of the proliferating cell nuclear antigen (PCNA), a crucial protein for DNA synthesis and a well-consolidated proliferation marker ($p < 0.01$ vs Cas9), (**Figure 10E**). Moreover, we investigated the effect of KLB depletion on the activation of several tumor markers and oncogenes, including *Jun Proto-Oncogene (cJUN)* ($p < 0.0001$ vs Cas9), *MCL1* ($p < 0.0001$ vs Cas9), *Fos Proto-Oncogene (cFOS)* ($p < 0.01$ vs Cas9), *BCL2 Apoptosis Regulator (BCL2)* ($p < 0.01$ vs Cas9) and *Dual Specificity Phosphatase 1 (DUSP1)* ($p < 0.0001$ vs Cas9), *Hypoxia Inducible Factor 1 Subunit Beta (HIF1 β)* ($p < 0.05$ vs Cas9), which mRNA levels were found increased in *KLB*^{-/-} cells (**Figure 11A**).

The effect of KLB depletion in inducing the pro-oncogenic phenotype in hepatocytes was also confirmed by data that revealed an increased ability of wound healing repair in *KLB*^{-/-}

cells compared to Cas9 cells ($p < 0.01$ at 24 hours and 48 hours vs Cas9), (**Figure 11B**). Finally, we evaluated the self-renewal ability of *KLB* KO cells by the analysis of free-floating cells aggregates in a 3D multicellular Tumor Spheroid model (TS) over 96 hours, using Incucyte® SX5 platform. Notably, from the analysis of phase contrast images (brightfield) carried out with a dedicated software, we observed that *KLB* KO caused a significant enlargement of the TS area and diameter in the last time points (72h, $p < 0.01$ vs Cas9; 96h, $p < 0.0001$ vs Cas9), (**Figure 11C**). These results together corroborate the hypothesis that *KLB* depletion triggers a constellation of pathological features, prompting cells to acquire a more malignant phenotype.

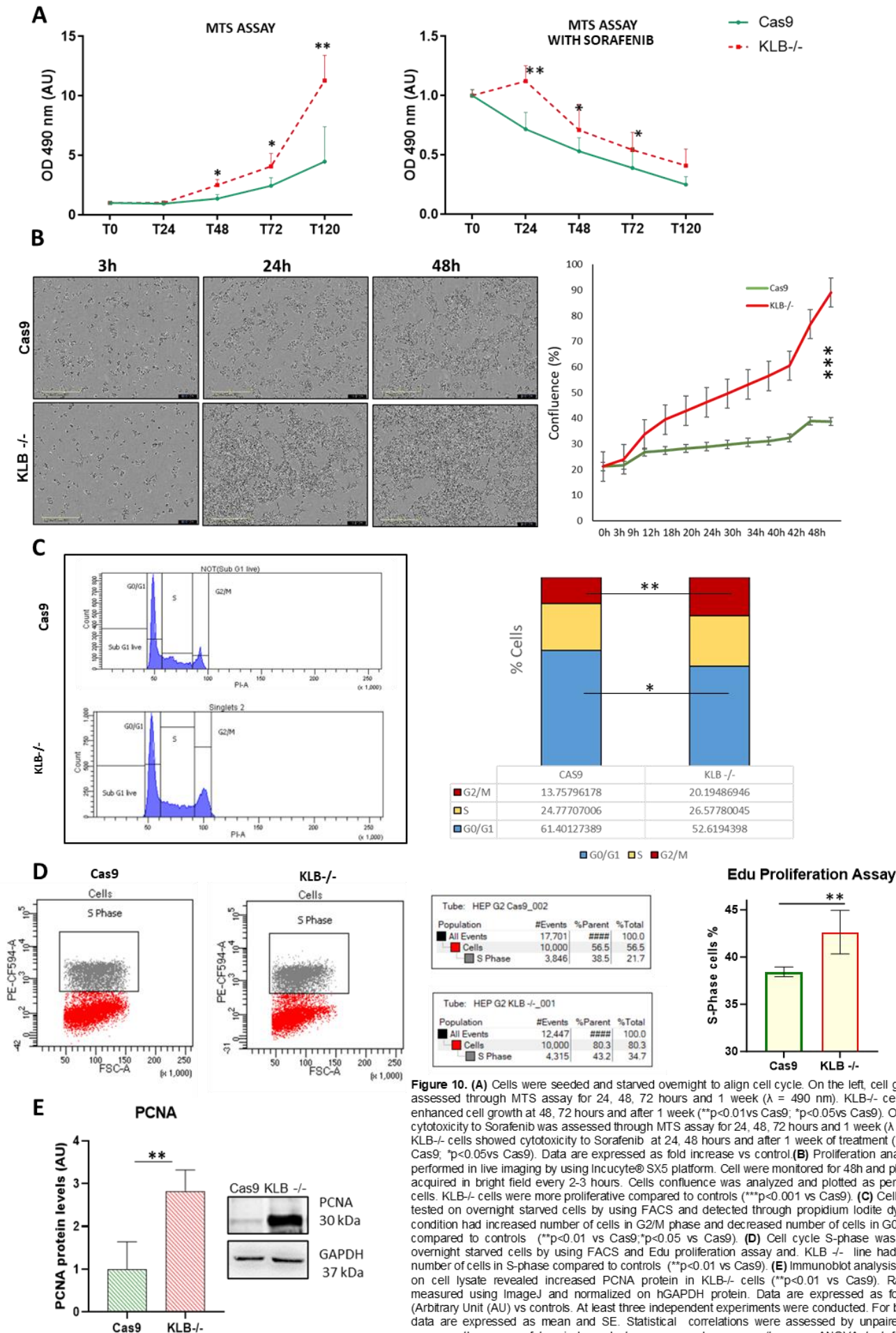


Figure 10. (A) Cells were seeded and starved overnight to align cell cycle. On the left, cell growth was assessed through MTS assay for 24, 48, 72 hours and 1 week ($\lambda = 490$ nm). KLB^{-/-} cells showed enhanced cell growth at 48, 72 hours and after 1 week (** $p < 0.01$ vs Cas9; * $p < 0.05$ vs Cas9). On the right, cytotoxicity to Sorafenib was assessed through MTS assay for 24, 48, 72 hours and 1 week ($\lambda = 490$ nm). KLB^{-/-} cells showed cytotoxicity to Sorafenib at 24, 48 hours and after 1 week of treatment (** $p < 0.01$ vs Cas9; * $p < 0.05$ vs Cas9). Data are expressed as fold increase vs control. (B) Proliferation analysis were performed in live imaging by using Incucyte® SX5 platform. Cell were monitored for 48h and photos were acquired in bright field every 2-3 hours. Cells confluence was plotted and expressed as percentage of cells. KLB^{-/-} cells were more proliferative compared to controls (** $p < 0.001$ vs Cas9). (C) Cell cycle was tested on overnight starved cells by using FACS and detected through propidium iodide dye. KLB^{-/-} condition had increased number of cells in G2/M phase and decreased number of cells in G0/G1 phase compared to controls (** $p < 0.01$ vs Cas9; * $p < 0.05$ vs Cas9). (D) Cell cycle S-phase was tested on overnight starved cells by using FACS and Edu proliferation assay and. KLB^{-/-} line had increased number of cells in S-phase compared to controls (** $p < 0.01$ vs Cas9). (E) Immunoblot analysis performed on cell lysate revealed increased PCNA protein in KLB^{-/-} cells (** $p < 0.01$ vs Cas9). Ratios were measured using ImageJ and normalized on hGAPDH protein. Data are expressed as fold change (Arbitrary Unit (AU) vs controls. At least three independent experiments were conducted. For bar graphs, data are expressed as mean and SE. Statistical correlations were assessed by unpaired t-test to compare the mean of two independent groups or by one-way/two-way ANOVA test for multiple parameters, adjusted for confounding factors. p values < 0.05 (two-tailed) will be considered statistically significant.

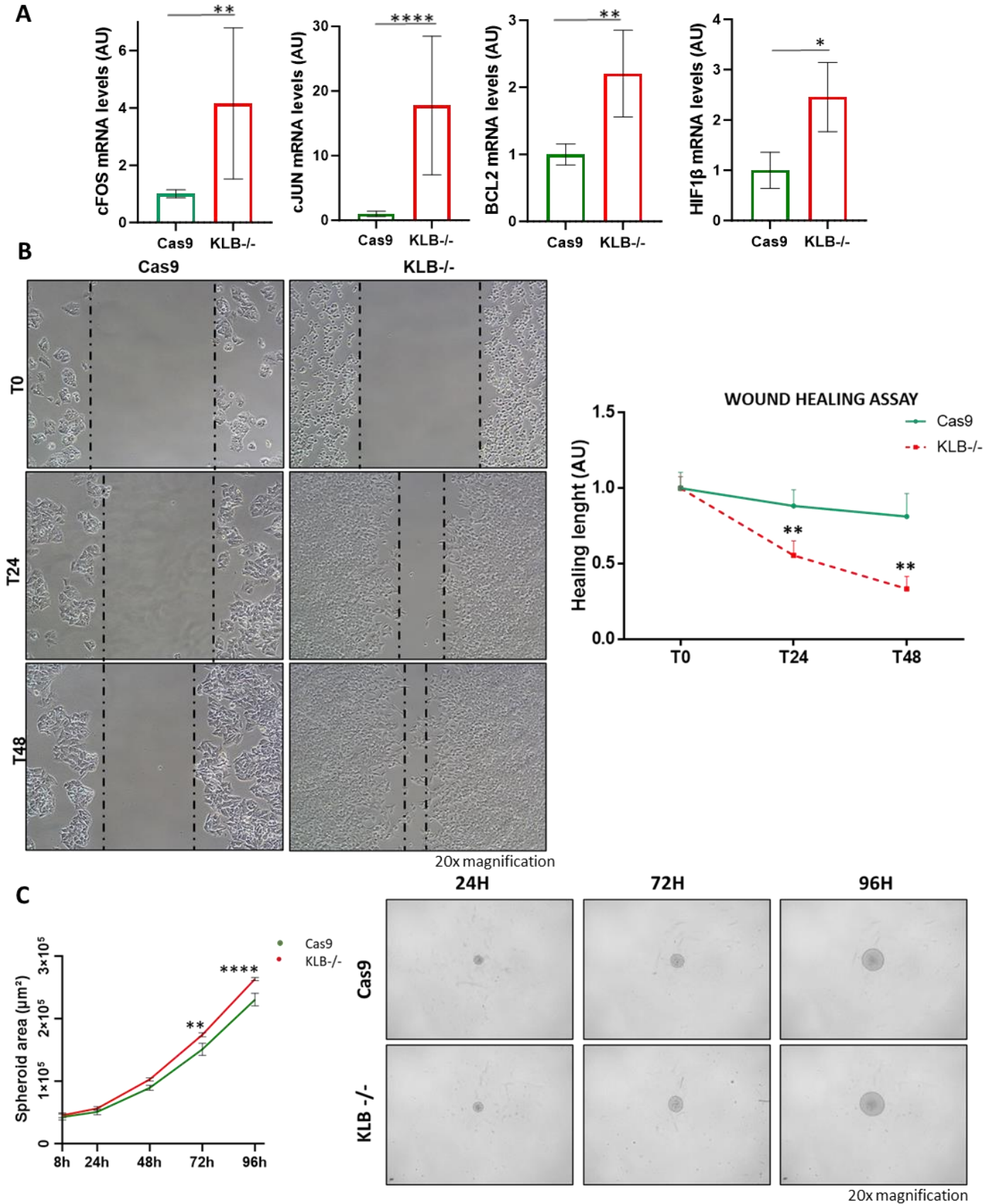


Figure 11. (A) *cFOS*, *cJUN*, *BCL2* and *HIF-1B* mRNA expression were evaluated by reverse transcription quantitative PCR and normalized to the *h-GAPDH* housekeeping. All the gene were found significantly increased in *KLB*^{-/-} cells (***p*<0.05 vs Cas9; ***p*<0.01 vs Cas9; *****p*<0.0001 vs Cas9). Data are expressed as fold change (Arbitrary Unit (AU) vs controls). At least three independent experiments were conducted. For bar graphs, data are expressed as mean and SE **(B)** Representative images of the wound healing assay were acquired in brightfield at 0, 24, 48 hours (magnification, 100X). The scratch width is indicated by the dotted lines and was measured by using ImageJ software. Wound healing repair was increased in *KLB*^{-/-} cells at 24 and 48 hours (***p*<0.01 vs Cas9). **(C)** For spheroid formation assay cells were seeded in ultra-low attachment plates for 96 hours and tumor spheroid area was measured with the Incucyte® SX5 software. Images were acquired in brightfield at 20x magnification using the Incucyte® SX5 platform. *KLB*^{-/-} cells generates larger tumor spheroid at 72h and 96h compared to controls (72h, ***p*<0.01 vs Cas9) (96 h, *****p*<0.0001 vs Cas9). Statistical correlations were assessed by unpaired t-test to compare the mean of two independent groups or by one-way/two-way ANOVA test for multiple parameters, adjusted for confounding factors. *p* values<0.05 (two-tailed) will be considered statistically significant

12. KLB depletion promotes the switching towards a mesenchymal phenotype:

Based on the latest results, we investigated the possible involvement of KLB in the processes related to the epithelial-mesenchymal transition (EMT). EMT is a very complex process at the molecular level which involves different biological events that converge in the loss by the epithelial cells of their organ-specific features leading to the acquisition of the typical properties of the mesenchymal cells. Thus, we analyzed the expression of 609 stem cell-related and pluripotency-related genes using the commercially available TaqMan™ OpenArray™ Human Stem Cell Panel, QuantStudio. Notably, the KLB KO induced the upregulation of a total of 114 genes and the downregulation of a total of 49 genes (**Figure 1A**). Next, we performed the Reactome enrichment analysis, considering separately the statistically significant upregulated and downregulated genes. As shown in **Figure 12B**, among the enriched terms, we found in our model, upregulation of pathways related to cellular response to stress, cell cycle and mitosis and to the transcriptional regulation of TP53. While, among the dampened entities, we found downregulated pathways related to signal transduction by growth factors, metabolisms of lipids, regulation of Insulin-like Growth factor and MAPK family signaling. Instead, genes belonging to the immune system, and to the cytokines and interleukins signaling were both up- and down-regulated in KLB $-/-$ cells compared to controls. Specifically, we found in KLB $-/-$ cells the upregulation of important mediators in the EMT process, such as *TGFB2*, ($p < 0.01$ vs Cas9) member of the transforming growth factor β (TGFB) family, the *matrix metalloproteinase-14 (MMP14)*, ($p < 0.01$ vs Cas9) which promotes cancer cell invasion and metastases, *WNT3a* ($p < 0.05$ vs Cas9) accountable for the modulation of β -catenin, *c-Myc* ($p < 0.01$ vs Cas9), and cyclin D1 during EMT. Moreover, we found in KLB $-/-$ cells the upregulation of the *Runt-Related Transcription Factor 2 (RUNX2)*, ($p < 0.01$ vs Cas9), which modulating Galectine-3 expression may regulate cell invasion and migration in HCC. Among the downregulated genes were listed several effectors of the lipid metabolism and storage, as observed in

previously reported data. Interestingly, was reported the downregulation of AFP ($p < 0.0001$ vs Cas9), a known hepato-specific cancer marker. EMT was further tested by evaluating the expression of important epithelial markers including E/N cadherin, cytocheratin8/18 (CK-18) and the phosphorylated Focal Adhesion Kinase (p-FAK). On the other hand, Vimentin (VIM) expression was evaluated as mesenchymal marker. Gene expression analyses showed that KLB KO was associated with a significant decrease in gene expression of all the four considered epithelial markers, *E-cadherin (CDH1)* ($p < 0.001$ vs Cas9), *N-cadherin (CDH2)* ($p < 0.01$ vs Cas9), *CK 18 (KRT18)* ($p < 0.001$ vs Cas9); while Vimentin gene and protein expression were increased ($p < 0.01$ vs Cas9; $p < 0.0001$ vs Cas9). Accordingly with these results, E-cadherin protein levels were decreased ($p < 0.001$ vs Cas9), while Vimentin and p-FAK protein levels were increased in our model (Vimentin, $p < 0.001$ vs Cas9; p-FAK, $p < 0.01$ vs Cas9) (**Figure 13A**). These analyses were further supported by the immunofluorescence imaging highlighting the loss of CK-18 protein, the different cytosolic compartmentalization of E-cadherin, the increase of Vimentin signal in KLB^{-/-} cells and the nuclear localization of p-FAK. (**Figure 13B**).

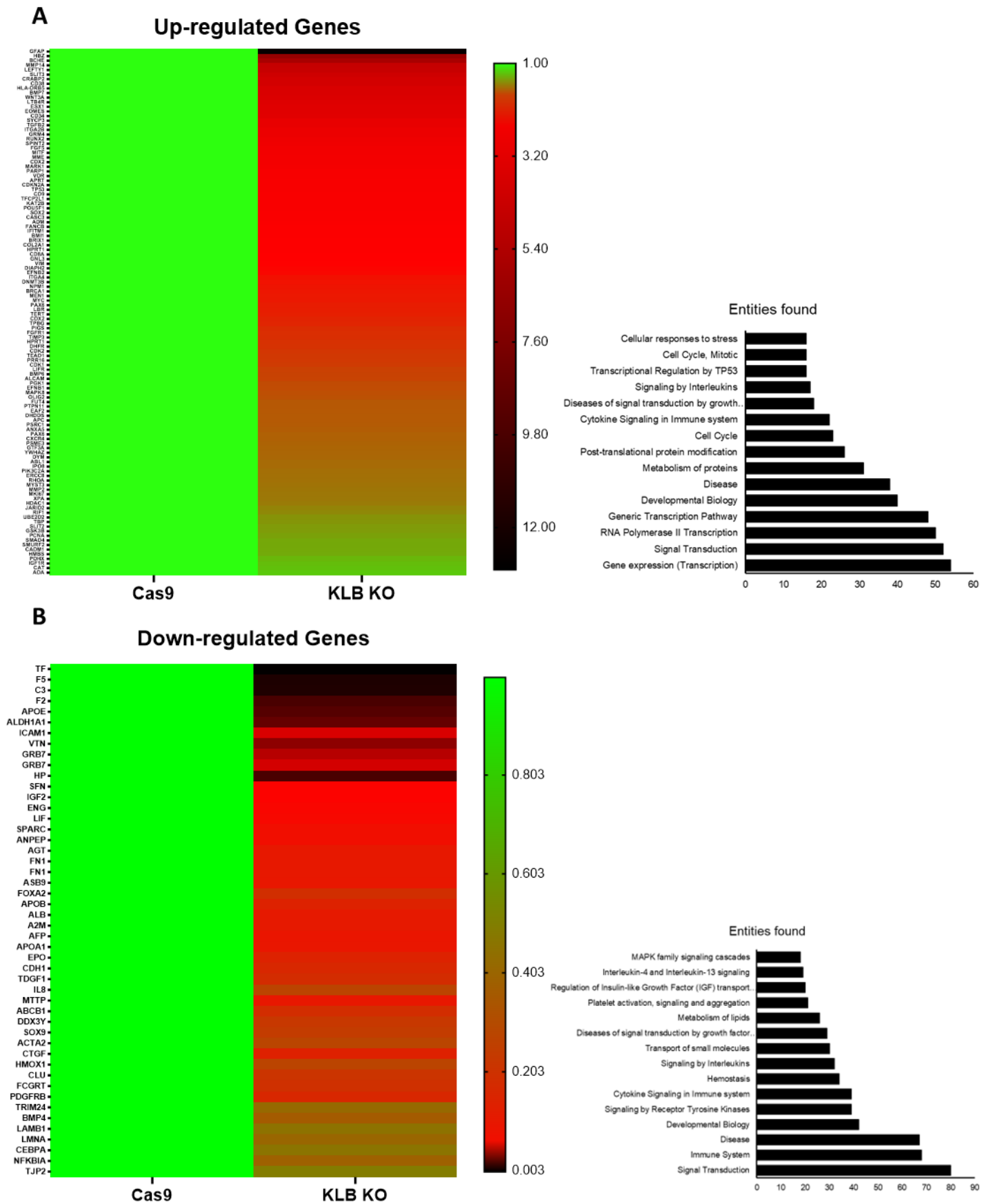


Figure 12. OpenArray™ Human Stem Cell Panel was performed on cDNA isolated from KLB^{-/-} cells and controls (2000ug). Gene expression curves were normalized on expression of multiple housekeeping genes and folded on controls. Heatmaps were plotted by using an online available tool. Reactome pathways associated with genes that are differently expressed between KLB^{-/-} cells and controls were ranked in entities graphed. **(A)** Heatmap and entities graph for differentially expressed and statistically significant upregulated gene. **(B)** Heatmap and entities graph for differentially expressed and statistically significant downregulated genes. Statistical correlations were assessed by unpaired t-test to compare the mean of two independent groups or by one-way/two-way ANOVA test for multiple parameters, adjusted for confounding factors. p values < 0.05 (two-tailed) will be considered statistically significant.

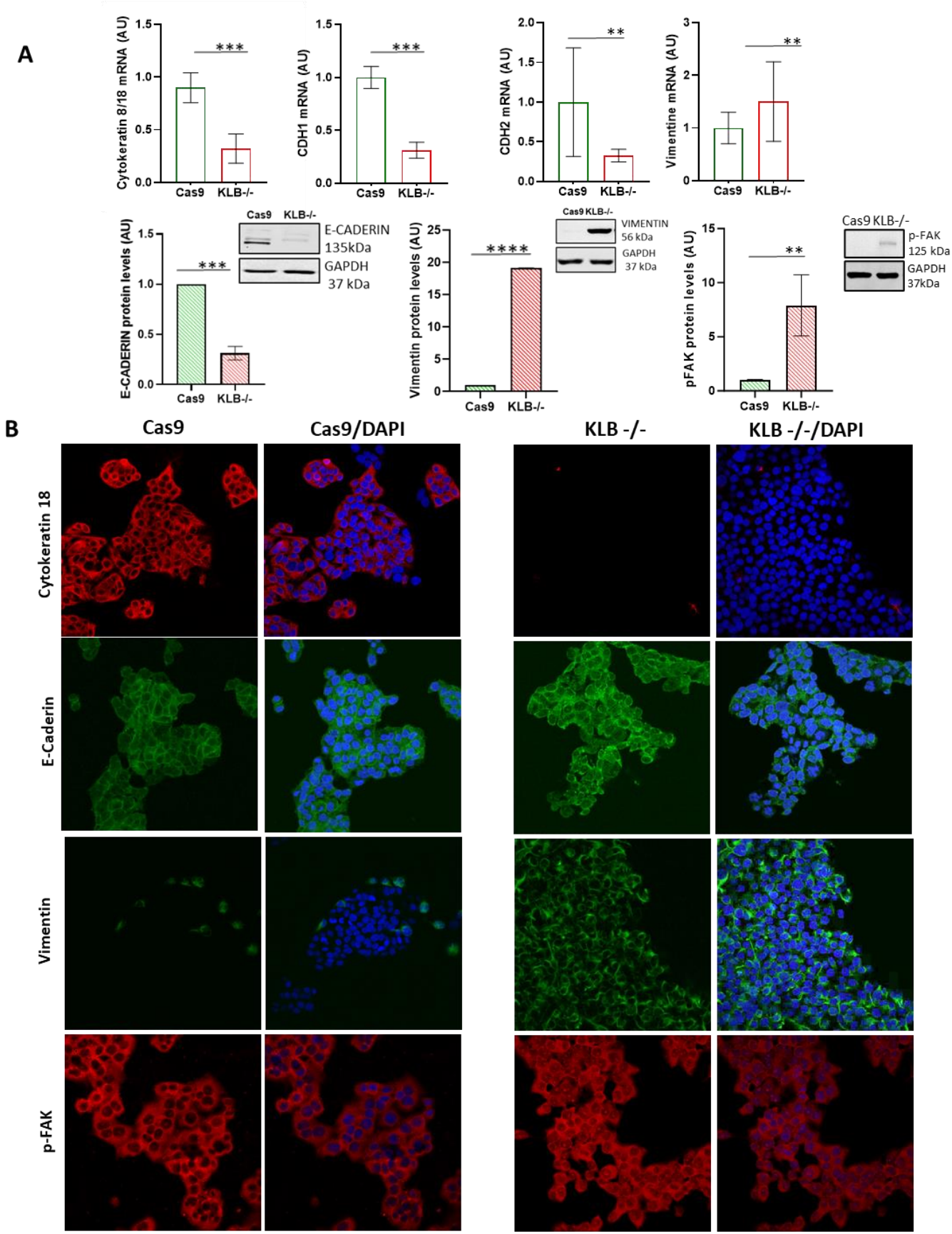


Figure 13 (A) Gene expression analyses were performed with TaqMan Real-time qPCR and expression curves were normalized on h-GAPDH. *Cytokeratin-18*, *E-Cadherin* (*CDH1*) and *N-Cadherin* (*CDH2*) were downregulated in *KLB*^{-/-} cells ($***p < 0.01$ vs Cas9), while *Vimentin* was upregulated in *KLB*^{-/-} cells ($**p < 0.01$ vs Cas9). Data are expressed as fold change (Arbitrary Unit (AU) vs controls). Immunoblot analysis performed on cell lysates revealed decreased levels of E-Cadherin protein and increased of Vimentin and pFAK protein levels in *KLB*^{-/-} cells ($**p < 0.01$; $***p < 0.001$; $****p < 0.0001$ vs Cas9). Ratios were measured using ImageJ and normalized on hGAPDH protein. Data are expressed as fold change (Arbitrary Unit (AU) vs controls). At least three independent experiments were conducted. For bar graphs, data are expressed as mean and SE. (B) Immunofluorescent assays were performed on fixed cells incubated with specific CK8/18 mouse antibody, E-Cadherin rabbit antibody, Vimentin rabbit antibody and pFAK rabbit antibody. Nuclei were stained with DAPI (1:10000, blue). Images were acquired at confocal microscopy, 40x magnification. *KLB*^{-/-} cells lose the expression of the epithelial marker CK-18 (red) compared to controls and showed a different distribution of E-cadherin protein (green), specifically cytosolic in *KLB*^{-/-} cells and of membrane in controls. Vimentin (green) signal was strongly increased in *KLB*^{-/-} cells which further report the nuclearization of pFAK (red) signal. Statistical correlations were assessed by unpaired t-test to compare the mean of two independent groups or by one-way/two-way ANOVA test for multiple parameters, adjusted for confounding factors. p values < 0.05 (two-tailed) will be considered statistically significant

AIM2: Characterization of the rs12152703 KLB variant in pediatric and adult patients with NAFLD

2.1 KLB rs12152703 variant may be protective against severe liver disease in NAFLD patients

The overall cohort consisted of 1311 consecutively enrolled patients with European descent NAFLD, of whom 261 were children. All the children were pediatric patients with biopsy-proven NAFLD, evaluated at Bambino Gesù Children's Hospital between September 2011 and December 2021, while the latter were 1050 unrelated adult patients with biopsy-proven NAFLD consecutively enrolled from the Metabolic Liver Diseases outpatient service at Fondazione IRCCS Ca' Granda of Milan between January 1999 and December 2021. Inclusion criteria were the availability of a liver biopsy specimen for suspected NASH or severe obesity, DNA samples, and clinical data. Other causes of liver disease including increased alcohol intake (>30/20 g/day in males/females), viral and autoimmune hepatitis, hereditary hemochromatosis, alpha1-antitrypsin deficiency, and history, Wilson disease, and infection with hepatitis B or hepatitis C were excluded.

The KLB rs12152703 G>T intronic variant was genotyped in the overall patient cohort and reported a frequency distribution of 0.41. This data was further compared with 1000 genomes Europeans not Finnish cohort that showed a similar frequency distribution of 0.38. At multivariate generalized linear model adjusted for age, sex, body mass index (BMI), T2D and the presence of the 3 risk variants for NAFLD (PNPLA3 G allele, TM6SF2 T allele and TMC4 T allele), the KLB rs12152703 G>T intronic variant was significantly correlated with dampened transaminase levels, marker of liver damage (ALT, $p = 0.06$, $\beta = -0.03$, 95% CI -0.06 to -0.002; AST, $p = 0.045$, $\beta = -0.04$, 95% CI -0.08 to -0.0008; GGT $p < 0.001$, $\beta = 0.13$, 95% CI -0.08 to -0.06), (**Figure 14A**). Furthermore, at two different ordinal logistic regression models adjusted as in the previous analysis, the rs12152703 variant was

associated negatively with the presence of NASH (p 0.031; β = -0.15; 95% CI, -0.28 to -0.013); and positively with a lower NAFLD activity score (NAS) (p = 0.023, β = -0.14 95% CI -0.25 to -0.02). **Figure 14A.**

2.2 Circulating levels and hepatic expression of KLB in association with the rs12152703 variant genotypes in a subset of pediatric patients.

Furthermore, we examined the soluble (sKLB) and hepatic (hKLB) KLB levels in patients within a pediatric cohort. The expression of sKLB was evaluated by a commercially available ELISA assay on the plasma from 137 children with NAFLD and stratified for genotype. The analysis (**Figure 14B**) showed that individuals carrying the KLB rs12152703 mutation, exhibited higher levels of sKLB than wt subjects (GG), with more pronounced effect with TT homozygote genotype (GG vs GT, $p < 0.05$, 95.00% CI of diff. : -46.69 to -0.1422; GG vs TT, $p < 0.0001$, 95.00% CI of diff: -124.5 to -44.12; GT vs TT, $p < 0.01$, 95.00% CI of diff: -102.3 to -19.51)

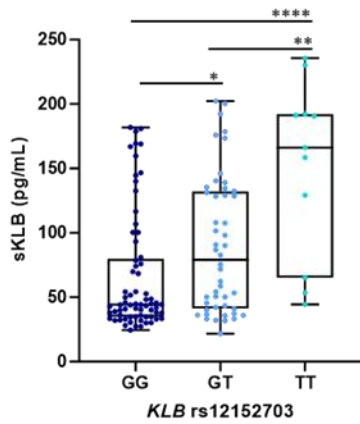
The expression of hKLB was assessed by quantitative analysis of immunofluorescent imaging in a subset of 80 children affected by NAFLD. As shown in **Figure 14C**, the rs12152703 variant was found to be associated with increased levels of hKLB, with a stronger effect with the TT genotype. (GG vs TT, $p < 0.0001$, 95.00% CI of diff: -0.4722 to -0.1491; GT vs TT, $p < 0.01$, 95.00% CI of diff: -0.3914 to -0.05331).

Therefore, these data suggest a probable gain-of-function of the KLB protein in individuals carrying the KLB rs12152703 mutation, with more pronounced effect in presence of the allele TT.

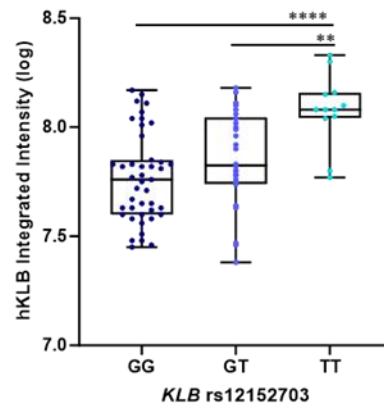
A

rs12152703	Estimate (β)	95% CI	P-value
ALT, IU/mL	-0.03 \pm 0.01	-0.06-0.002	0.06
AST, IU/mL	-0.04 \pm 0.02	-0.08- -0.0008	0.045*
GGT, IU/mL	-0.13 \pm 0.04	-0.20- -0.06	0.0004*
Histological NASH	-0.15 \pm 0.07	-0.28- -0.013	0.031*
NAFLD Activity Score (NAS)	-0.14 \pm 0.06	-0.25- -0.02	0.023*

B



C



hKLB/DAPI

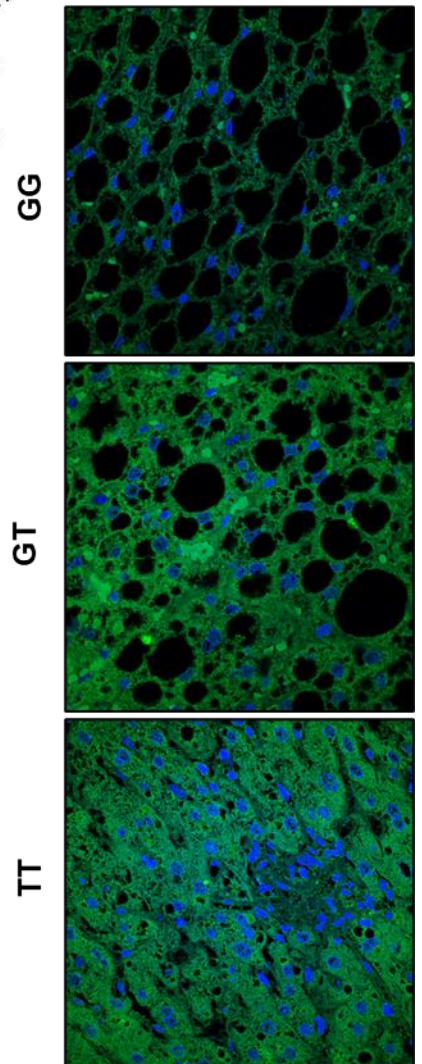


Figure 14. (A) Different multivariate model, adjusted for sex, age, BMI, Type 2 diabetes (T2D), *PNPLA3* rs738409 I14M G allele, *TM6SF2* rs58542926 E167K T allele and *TMC4* rs641738 T allele. The analysis was performed on a total of 1311 subjects and the presence rs12152703 variant was used as dependent variable **(B)** sKLB levels were detected by using commercially available ELISA kit and **(C)** hKLB levels were quantified from immunofluorescence analyses on NAFLD patients divided for KLB rs12152703 variant genotypes. Both sKLB and hKLB levels increase in presence of KLB rs12152703 variant T allele. **(C)** Representative immunofluorescent images were reported based on KLB rs12152703 variant genotypes. Statistical correlations were assessed by multivariate analysis to correlate multiple parameters and by one-way/two-way ANOVA test to analyze KLB levels depending on genotype, adjusted for confounding factors. p values < 0.05 (two-tailed) were considered statistically significant.

DISCUSSION

This study was aimed at elucidating the implication of KLB on NAFLD pathogenesis. The project has been exploited by evaluating in *in vitro* the effect of the full *KLB* knock-out, and the impact of the less-known rs12152703 *KLB* variant on NAFLD patients. The preliminary data underpinning this study, showed that the *KLB* rs17618244 variant was associated with more severe liver damage, but not with steatosis in pediatric and adult patients with NAFLD. Moreover, carriers of this variant had increased risk of developing ballooning and lobular inflammation. In an adult cohort the rs17618244 variant was demonstrated to be further associated with hepatic fibrosis and with traits of advanced liver damage [56]. In our series, patients carrying the variant showed a significant reduction of soluble *KLB* and FGF19 plasma levels with a parallel decreased of the hepatic *KLB* expression (h*KLB*), suggesting that rs17618244 variant was associated to reduction of both soluble and hepatic *KLB*.

On these premises, the laboratory of metabolic diseases at the Policlinico Ca' Granda of Milan generated a full *KLB* KO HepG2 cell line, aimed at reproducing in *in vitro* the effects of the *KLB* rs17618244 variant. The resulting cells reported almost the total absence of *KLB* both at gene and protein level and exhibited a significant reduction of the active auto phosphorylated form of FGFR4 at the baseline and in presence of FGF19 stimulus, highlighting *KLB*/FGFR4 signal interruption. Accordingly, we observed that the *KLB* KO, shut down the signaling triggered from *KLB*/FGFR4 complex activation. This resulted in the downregulation of p-ERK and p-P38 two important *KLB* downstream effectors [70, 105]. Notably, p-ERK lowering was maintained also after the stimulus with FGF19, correlating the absence of *KLB* to the impairment of its downstream signaling. Interestingly, all these findings highlight the *KLB* dependent regulation of FGFR4 also without FGF19, revealing a possible alternative mechanism for the *KLB*/FGFR4 complex activation independent from their specific ligand. One possible hypothesis is that FGFR4/*KLB* complex in the liver,

independently of FGF19 binding, may trigger other pathways by the interaction with other membrane-related proteins, such as Galectin-3 [106]. This hypothesis could be relevant for the treatment of NASH-related fibrosis because trials with Galectin-3 inhibitors are currently ongoing in patients with NASH [107]. Next, we evaluated the impact of KLB depletion on hepatocytes homeostasis and we observed that lipid metabolism was strongly impaired in *KLB* *-/-* cells, resulting in the downregulation of pivotal genes involved in lipogenesis, lipid absorption, lipid uptake and transports, such as *FAS*, *PPAR γ* , *CD36* and *ACSL1*. KLB impact on the dysregulation of the lipid handling was further confirmed through cell imaging, showing that *KLB* *-/-* cells were characterized by decreased number and size of lipid droplets within and decreased levels of ApoB [108]. Accordingly, important mediators involved in triglycerides biosynthesis such as *DGAT1* and *DGAT2*, as well as factors involved in FA β -oxidation, such as *CPT1*, *PPAR α* and *PGC1 α* [109], were found downregulated in our model also after exposing cells to a lipid load with FAs. This implies that the deleterious effects of the *KLB* KO on lipid metabolism seems to be independent of the lipid accumulation, resembling what observed in patients carrying the rs17618244 variant, which was not correlated with hepatic steatosis [55, 56]. We further demonstrated that the absence of KLB negatively affects the cholesterol production, uptake and transport. Thus, we observed in our model the downregulation of *HMGCoA*, *SREBP2*, *ACSS2*, *DHCR7*, *LDLR*, *SR-B1*, *LXR α* and of the ABC transporters genes. Nevertheless, the *KLB* *-/-* cells showed the upregulation of BAs production at gene level and increased intracellular BAs content. We assume that this increase may be caused by the disruption of the FGF19 signaling, being no longer able to inhibit BAs production. As consequence, all the cholesterol available would be rapidly converted into BAs that are accumulated within the cell, inducing toxicity [83, 110]. Nevertheless, further analyses on the BAs should be performed to confirm these findings. These evidence together support the establishment of several typical NAFLD traits driving to disease worsening and progression to NASH [111]. Indeed, in NAFLD, is reported also

an increased ER stress with consequent rise in ROS levels that exacerbate in patients and in high-fat-diet (HFD) mice the liver damage [112, 113]. Accordingly, in our experiments *KLB*^{-/-} cells reported the up-regulation of key ER stress effectors such as *ATF4* and *ATF6*. Oxidative stress was also augmented through the increasing of ROS, RNS and H₂O₂ levels, suggesting a disruptions of the hepatocyte homeostasis [114]. In these conditions, ROS work as signaling molecules, and their production is countered by non-enzymatic and enzymatic antioxidant mechanisms such as MnSOD2 and NRF2, found activated in our model. As was reported in patients, during NAFLD the liver damage is exacerbated by cellular stress and chronic JNK stimulation which together prompt cells apoptosis [114, 115]. As expected, *KLB*^{-/-} cells reported the activation of the JNK signaling and were more apoptotic compared to controls, in terms of early and late apoptosis. Apoptosis was further supported in *KLB* KO model from the activation of key apoptotic effectors such as BAX and the cleaved Caspase-3 [116]. Considering the wide effect of *KLB* depletion on the hepatocyte homeostasis, we supposed that the high load of breakdown products, accumulated by *KLB*^{-/-} cells, as a consequence of the enhanced cellular stress and apoptosis, would have triggered the activation of the canonical macro-autophagy process in attempt to restore physiological conditions. Indeed, our results highlighted a central role of *KLB* in the regulation of the autophagic flux. Specifically, *KLB*^{-/-} cells reported the up-regulation of the Beclin-1, probably the phosphorylated form, indicating the initial effort to up-stream regulating the autophagic flux, in response to stress [117]. On the other hand, *KLB* depletion may have a dual effect, downregulating p62 and abolishing the lipidation of LC3, necessary for its activation. This resulted in an aberrant formation of functional autophagosomes determined also by the downregulation of the autophagolysosome protein LAMP2 [118]. As result, the whole autophagic flux was dysfunctional after *KLB* KO. Although we still have to demonstrate the underlining mechanism, it is conceivable that this impairment could be caused by the downregulation of crucial enzymes, such as the one

belongs to the ATG family, involved in LC3 lipidation and needed for the autophagosome elongation [119].

The resulting conditions, triggered the activation of the inflammatory response in *KLB* ^{-/-} cells [120]. Indeed, we found that *KLB* depleted cells had higher nuclear expression of the active NF- κ B form, which usually initiates liver inflammation in NAFLD patients [121]. The activation of the NF- κ B transcriptional activity in *KLB* ^{-/-} cells, led to higher cytokine and interleukins production, resulting in increased levels of TNF α , IL1 β , IL-6 [122]. The inflammatory response was further supported by the upregulation of important genes involved in chemokines expression and signaling, reflecting in *in vitro* what previously observed in patients carrying the *KLB* rs17618244 genetic variant [55, 56].

In summary, all the pathological traits observed in *KLB* KO cells suggest the establishment of severe damage of the hepatocyte homeostasis, experienced, in patients during NAFLD progression and advanced stage of liver injury.

Considering that the chronic liver injury during NAFLD progression provided a fertile soil for the onset of hepatocarcinogenesis [123], we also evaluated the effect of *KLB* depletion on the acquisition of a malignant phenotype. In particular, we evaluated the impact of the *KLB* KO on several tumorigenic traits. Interestingly, we observed that hepatocytes in the absence of *KLB* are more proliferative compared to controls, in term of cell growth and of cell proliferation. These data were also supported by cell cycle analysis, highlighting in *KLB* KO model, a higher number of cells in phase S and in phase M along with gained expression of PCNA, a well consolidated tumorigenic marker for HCC [124, 125]. The acquisition of a pro-tumorigenic phenotype was further supported by the upregulation of important liver proto-oncogenes such as *cFOS*, *cJUN*, *BCL2*, and *HIF1 β* , suggesting the establishment of pro-carcinogenic conditions [126]. Moreover, *KLB* ^{-/-} cells were more resistant to Sorafenib, an anticancer therapy which has been firstly delivered to HCC patients, and showed increased

invasiveness to the wound healing assay [127]. All these findings corroborate the hypothesis that *KLB* deficiency may predispose to the acquisition of a more malignant phenotype in hepatoma cells lines promoting also other cancerogenic pathways such as cell migration, metastasis and the EMT. In this regard, we assessed the tumorigenic and stemness behavior through the 3D Tumor Spheroid assay and performing a RT qPCR-based gene panel, evaluating simultaneously the expression of 609 stemness- and pluripotency-related genes. The results of these analyses reveal that *KLB* *-/-* cells generate larger tumor spheroids compared to controls and overexpress pivotal effectors involved in the transition towards a mesenchymal phenotype. Among these effectors we reported the upregulation of genes belonging to the transforming growth factor β (TGFB) family, genes encoding for the matrix metalloproteinases, and mediators of the β -catenin signaling [28, 128, 129]. Moreover, we demonstrated that *KLB* KO confers stemness and pluripotency features and upregulates pathways related to cellular response to stress, cell cycle and mitosis, and to the transcriptional regulation of TP53, further supporting all the previous data. Moreover, *KLB* *-/-* cells lose the expression both at gene and protein level of important epithelial markers such as E/N-cadherin and CK-18. Concomitantly these cells acquire the expression of Vimentin and nuclear pFAK, two markers associated to the mesenchymal phenotype.

On the other hand, regarding patients, the poorly investigated *KLB* intronic variant rs12152703 was evaluated in the overall cohort of 1311 NAFLD patients and controls. Notably, the variant was found to be protective against advanced NAFLD, in terms of lowered predisposition to develop NASH, lowered NAFLD activity score (NAS) and decreased transaminase levels. The effect of this variant seems to be the opposite of the previously characterized rs17618244 at-risk variation which abolish *KLB* activity driving towards NAFLD worsening [5]. Moreover, in a subset of patients belonging to the pediatric cohort, the rs12152703 variant was associated with higher levels hepatic *KLB* and of soluble

KLB compared to the *WT* genotype. Therefore, this new variant might encode for a more stable KLB protein thus reducing the risk of a severe liver damage in patients. Nevertheless, even if promising, our results remain preliminary and a deeper assessment of hKLB and sKLB forms on a larger number of patients including also adult subjects is deemed. Thus, further studies are necessary in order to better evaluate the effect of this variant on the overall NAFLD spectrum such as the impact of the variant on cellular stress and liver inflammation could be helpful to explain its protective effect on liver disease.

CONCLUDING REMARKS

In summary, the KLB rs17618244 variant was associated with a more severe liver disease and with decreased hepatic and soluble KLB levels in a large cohort of pediatric and adult patients with NAFLD. Based on previously published results the rs17618244 variant was correlated to the loss of function of KLB protein with deleterious effects on liver damage and NAFLD progression. In HepG2 cells the complete depletion of KLB protein, through CRISPR/Cas9 technology, was demonstrated to have a strong impact on the hepatocyte homeostasis, bringing to the onset of severe NAFLD traits. Therefore, *KLB* ^{-/-} cells showed deficiencies in cholesterol and lipid metabolism, suggesting the loss of important hepatocyte functions and a major impairment of the cell homeostasis at different levels. All these events in turn may trigger apoptosis sustained by a defective autophagy process. As consequence, the inflammatory response is induced, resembling NAFLD in humans. In addition, *KLB* ^{-/-} cells showed typical pro-oncogenic features, such as increased proliferation, cell growth and invasiveness and upregulated important oncogenes. These acquired features prompt the formation of tumor spheroids and led to the upregulation of key modulators of the EMT process, suggesting the shift towards a mesenchymal tumorigenic phenotype.

Considering that our model resembled in several aspects the stages of NAFLD progression and HCC tumorigenesis observed in patients, we possibly may hypothesize that KLB depletion may have a central role in the switching towards a different non-hepatocellular phenotype that could have acquired pro-oncogenic features. Moreover, the FGF19-independent multiple effects of KLB observed in our model could be related to still unknown functional roles of this co-receptor.

The translational relevance of our data was supported by published studies performed in patients carrying or not the KLB variants rs17618244 [55, 56] or rs12152703. In this regard, the new KLB rs12152703 variant was associated for the first time, with enhanced levels of

hepatic and soluble KLB and seems to have a protective effect on NAFLD onset and progression. The results obtained also suggests a central function of the sKLB, which may be shed after the binding to FGF19 and could have its own function. Nevertheless, these are speculations that still must be proved with tailored studies.

To date, KLB/FGFR4/FGF19 axis is considered a promising target against NASH and fibrosis [81]. Indeed, in a phase 2 clinical trial the treatment with Aldafermin, the best FGF19 analogue, was associated with a significant decrease of hepatic steatosis, up to 70%, lowering of transaminases levels and to an improvement in NAS score by 2 or more points with decreasing of fibrosis. However, several side effects, such as medium-severe gastrointestinal disorders related with changes in BAs metabolism, were reported in patients [93]. Moreover, excess of FGF19 is known to have a tumorigenic effect on the liver [130]. Thus, considering that FGFR4/KLB complex has a pivotal role for the hepatic binding of FGF19, the recombinant isoforms of KLB could be used for the treatment of NASH and might have stronger effects on liver disease. In this picture, the restoration of KLB levels per se, at least in those patients reporting KLB downregulation, might constitute a possible novel therapeutic strategy for the prevention of severe NAFLD.

FUTURE PERSPECTIVES

In the next future, a deeper exploration of KLB functionality in the liver and in the NAFLD context is deemed to translate our findings to patients. However, in order to clarify how KLB is capable to modulate all the constellation of factors we reported in this study, additional *in vitro* experiments are required. Among these, an additional cell line reporting KLB KO will have to be generated to validate the data obtained on HepG2 cells. For this purpose, immortalized human hepatocytes could be a reliable model to reproduce key experiments. Moreover, cell lines overexpressing the WT form of KLB will be generated by using both KLB KO cells and HepG2 cells to respectively assess the impact of KLB rescue and the overproduction on hepatocyte homeostasis. Moreover, the overexpression of KLB in these models could also help in clarifying the potential beneficial effects of KLB expression on NAFLD spectrum observed in patients. In order to reproduce more accurately the effects of the rs17618244 variant in *in vitro* a knock-in model introducing the corresponding sequence of the variant should be generated by using CRISPR/Cas9 technique, and the main aspects featuring NAFLD pathogenesis should be evaluated and compared to the KLB full knock-out model. Finally, the tumorigenic potential of *KLB KO* cells should be further evaluated in *in vivo* inoculating these cells in nude mice.

Since what we observed on patients carrying the KLB rs12152703 variant, we hypothesize that not only the full protein of KLB (fKLB) but also sKLB, may impact on NAFLD onset and progression. Therefore, pre-clinical data obtained by administering different synthetic KLB forms, including both the fKLB and sKLB, to 2D and 3D *in vitro* models of NAFLD/NASH, could provide further evidenced on the therapeutic potential of KLB mimetics.

BIBLIOGRAPHY

- [1] A. S. Aaldijk, C. R. C. Verzijl, J. W. Jonker, and D. Struik, "Biological and pharmacological functions of the FGF19- and FGF21-coreceptor beta klotho," *Frontiers in Endocrinology*, Review vol. 14, 2023.
- [2] E. Buzzetti, M. Pinzani, and E. A. Tsochatzis, "The multiple-hit pathogenesis of non-alcoholic fatty liver disease (NAFLD)," (in eng), *Metabolism*, vol. 65, no. 8, pp. 1038-48, Aug 2016, doi: 10.1016/j.metabol.2015.12.012.
- [3] A. F. Godoy-Matos, W. S. Silva Júnior, and C. M. Valerio, "NAFLD as a continuum: from obesity to metabolic syndrome and diabetes," *Diabetology & Metabolic Syndrome*, vol. 12, no. 1, p. 60, 2020/07/14 2020, doi: 10.1186/s13098-020-00570-y.
- [4] W. Jonas and A. Schürmann, "Genetic and epigenetic factors determining NAFLD risk," *Molecular Metabolism*, vol. 50, p. 101111, 2021/08/01/ 2021, doi: <https://doi.org/10.1016/j.molmet.2020.101111>.
- [5] M. H. Le *et al.*, "Forecasted 2040 global prevalence of nonalcoholic fatty liver disease using hierarchical bayesian approach," (in eng), *Clin Mol Hepatol*, vol. 28, no. 4, pp. 841-850, Oct 2022, doi: 10.3350/cmh.2022.0239.
- [6] B. J. Perumpail, M. A. Khan, E. R. Yoo, G. Cholankeril, D. Kim, and A. Ahmed, "Clinical epidemiology and disease burden of nonalcoholic fatty liver disease," (in eng), *World J Gastroenterol*, vol. 23, no. 47, pp. 8263-8276, Dec 21 2017, doi: 10.3748/wjg.v23.i47.8263.
- [7] S. Pouwels *et al.*, "Non-alcoholic fatty liver disease (NAFLD): a review of pathophysiology, clinical management and effects of weight loss," (in eng), *BMC Endocr Disord*, vol. 22, no. 1, p. 63, Mar 14 2022, doi: 10.1186/s12902-022-00980-1.
- [8] G. C. Farrell, V. W. Wong, and S. Chitturi, "NAFLD in Asia--as common and important as in the West," (in eng), *Nat Rev Gastroenterol Hepatol*, vol. 10, no. 5, pp. 307-18, May 2013, doi: 10.1038/nrgastro.2013.34.
- [9] Z. M. Younossi *et al.*, "The economic and clinical burden of nonalcoholic fatty liver disease in the United States and Europe," (in eng), *Hepatology*, vol. 64, no. 5, pp. 1577-1586, Nov 2016, doi: 10.1002/hep.28785.
- [10] S. H. Koo, "Nonalcoholic fatty liver disease: molecular mechanisms for the hepatic steatosis," (in eng), *Clin Mol Hepatol*, vol. 19, no. 3, pp. 210-5, Sep 2013, doi: 10.3350/cmh.2013.19.3.210.
- [11] B. A. Neuschwander-Tetri, "Hepatic lipotoxicity and the pathogenesis of nonalcoholic steatohepatitis: the central role of nontriglyceride fatty acid metabolites," (in eng), *Hepatology*, vol. 52, no. 2, pp. 774-88, Aug 2010, doi: 10.1002/hep.23719.
- [12] F. M. Perla, M. Prelati, M. Lavorato, D. Visicchio, and C. Anania, "The Role of Lipid and Lipoprotein Metabolism in Non-Alcoholic Fatty Liver Disease," (in eng), *Children (Basel)*, vol. 4, no. 6, Jun 6 2017, doi: 10.3390/children4060046.
- [13] R. Ramanathan, A. H. Ali, and J. A. Ibdah, "Mitochondrial Dysfunction Plays Central Role in Nonalcoholic Fatty Liver Disease," *International Journal of Molecular Sciences*, vol. 23, no. 13, doi: 10.3390/ijms23137280.
- [14] Z. Li *et al.*, "Mitochondria-Mediated Pathogenesis and Therapeutics for Non-Alcoholic Fatty Liver Disease," *Molecular Nutrition & Food Research*, vol. 63, no. 16, p. 1900043, 2019/08/01 2019, doi: <https://doi.org/10.1002/mnfr.201900043>.
- [15] J. P. Arab, M. Arrese, and M. Trauner, "Recent Insights into the Pathogenesis of Nonalcoholic Fatty Liver Disease," (in eng), *Annu Rev Pathol*, vol. 13, pp. 321-350, Jan 24 2018, doi: 10.1146/annurev-pathol-020117-043617.
- [16] T. Higashi, S. L. Friedman, and Y. Hoshida, "Hepatic stellate cells as key target in liver fibrosis," *Advanced Drug Delivery Reviews*, vol. 121, pp. 27-42, 2017/11/01/ 2017, doi: <https://doi.org/10.1016/j.addr.2017.05.007>.
- [17] Y. Koyama and D. A. Brenner, "Liver inflammation and fibrosis," *The Journal of Clinical Investigation*, vol. 127, no. 1, pp. 55-64, 01/03/ 2017, doi: 10.1172/JCI88881.
- [18] J. E. Puche, Y. Saiman, and S. L. Friedman, "Hepatic Stellate Cells and Liver Fibrosis," in *Comprehensive Physiology*, 2013, pp. 1473-1492.

- [19] P. Acharya, K. Chouhan, S. Weiskirchen, and R. Weiskirchen, "Cellular Mechanisms of Liver Fibrosis," (in eng), *Front Pharmacol*, vol. 12, p. 671640, 2021, doi: 10.3389/fphar.2021.671640.
- [20] Q. Song and X. Zhang, "The Role of Gut-Liver Axis in Gut Microbiome Dysbiosis Associated NAFLD and NAFLD-HCC," (in eng), *Biomedicines*, vol. 10, no. 3, Feb 23 2022, doi: 10.3390/biomedicines10030524.
- [21] L. Xu, N. Nagata, and T. Ota, "Impact of Glucoraphanin-Mediated Activation of Nrf2 on Non-Alcoholic Fatty Liver Disease with a Focus on Mitochondrial Dysfunction," (in eng), *Int J Mol Sci*, vol. 20, no. 23, Nov 25 2019, doi: 10.3390/ijms20235920.
- [22] A. Hwang *et al.*, "Supervised learning reveals circulating biomarker levels diagnostic of hepatocellular carcinoma in a clinically relevant model of non-alcoholic steatohepatitis; An OAD to NASH," (in eng), *PLoS one*, vol. 13, no. 6, pp. e0198937-e0198937, 2018, doi: 10.1371/journal.pone.0198937.
- [23] A. Khan and X. Zhang, "Function of the Long Noncoding RNAs in Hepatocellular Carcinoma: Classification, Molecular Mechanisms, and Significant Therapeutic Potentials," (in eng), *Bioengineering (Basel)*, vol. 9, no. 8, Aug 21 2022, doi: 10.3390/bioengineering9080406.
- [24] R. Piciotti *et al.*, "Old-fashioned and newly discovered biomarkers: the future of NAFLD-related HCC screening and monitoring," *Hepatoma Research*, vol. 8, p. 37, 2022, doi: 10.20517/2394-5079.2022.46.
- [25] G. A. Michelotti, M. V. Machado, and A. M. Diehl, "NAFLD, NASH and liver cancer," *Nature Reviews Gastroenterology & Hepatology*, vol. 10, no. 11, pp. 656-665, 2013/11/01 2013, doi: 10.1038/nrgastro.2013.183.
- [26] H. Son and A. Moon, "Epithelial-mesenchymal Transition and Cell Invasion," (in eng), *Toxicol Res*, vol. 26, no. 4, pp. 245-52, Dec 2010, doi: 10.5487/tr.2010.26.4.245.
- [27] M. Garg, "Epithelial-mesenchymal transition - activating transcription factors - multifunctional regulators in cancer," (in eng), *World J Stem Cells*, vol. 5, no. 4, pp. 188-95, Oct 26 2013, doi: 10.4252/wjsc.v5.i4.188.
- [28] M. Deldar Abad Paskeh, S. Mirzaei, M. Ashrafzadeh, A. Zarrabi, and G. Sethi, "Wnt/ β -Catenin Signaling as a Driver of Hepatocellular Carcinoma Progression: An Emphasis on Molecular Pathways," (in eng), *J Hepatocell Carcinoma*, vol. 8, pp. 1415-1444, 2021, doi: 10.2147/jhc.s336858.
- [29] G. Giannelli, P. Koudelkova, F. Dituri, and W. Mikulits, "Role of epithelial to mesenchymal transition in hepatocellular carcinoma," (in eng), *J Hepatol*, vol. 65, no. 4, pp. 798-808, Oct 2016, doi: 10.1016/j.jhep.2016.05.007.
- [30] Z.-Q. Qiu *et al.*, "The clinical relevance of epithelial-mesenchymal transition and its correlations with tumorigenic immune infiltrates in hepatocellular carcinoma," *Immunology*, vol. 166, no. 2, pp. 185-196, 2022/06/01 2022, doi: <https://doi.org/10.1111/imm.13465>.
- [31] D. Xu, Y. Wang, J. Wu, S. Lin, Y. Chen, and J. Zheng, "Identification and clinical validation of EMT-associated prognostic features based on hepatocellular carcinoma," *Cancer Cell International*, vol. 21, no. 1, p. 621, 2021/11/24 2021, doi: 10.1186/s12935-021-02326-8.
- [32] M. E. Rinella and S. Sookoian, "From NAFLD to MASLD: updated naming and diagnosis criteria for fatty liver disease," (in eng), *J Lipid Res*, vol. 65, no. 1, p. 100485, Jan 2024, doi: 10.1016/j.jlr.2023.100485.
- [33] R. Loomba and V. W. Wong, "Implications of the new nomenclature of steatotic liver disease and definition of metabolic dysfunction-associated steatotic liver disease," (in eng), *Aliment Pharmacol Ther*, vol. 59, no. 2, pp. 150-156, Jan 2024, doi: 10.1111/apt.17846.
- [34] K. Cusi, "From NAFLD to MASLD: Promise and pitfalls of a new definition," *Annals of Hepatology*, 10.1016/j.aohep.2023.101179, doi: 10.1016/j.aohep.2023.101179.
- [35] L. He, W. Zheng, K. Qiu, W. Kong, and T. Zeng, "Changing from NAFLD to MASLD: The new definition can more accurately identify individuals at higher risk for diabetes," *Journal of Hepatology*, vol. 80, no. 2, pp. e85-e87, 2024, doi: 10.1016/j.jhep.2023.09.035.
- [36] D. Sharma and P. Mandal, "NAFLD: genetics and its clinical implications," *Clinics and Research in Hepatology and Gastroenterology*, vol. 46, no. 9, p. 102003, 2022/11/01/ 2022, doi: <https://doi.org/10.1016/j.clinre.2022.102003>.

- [37] Y. Rotman, C. Koh, J. M. Zmuda, D. E. Kleiner, and T. J. Liang, "The association of genetic variability in patatin-like phospholipase domain-containing protein 3 (PNPLA3) with histological severity of nonalcoholic fatty liver disease," (in eng), *Hepatology*, vol. 52, no. 3, pp. 894-903, Sep 2010, doi: 10.1002/hep.23759.
- [38] Q. M. Anstee *et al.*, "Genome-wide association study of non-alcoholic fatty liver and steatohepatitis in a histologically characterised cohort(☆)," (in eng), *J Hepatol*, vol. 73, no. 3, pp. 505-515, Sep 2020, doi: 10.1016/j.jhep.2020.04.003.
- [39] S. Sookoian *et al.*, "Lack of evidence supporting a role of TMC4-rs641738 missense variant-MBOAT7- intergenic downstream variant-in the Susceptibility to Nonalcoholic Fatty Liver Disease," (in eng), *Sci Rep*, vol. 8, no. 1, p. 5097, Mar 23 2018, doi: 10.1038/s41598-018-23453-9.
- [40] R. M. Mancina *et al.*, "The MBOAT7-TMC4 Variant rs641738 Increases Risk of Nonalcoholic Fatty Liver Disease in Individuals of European Descent," (in eng), *Gastroenterology*, vol. 150, no. 5, pp. 1219-1230.e6, May 2016, doi: 10.1053/j.gastro.2016.01.032.
- [41] S. Petta *et al.*, "Glucokinase regulatory protein gene polymorphism affects liver fibrosis in non-alcoholic fatty liver disease," (in eng), *PLoS One*, vol. 9, no. 2, p. e87523, 2014, doi: 10.1371/journal.pone.0087523.
- [42] M. Di Filippo *et al.*, "Homozygous MTTP and APOB mutations may lead to hepatic steatosis and fibrosis despite metabolic differences in congenital hypocholesterolemia," *Journal of Hepatology*, vol. 61, no. 4, pp. 891-902, 2014/10/01/ 2014, doi: <https://doi.org/10.1016/j.jhep.2014.05.023>.
- [43] C. S. Faulkner, C. M. White, V. H. Shah, and L. L. Jophlin, "A single nucleotide polymorphism of PLIN2 is associated with nonalcoholic steatohepatitis and causes phenotypic changes in hepatocyte lipid droplets: A pilot study," *Biochimica et Biophysica Acta (BBA) - Molecular and Cell Biology of Lipids*, vol. 1865, no. 5, p. 158637, 2020/05/01/ 2020, doi: <https://doi.org/10.1016/j.bbalip.2020.158637>.
- [44] K. Kuramoto *et al.*, "Perilipin 5, a lipid droplet-binding protein, protects heart from oxidative burden by sequestering fatty acid from excessive oxidation," (in eng), *J Biol Chem*, vol. 287, no. 28, pp. 23852-63, Jul 6 2012, doi: 10.1074/jbc.M111.328708.
- [45] C. Namikawa *et al.*, "Polymorphisms of microsomal triglyceride transfer protein gene and manganese superoxide dismutase gene in non-alcoholic steatohepatitis," *Journal of Hepatology*, vol. 40, no. 5, pp. 781-786, 2004/05/01/ 2004, doi: <https://doi.org/10.1016/j.jhep.2004.01.028>.
- [46] F. Mohseni, S. Farajnia, M. A. Farhangi, M. Khoshbaten, and M.-A. Jafarabadi, "Association of UCP2 -866G>A Polymorphism With Nonalcoholic Fatty Liver Disease in Patients From North-West of Iran," *Laboratory Medicine*, vol. 48, no. 1, pp. 65-72, 2017, doi: 10.1093/labmed/lmw052.
- [47] Y. Ma *et al.*, "17-Beta Hydroxysteroid Dehydrogenase 13 Is a Hepatic Retinol Dehydrogenase Associated With Histological Features of Nonalcoholic Fatty Liver Disease," (in eng), *Hepatology*, vol. 69, no. 4, pp. 1504-1519, Apr 2019, doi: 10.1002/hep.30350.
- [48] H. Gellert-Kristensen, T. G. Richardson, G. Davey Smith, B. G. Nordestgaard, A. Tybjaerg-Hansen, and S. Stender, "Combined Effect of PNPLA3, TM6SF2, and HSD17B13 Variants on Risk of Cirrhosis and Hepatocellular Carcinoma in the General Population," (in eng), *Hepatology*, vol. 72, no. 3, pp. 845-856, Sep 2020, doi: 10.1002/hep.31238.
- [49] B. Carlsson *et al.*, "Review article: the emerging role of genetics in precision medicine for patients with non-alcoholic steatohepatitis," (in eng), *Aliment Pharmacol Ther*, vol. 51, no. 12, pp. 1305-1320, Jun 2020, doi: 10.1111/apt.15738.
- [50] C. De Benedittis *et al.*, "Interplay of PNPLA3 and HSD17B13 Variants in Modulating the Risk of Hepatocellular Carcinoma among Hepatitis C Patients," (in eng), *Gastroenterol Res Pract*, vol. 2020, p. 4216451, 2020, doi: 10.1155/2020/4216451.
- [51] C. Bianco *et al.*, "Non-invasive stratification of hepatocellular carcinoma risk in non-alcoholic fatty liver using polygenic risk scores," (in eng), *J Hepatol*, vol. 74, no. 4, pp. 775-782, Apr 2021, doi: 10.1016/j.jhep.2020.11.024.
- [52] A. De Vincentis *et al.*, "A Polygenic Risk Score to Refine Risk Stratification and Prediction for Severe Liver Disease by Clinical Fibrosis Scores," *Clinical Gastroenterology and Hepatology*, vol. 20, no. 3, pp. 658-673, 2022, doi: 10.1016/j.cgh.2021.05.056.

- [53] B. S. Wong *et al.*, "A Klotho β variant mediates protein stability and associates with colon transit in irritable bowel syndrome with diarrhea," (in eng), *Gastroenterology*, vol. 140, no. 7, pp. 1934-42, Jun 2011, doi: 10.1053/j.gastro.2011.02.063.
- [54] F. Ji *et al.*, "KLB gene polymorphism is associated with obesity and non-alcoholic fatty liver disease in the Han Chinese," (in eng), *Aging (Albany NY)*, vol. 11, no. 18, pp. 7847-7858, Sep 23 2019, doi: 10.18632/aging.102293.
- [55] P. Dongiovanni *et al.*, " β -Klotho gene variation is associated with liver damage in children with NAFLD," (in eng), *J Hepatol*, vol. 72, no. 3, pp. 411-419, Mar 2020, doi: 10.1016/j.jhep.2019.10.011.
- [56] N. Panera *et al.*, "The KLB rs17618244 gene variant is associated with fibrosing MAFLD by promoting hepatic stellate cell activation," (in eng), *EBioMedicine*, vol. 65, p. 103249, Mar 2021, doi: 10.1016/j.ebiom.2021.103249.
- [57] M. Meroni, M. Longo, G. Tria, and P. Dongiovanni, "Genetics Is of the Essence to Face NAFLD," (in eng), *Biomedicines*, vol. 9, no. 10, Sep 30 2021, doi: 10.3390/biomedicines9101359.
- [58] S. Ito *et al.*, "Molecular cloning and expression analyses of mouse betaklotho, which encodes a novel Klotho family protein," (in eng), *Mech Dev*, vol. 98, no. 1-2, pp. 115-9, Nov 2000, doi: 10.1016/s0925-4773(00)00439-1.
- [59] L. Geng *et al.*, " β -Klotho promotes glycolysis and glucose-stimulated insulin secretion via GP130," *Nature Metabolism*, vol. 4, no. 5, pp. 608-626, 2022/05/01 2022, doi: 10.1038/s42255-022-00572-2.
- [60] M. S. Razzaque, "The role of Klotho in energy metabolism," *Nature Reviews Endocrinology*, vol. 8, no. 10, pp. 579-587, 2012/10/01 2012, doi: 10.1038/nrendo.2012.75.
- [61] K. Fon Tacer *et al.*, "Research resource: Comprehensive expression atlas of the fibroblast growth factor system in adult mouse," (in eng), *Mol Endocrinol*, vol. 24, no. 10, pp. 2050-64, Oct 2010, doi: 10.1210/me.2010-0142.
- [62] Y. Xu and Z. Sun, "Molecular basis of Klotho: from gene to function in aging," (in eng), *Endocr Rev*, vol. 36, no. 2, pp. 174-93, Apr 2015, doi: 10.1210/er.2013-1079.
- [63] T. Lan *et al.*, "FGF19, FGF21, and an FGFR1/ β -Klotho-Activating Antibody Act on the Nervous System to Regulate Body Weight and Glycemia," (in eng), *Cell Metab*, vol. 26, no. 5, pp. 709-718.e3, Nov 7 2017, doi: 10.1016/j.cmet.2017.09.005.
- [64] G. Guthrie, C. Vonderohe, and D. Burrin, "Fibroblast growth factor 15/19 expression, regulation, and function: An overview," *Molecular and Cellular Endocrinology*, vol. 548, p. 111617, 2022/05/15/ 2022, doi: <https://doi.org/10.1016/j.mce.2022.111617>.
- [65] E. P. van Loon *et al.*, "Shedding of klotho by ADAMs in the kidney," (in eng), *Am J Physiol Renal Physiol*, vol. 309, no. 4, pp. F359-68, Aug 15 2015, doi: 10.1152/ajprenal.00240.2014.
- [66] C. D. Chen *et al.*, "Identification of cleavage sites leading to the shed form of the anti-aging protein klotho," (in eng), *Biochemistry*, vol. 53, no. 34, pp. 5579-87, Sep 2 2014, doi: 10.1021/bi500409n.
- [67] S. Lee *et al.*, "Structures of β -klotho reveal a 'zip code'-like mechanism for endocrine FGF signalling," *Nature*, vol. 553, no. 7689, pp. 501-505, 2018/01/01 2018, doi: 10.1038/nature25010.
- [68] S. Y. Shi *et al.*, "A systematic dissection of sequence elements determining β -Klotho and FGF interaction and signaling," *Scientific Reports*, vol. 8, no. 1, p. 11045, 2018/07/23 2018, doi: 10.1038/s41598-018-29396-5.
- [69] R. Micanovic *et al.*, "Different roles of N- and C- termini in the functional activity of FGF21," (in eng), *J Cell Physiol*, vol. 219, no. 2, pp. 227-34, May 2009, doi: 10.1002/jcp.21675.
- [70] Y. Liu, M. Cao, Y. Cai, X. Li, C. Zhao, and R. Cui, "Dissecting the Role of the FGF19-FGFR4 Signaling Pathway in Cancer Development and Progression," (in eng), *Front Cell Dev Biol*, vol. 8, p. 95, 2020, doi: 10.3389/fcell.2020.00095.
- [71] R. Goetz and M. Mohammadi, "Exploring mechanisms of FGF signalling through the lens of structural biology," (in eng), *Nat Rev Mol Cell Biol*, vol. 14, no. 3, pp. 166-80, Mar 2013, doi: 10.1038/nrm3528.
- [72] S. Kan *et al.*, "FGF19 increases mitochondrial biogenesis and fusion in chondrocytes via the AMPK α -p38/MAPK pathway," (in eng), *Cell Commun Signal*, vol. 21, no. 1, p. 55, Mar 13 2023, doi: 10.1186/s12964-023-01069-5.

- [73] Q. Zhou, V. W. Lui, and W. Yeo, "Targeting the PI3K/Akt/mTOR pathway in hepatocellular carcinoma," (in eng), *Future Oncol*, vol. 7, no. 10, pp. 1149-67, Oct 2011, doi: 10.2217/fon.11.95.
- [74] K. Dolegowska, M. Marchelek-Mysliwiec, M. Nowosiad-Magda, M. Slawinski, and B. Dolegowska, "FGF19 subfamily members: FGF19 and FGF21," (in eng), *J Physiol Biochem*, vol. 75, no. 2, pp. 229-240, Jun 2019, doi: 10.1007/s13105-019-00675-7.
- [75] J. Y. L. Chiang and J. M. Ferrell, "Up to date on cholesterol 7 alpha-hydroxylase (CYP7A1) in bile acid synthesis," (in eng), *Liver Res*, vol. 4, no. 2, pp. 47-63, Jun 2020, doi: 10.1016/j.livres.2020.05.001.
- [76] T. Li and J. Y. L. Chiang, "Bile Acid Metabolism in Health and Disease," in *The Liver*, 2020, pp. 269-285.
- [77] B. C. Lin, M. Wang, C. Blackmore, and L. R. Desnoyers, "Liver-specific Activities of FGF19 Require Klotho beta *," *Journal of Biological Chemistry*, vol. 282, no. 37, pp. 27277-27284, 2007, doi: 10.1074/jbc.M704244200.
- [78] T. C. Schreuder *et al.*, "The hepatic response to FGF19 is impaired in patients with nonalcoholic fatty liver disease and insulin resistance," (in eng), *Am J Physiol Gastrointest Liver Physiol*, vol. 298, no. 3, pp. G440-5, Mar 2010, doi: 10.1152/ajpgi.00322.2009.
- [79] Q. Fang *et al.*, "Serum Fibroblast Growth Factor 19 Levels Are Decreased in Chinese Subjects With Impaired Fasting Glucose and Inversely Associated With Fasting Plasma Glucose Levels," *Diabetes Care*, vol. 36, no. 9, pp. 2810-2814, 2013, doi: 10.2337/dc12-1766.
- [80] A. Alisi *et al.*, "Association between Serum Atypical Fibroblast Growth Factors 21 and 19 and Pediatric Nonalcoholic Fatty Liver Disease," (in eng), *PLoS One*, vol. 8, no. 6, p. e67160, 2013, doi: 10.1371/journal.pone.0067160.
- [81] E. Henriksson and B. Andersen, "FGF19 and FGF21 for the Treatment of NASH—Two Sides of the Same Coin? Differential and Overlapping Effects of FGF19 and FGF21 From Mice to Human," (in eng), *Front Endocrinol (Lausanne)*, vol. 11, p. 601349, 2020, doi: 10.3389/fendo.2020.601349.
- [82] C. Cicione, C. Degirolamo, and A. Moschetta, "Emerging role of fibroblast growth factors 15/19 and 21 as metabolic integrators in the liver," *Hepatology*, vol. 56, no. 6, pp. 2404-2411, 2012/12/01 2012, doi: <https://doi.org/10.1002/hep.25929>.
- [83] E. Somm *et al.*, "β-Klotho deficiency shifts the gut-liver bile acid axis and induces hepatic alterations in mice," (in eng), *Am J Physiol Endocrinol Metab*, vol. 315, no. 5, pp. E833-e847, Nov 1 2018, doi: 10.1152/ajpendo.00182.2018.
- [84] S. A. Polyzos, E. S. Kang, C. Boutari, E. J. Rhee, and C. S. Mantzoros, "Current and emerging pharmacological options for the treatment of nonalcoholic steatohepatitis," (in eng), *Metabolism*, vol. 111s, p. 154203, Oct 2020, doi: 10.1016/j.metabol.2020.154203.
- [85] Z. M. Younossi *et al.*, "Obeticholic acid for the treatment of non-alcoholic steatohepatitis: interim analysis from a multicentre, randomised, placebo-controlled phase 3 trial," (in eng), *Lancet*, vol. 394, no. 10215, pp. 2184-2196, Dec 14 2019, doi: 10.1016/s0140-6736(19)33041-7.
- [86] S. Frey, N. Petrucciani, and A. Iannelli, "Bariatric Surgery in the Setting of Liver Cirrhosis with Portal Hypertension: the Confection and Particularities of Roux-en-Y Gastric Bypass in a High-Risk Patient," *Obesity Surgery*, vol. 30, no. 10, pp. 4165-4166, 2020/10/01 2020, doi: 10.1007/s11695-020-04715-w.
- [87] M. Zhou, R. M. Learned, S. J. Rossi, A. M. DePaoli, H. Tian, and L. Ling, "Engineered FGF19 eliminates bile acid toxicity and lipotoxicity leading to resolution of steatohepatitis and fibrosis in mice," (in eng), *Hepatol Commun*, vol. 1, no. 10, pp. 1024-1042, Dec 2017, doi: 10.1002/hep4.1108.
- [88] B. C. Lin and L. R. Desnoyers, "FGF19 and cancer," (in eng), *Adv Exp Med Biol*, vol. 728, pp. 183-94, 2012, doi: 10.1007/978-1-4614-0887-1_12.
- [89] S. Talukdar and A. Kharitonov, "FGF19 and FGF21: In NASH we trust," (in eng), *Mol Metab*, vol. 46, p. 101152, Apr 2021, doi: 10.1016/j.molmet.2020.101152.
- [90] M. E. Rinella *et al.*, "Rosuvastatin improves the FGF19 analogue NGM282-associated lipid changes in patients with non-alcoholic steatohepatitis," *Journal of Hepatology*, vol. 70, no. 4, pp. 735-744, 2019, doi: 10.1016/j.jhep.2018.11.032.

- [91] M. E. Rinella *et al.*, "A randomized, double-blind, placebo-controlled trial of aldafermin in patients with NASH and compensated cirrhosis," (in eng), *Hepatology*, vol. 79, no. 3, pp. 674-689, Mar 1 2024, doi: 10.1097/hep.0000000000000607.
- [92] S. A. Harrison *et al.*, "Efficacy and Safety of Aldafermin, an Engineered FGF19 Analog, in a Randomized, Double-Blind, Placebo-Controlled Trial of Patients With Nonalcoholic Steatohepatitis," (in eng), *Gastroenterology*, vol. 160, no. 1, pp. 219-231.e1, Jan 2021, doi: 10.1053/j.gastro.2020.08.004.
- [93] S. A. Harrison *et al.*, "NGM282 for treatment of non-alcoholic steatohepatitis: a multicentre, randomised, double-blind, placebo-controlled, phase 2 trial," (in eng), *Lancet*, vol. 391, no. 10126, pp. 1174-1185, Mar 24 2018, doi: 10.1016/s0140-6736(18)30474-4.
- [94] S. A. Harrison *et al.*, "Safety and efficacy of once-weekly efruxifermin versus placebo in non-alcoholic steatohepatitis (HARMONY): a multicentre, randomised, double-blind, placebo-controlled, phase 2b trial," *The Lancet Gastroenterology & Hepatology*, vol. 8, no. 12, pp. 1080-1093, 2023, doi: 10.1016/S2468-1253(23)00272-8.
- [95] N. Alkhouri *et al.*, "Clinical trial: Effects of pegozafermin on the liver and on metabolic comorbidities in subjects with biopsy-confirmed nonalcoholic steatohepatitis," *Alimentary Pharmacology & Therapeutics*, vol. 58, no. 10, pp. 1005-1015, 2023/11/01 2023, doi: <https://doi.org/10.1111/apt.17709>.
- [96] J. Sonoda, M. Z. Chen, and A. Baruch, "FGF21-receptor agonists: an emerging therapeutic class for obesity-related diseases," vol. 30, no. 2, 2017, doi: doi:10.1515/hmbci-2017-0002.
- [97] C. Wong *et al.*, "Fibroblast growth factor receptor 1/Klotho β agonist BFKB8488A improves lipids and liver health markers in patients with diabetes or NAFLD: A phase 1b randomized trial," (in eng), *Hepatology*, vol. 78, no. 3, pp. 847-862, Sep 1 2023, doi: 10.1002/hep.32742.
- [98] M. H. Le *et al.*, "Global incidence of non-alcoholic fatty liver disease: A systematic review and meta-analysis of 63 studies and 1,201,807 persons," (in eng), *J Hepatol*, vol. 79, no. 2, pp. 287-295, Aug 2023, doi: 10.1016/j.jhep.2023.03.040.
- [99] S. Sookoian, C. J. Pirola, L. Valenti, and N. O. Davidson, "Genetic Pathways in Nonalcoholic Fatty Liver Disease: Insights From Systems Biology," (in eng), *Hepatology*, vol. 72, no. 1, pp. 330-346, Jul 2020, doi: 10.1002/hep.31229.
- [100] D. E. Kleiner *et al.*, "Design and validation of a histological scoring system for nonalcoholic fatty liver disease," (in eng), *Hepatology*, vol. 41, no. 6, pp. 1313-21, Jun 2005, doi: 10.1002/hep.20701.
- [101] M. Meroni *et al.*, "Modeling KLB deficiency by genome editing in hepatocytes: from oxidative stress and inflammation towards enhanced proliferation," *Digestive and Liver Disease*, vol. 54, p. S50, 2022, doi: 10.1016/j.dld.2022.01.098.
- [102] K. Jakobi *et al.*, "Sorafenib Treatment and Modulation of the Sphingolipid Pathway Affect Proliferation and Viability of Hepatocellular Carcinoma In Vitro," (in eng), *Int J Mol Sci*, vol. 21, no. 7, Mar 31 2020, doi: 10.3390/ijms21072409.
- [103] Z. Ezzoukhry *et al.*, "EGFR activation is a potential determinant of primary resistance of hepatocellular carcinoma cells to sorafenib," (in eng), *Int J Cancer*, vol. 131, no. 12, pp. 2961-9, Dec 15 2012, doi: 10.1002/ijc.27604.
- [104] K. J. Livak and T. D. Schmittgen, "Analysis of relative gene expression data using real-time quantitative PCR and the 2⁻(Delta Delta C(T)) Method," (in eng), *Methods*, vol. 25, no. 4, pp. 402-8, Dec 2001, doi: 10.1006/meth.2001.1262.
- [105] Y. Xie *et al.*, "FGF/FGFR signaling in health and disease," *Signal Transduction and Targeted Therapy*, vol. 5, no. 1, p. 181, 2020/09/02 2020, doi: 10.1038/s41392-020-00222-7.
- [106] A. Y. Ming, E. Yoo, E. N. Vorontsov, S. M. Altamentova, D. M. Kilkenny, and J. V. Rocheleau, "Dynamics and Distribution of Klotho β (KLB) and fibroblast growth factor receptor-1 (FGFR1) in living cells reveal the fibroblast growth factor-21 (FGF21)-induced receptor complex," (in eng), *J Biol Chem*, vol. 287, no. 24, pp. 19997-20006, Jun 8 2012, doi: 10.1074/jbc.M111.325670.
- [107] M. Kram, "Galectin-3 inhibition as a potential therapeutic target in non-alcoholic steatohepatitis liver fibrosis," (in eng), *World J Hepatol*, vol. 15, no. 2, pp. 201-207, Feb 27 2023, doi: 10.4254/wjh.v15.i2.201.

- [108] M. Hoekstra and M. Van Eck, "High-density lipoproteins and non-alcoholic fatty liver disease," *Atherosclerosis Plus*, vol. 53, pp. 33-41, 2023/09/01/ 2023, doi: <https://doi.org/10.1016/j.athplu.2023.08.001>.
- [109] S. Lamichane, B. Dahal Lamichane, and S.-M. Kwon, "Pivotal Roles of Peroxisome Proliferator-Activated Receptors (PPARs) and Their Signal Cascade for Cellular and Whole-Body Energy Homeostasis," *International Journal of Molecular Sciences*, vol. 19, no. 4, doi: 10.3390/ijms19040949.
- [110] S. A. Kliewer and D. J. Mangelsdorf, "Bile Acids as Hormones: The FXR-FGF15/19 Pathway," (in eng), *Dig Dis*, vol. 33, no. 3, pp. 327-31, 2015, doi: 10.1159/000371670.
- [111] R. Amorim, C. C. Magalhães, F. Borges, P. J. Oliveira, and J. Teixeira, "From Non-Alcoholic Fatty Liver to Hepatocellular Carcinoma: A Story of (Mal)Adapted Mitochondria," (in eng), *Biology (Basel)*, vol. 12, no. 4, Apr 14 2023, doi: 10.3390/biology12040595.
- [112] J. Le, W. Jia, and Y. Sun, "Sennoside A protects mitochondrial structure and function to improve high-fat diet-induced hepatic steatosis by targeting VDAC1," (in eng), *Biochem Biophys Res Commun*, vol. 500, no. 2, pp. 484-489, Jun 2 2018, doi: 10.1016/j.bbrc.2018.04.108.
- [113] Y. Zheng, S. Wang, J. Wu, and Y. Wang, "Mitochondrial metabolic dysfunction and non-alcoholic fatty liver disease: new insights from pathogenic mechanisms to clinically targeted therapy," (in eng), *J Transl Med*, vol. 21, no. 1, p. 510, Jul 28 2023, doi: 10.1186/s12967-023-04367-1.
- [114] J. H. Koo and C. Y. Han, "Signaling Nodes Associated with Endoplasmic Reticulum Stress during NAFLD Progression," (in eng), *Biomolecules*, vol. 11, no. 2, Feb 8 2021, doi: 10.3390/biom11020242.
- [115] T. Zhou, L. Chang, Y. Luo, Y. Zhou, and J. Zhang, "Mst1 inhibition attenuates non-alcoholic fatty liver disease via reversing Parkin-related mitophagy," (in eng), *Redox Biol*, vol. 21, p. 101120, Feb 2019, doi: 10.1016/j.redox.2019.101120.
- [116] T. Kanda *et al.*, "Apoptosis and non-alcoholic fatty liver diseases," (in eng), *World J Gastroenterol*, vol. 24, no. 25, pp. 2661-2672, Jul 7 2018, doi: 10.3748/wjg.v24.i25.2661.
- [117] J.-P. Decuypere, J. B. Parys, and G. Bultynck, "Regulation of the Autophagic Bcl-2/Beclin 1 Interaction," *Cells*, vol. 1, no. 3, pp. 284-312, doi: 10.3390/cells1030284.
- [118] E.-L. Eskelinen *et al.*, "Role of LAMP-2 in Lysosome Biogenesis and Autophagy," *Molecular Biology of the Cell*, vol. 13, no. 9, pp. 3355-3368, 2002/09/01 2002, doi: 10.1091/mbc.e02-02-0114.
- [119] A. Vainshtein and D. A. Hood, "The regulation of autophagy during exercise in skeletal muscle," (in eng), *J Appl Physiol (1985)*, vol. 120, no. 6, pp. 664-73, Mar 15 2016, doi: 10.1152/jappphysiol.00550.2015.
- [120] P. Middleton and N. Vergis, "Mitochondrial dysfunction and liver disease: role, relevance, and potential for therapeutic modulation," (in eng), *Therap Adv Gastroenterol*, vol. 14, p. 17562848211031394, 2021, doi: 10.1177/17562848211031394.
- [121] T. Luedde and R. F. Schwabe, "NF- κ B in the liver--linking injury, fibrosis and hepatocellular carcinoma," (in eng), *Nat Rev Gastroenterol Hepatol*, vol. 8, no. 2, pp. 108-18, Feb 2011, doi: 10.1038/nrgastro.2010.213.
- [122] Q. Chen, X. Lu, and X. Zhang, "Noncanonical NF- κ B Signaling Pathway in Liver Diseases," (in eng), *J Clin Transl Hepatol*, vol. 9, no. 1, pp. 81-89, Feb 28 2021, doi: 10.14218/jcth.2020.00063.
- [123] D. Geh, D. M. Manas, and H. L. Reeves, "Hepatocellular carcinoma in non-alcoholic fatty liver disease-a review of an emerging challenge facing clinicians," (in eng), *Hepatobiliary Surg Nutr*, vol. 10, no. 1, pp. 59-75, Jan 2021, doi: 10.21037/hbsn.2019.08.08.
- [124] L. Gramantieri *et al.*, "In human hepatocellular carcinoma in cirrhosis proliferating cell nuclear antigen (PCNA) is involved in cell proliferation and cooperates with P21 in DNA repair," *Journal of Hepatology*, vol. 39, no. 6, pp. 997-1003, 2003/12/01/ 2003, doi: [https://doi.org/10.1016/S0168-8278\(03\)00458-6](https://doi.org/10.1016/S0168-8278(03)00458-6).
- [125] H. Cheng *et al.*, "Heat-Shock protein A12A is a novel PCNA-binding protein and promotes hepatocellular carcinoma growth," *The FEBS Journal*, vol. 287, no. 24, pp. 5464-5477, 2020/12/01 2020, doi: <https://doi.org/10.1111/febs.15276>.

- [126] M.-F. Yuen, P.-C. Wu, V. C.-H. Lai, J. Y.-N. Lau, and C.-L. Lai, "Expression of c-Myc, c-Fos, and c-Jun in hepatocellular carcinoma," *Cancer*, vol. 91, no. 1, pp. 106-112, 2001/01/01 2001, doi: [https://doi.org/10.1002/1097-0142\(20010101\)91:1<106::AID-CNCR14>3.0.CO;2-2](https://doi.org/10.1002/1097-0142(20010101)91:1<106::AID-CNCR14>3.0.CO;2-2).
- [127] O. Abdel-Rahman and M. Fouad, "Sorafenib-based combination as a first line treatment for advanced hepatocellular carcinoma: A systematic review of the literature," *Critical Reviews in Oncology/Hematology*, vol. 91, no. 1, pp. 1-8, 2014/07/01/ 2014, doi: <https://doi.org/10.1016/j.critrevonc.2013.12.013>.
- [128] E. Gonzalez-Sanchez *et al.*, "The TGF- β Pathway: A Pharmacological Target in Hepatocellular Carcinoma?," (in eng), *Cancers (Basel)*, vol. 13, no. 13, Jun 29 2021, doi: 10.3390/cancers13133248.
- [129] C. Scheau *et al.*, "The Role of Matrix Metalloproteinases in the Epithelial-Mesenchymal Transition of Hepatocellular Carcinoma," (in eng), *Anal Cell Pathol (Amst)*, vol. 2019, p. 9423907, 2019, doi: 10.1155/2019/9423907.
- [130] Z. Shan *et al.*, "Fibroblast growth factors 19 and 21 in acute liver damage," (in eng), *Annals of translational medicine*, vol. 6, no. 12, pp. 257-257, 2018, doi: 10.21037/atm.2018.05.26.